A study of self-consistent equations of state

Alv Borge

Department of Physics
Norwegian University of Science and Technology
Trondheim, Norway

February, 2001

Preface

This thesis is submitted to the Norwegian University of Science and Technology in partial fulfillment of the requirements for the degree Doktor Ingeniør. It consists of an introduction to the field of research in which I have been working, two scientific papers, and some calculational details not covered by the articles.

The work was carried out at the Institute of Physics in the Group of theoretical physics at the Norwegian University of Science and Technology.

I wish to express my gratitude to Professor Johan Skule Høye for his kind help and patience, and for a lot of good ideas.

I finally acknowledge the financial support from the Norwegian University of Science and Technology and from the Norwegian Research Council.

Alv Borge

February, 2001

Contents

Papers

Paper I A. Borge and J. S. Høye, *"Critical properties of the self-consistent Ornstein-Zernike approximation for 3-dimensional lattice gases with varying range of interaction"*, J. Chem. Phys. **108**, 4516 (1998).

Paper II J. S. Høye and A. Borge, *"Self Consistent Ornstein-Zernike Approximation compared with exact results for lattice gases in one and two dimensions"*, J. Chem. Phys. **108**, 8830 (1998).

Chapter 1

Basis

1.1 Introduction

The noble aim of statistical mechanics is to provide the link between macrophysics and microphysics. A particular important task is to connect the equation of state for a substance with the interactions between its molecules.

For liquids and dense gases this is particularly difficult, since one lacks a simple model, like the ideal gas or the perfect crystal, as the starting point[1].

The concern of this thesis is precisely to calculate the properties of a classical fluid, in particular near its critical point, the endpoint of the liquid-gas phase transition (Fig. 1.1(a)) at which the coexisting liquid and gas become identical. Due to the long-ranged density fluctuations which make the compressibility diverge (Fig. 1.1(b)), this is undoubtedly the most difficult situation.

To meet the challenges several methods have been developed, some rather recently. These methods may not be well known, and the thesis therefore contains a rather lengthy introduction to the field, with concise descriptions of those methods that will be relevant for the calculations to follow. I hope this makes the thesis more self-contained.

In Sec. 1.2 I review the similarities between fluid and magnetic systems. Definitions of correlation functions and the recipes for calculating the equation of state for a discrete system are given in Sec. 1.3. Chapter 2 deals

[1] Croxton in his book [1] says that "Liquid state physics no longer has the luxury status of an intellectual plaything –a kind of purgatory between gas and solid, a statistical mechanical jungle populated only by the foolhardy and/or academics".

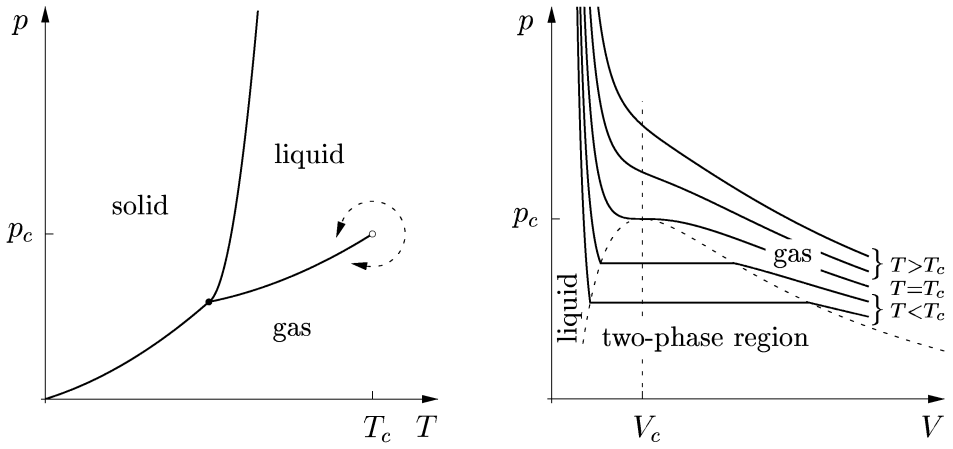

(a) PT-diagram (b) PV-diagram

Figure 1.1: Phase diagrams for a pure substance of simplest kind with a solid, a liquid, and a gasous phase: (a) Projection of the surface of state in the pressure-temperature (PT) plane, with (b) corresponding isothermal cross-sections in the fluid regime. The gas-liquid coexistence curve terminates in the critical point denoted (p_c, V_c, T_c), where p_c, V_c, and T_c are the critical pressure, critical volume, and critical temperature, respectively. Following the dashed line in (a) one sees that there is no clear division between a gas and a liquid.

with approximation methods for calculating the correlation functions. The situation close to the critical point is reviewed in Chapter 3. In Secs. 4.1 and 4.2 we deduce the SCOZA partial differential equation and in Secs. 4.3–4.5 it is solved numerically in three, two, and one dimensions, respectively. These latter calculations supplement those reported in the papers.

1.2 The lattice gas and the analogy with Ising spins

A variety of physical systems exhibit critical phenomena similar to the gas-liquid transition. Theoretically the magnetic ones have been of great impor-

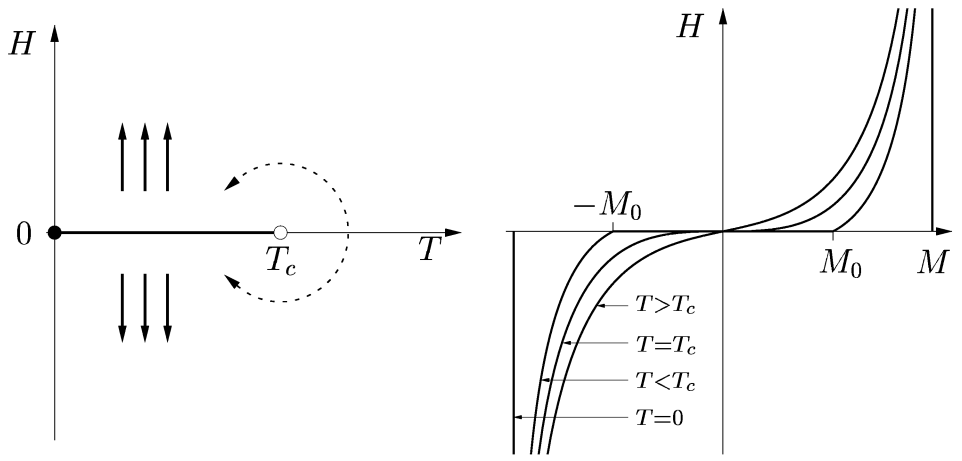

(a) HT-diagram (b) HM-diagram

Figure 1.2: (a) Projection of the equation of state for a ferromagnetic substance in the magnetic field-temperature (HT) plane, with (b) corresponding isothermal cross-sections (projection in the field-magnetisation (HM) plane). The coexistence curve for $H = 0$ terminates at the critical point, $T = T_c$ and $M = 0$.

tance.

Analogous to increasing the density by compressing a fluid, a magnetic field H applied to a ferromagnetic material will increase its magnetisation M. In a sense H and M correspond respectively to the pressure p and the density ρ in the fluid case [2]. At the critical point the fluctuations in the magnetisation will increase enormously and the isothermal susceptibility will diverge. Below the critical temperature, and in zero field, one gets spontaneous magnetisation and equilibrium between the positively and the negatively magnetized phase, $\pm M_0(T)$ (Fig. 1.2).

The well-known Ising model is the simplest model of a ferromagnetic substance. The N dimensionless spins, situated on a periodic lattice, are allowed to point either up or down ($s_i = \pm 1$) along an easy axis of magnetisation defined by the applied magnetic field $\boldsymbol{H}$ (in the Hamiltonian (1.1) below, H is the orientational energy of one spin in the field). With ferromagnetic pair interaction J_{ij} between spins i and j the Hamiltonian and canonical partition

function for a given spin configuration $\{s\}$ read

$$\mathcal{H}(\{s\}) = -\sum_{i<j} J_{ij} s_i s_j - H \sum_i s_i \tag{1.1}$$

and

$$Z_N(H,T) = \sum_{\{s\}} e^{-\beta \mathcal{H}(\{s\})}, \tag{1.2}$$

where $\beta = 1/k_B T$, k_B is the Boltzmann constant, and T is the absolute temperature. The magnetic field $\boldsymbol{H}$ regulates the net magnetisation

$$M = < \sum_i s_i > = \frac{\partial \ln Z_N(H,T)}{\partial \beta H} \tag{1.3}$$

In spatial dimension higher than one a critical point is achieved. In zero magnetic field, above the critical temperature, there is no net magnetisation due to random spin flipping, while below T_c one gets spontaneous magnetisation and symmetry breaking with coexistence between the spin up and the spin down phase. Thus the scalar spontaneous magnetisation describes the ordered phase analogous to the density difference $|\rho_l - \rho_c|$ in the gas-liquid transition (Fig. 1.3). Both theoretically and experimentally the gas-liquid phase transition has been found to have the same critical behavior as the Ising model [3].

The lattice gas is a discrete version of the gas-liquid system analogous to the Ising model with spin variables $s_i = \pm 1$. In the grand canonical ensemble the volume V is divided into N cells each with volume $v_0 = V/N$. The cells form a lattice. These cells are so small that at most one particle can occupy a cell, which gives a particle-hole symmetry that corresponds to the up-down symmetry in the spin case. By defining the occupation number

$$n_i = 1, 0 \tag{1.4}$$

denoting an occupied and empty cell, respectively, and again assuming pair interaction ϕ_{ij} between particles i and j, the potential energy for a given occupation configuration $\{n\}$ equals

$$V(\{n\}) = \sum_{i<j} \phi_{ij} n_i n_j. \tag{1.5}$$

Here a chemical potential μ regulates the mean particle numbers $\langle n_i \rangle$ and hence the the number density ρ, analogous to how the magnetic field influences the magnetisation in the Ising model. In terms of the fugacity

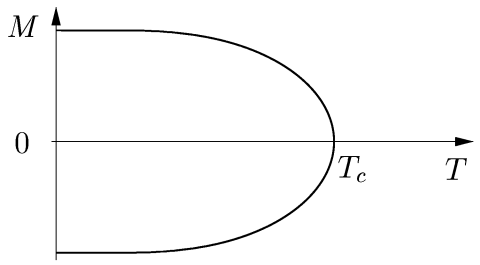

Figure 1.3: Projection of the equation of state for a ferromagnetic substance in the magnetisation-temperature (MT) plane (or $H = 0$ cross-section). Below the critical temperature T_c, and in zero magnetic field, the ferromagnet has a residual or spontaneous magnetisation $\pm M_0(T)$ in the coexisting phases.

$z = e^{\beta\mu}/\Lambda^3$, where $\Lambda = h/\sqrt{2\pi m k_B T}$ is the thermal de Broglie wavelength, the grand canonical partition function is

$$\begin{aligned} \Xi(\mu, T) &= \sum_{\{n\}} (z v_0)^{\sum_i n_i} e^{-\beta V(\{n\})} \\ &= \sum_{\{n\}} e^{\beta\left\{-\sum_{i<j}\phi_{ij} n_i n_j + \left[\frac{1}{\beta}\ln(v_0/\Lambda^3)+\mu\right]\sum_i n_i\right\}}. \end{aligned} \tag{1.6}$$

Except for an unimportant prefactor, Eq. (1.6) equals Eq. (1.2) when one makes the substitutions

$$n_i = \frac{1}{2}(1 + s_i) \tag{1.7}$$

$$\phi_{ij} = -4J_{ij} \tag{1.8}$$

$$\Delta\mu \equiv \mu - \mu_0(T) = 2H \tag{1.9}$$

where

$$\mu_0(T) = \frac{1}{2}\sum_{j(\neq i)} \phi_{ij} - k_B T \ln(v_0/\Lambda^3). \tag{1.10}$$

The term $\sum_{j(\neq i)} \phi_{ij}$ is considered to be independent of the position i in the thermodynamical limit. For subcritical temperatures $\Delta\mu$ gives the deviation in chemical potential from the gas-liquid coexistence curve $\mu_0(T)$, in the same way as the H-field measures the vertical distance from the coexistence

line $H = 0$ in the phase diagram for the Ising model (see Fig. 1.2(a)). In a spatially homogeneous system one gets from Eqs. (1.7) and (1.3) the mean number density

$$\rho = \rho_i \equiv \frac{< n_i >}{v_0} = \frac{1}{2v_0}(1+ < s_i >) = \frac{1}{2v_0}(1+m) \tag{1.11}$$

with the mean magnetisation per spin $m = M/N$ for an N-spin system.

1.3 Correlation functions

In the canonical ensemble for a continuum fluid the probability of finding any two particles in volume elements $d\boldsymbol{r}_1$ and $d\boldsymbol{r}_2$ at positions $\boldsymbol{r}_1$ and $\boldsymbol{r}_2$ is

$$\rho_N^{(2)}(\boldsymbol{r}_1, \boldsymbol{r}_2) d\boldsymbol{r}_1 d\boldsymbol{r}_2 = N(N-1) d\boldsymbol{r}_1 d\boldsymbol{r}_2 \frac{\int e^{-\beta V_N(\boldsymbol{r}^N)}\, d\boldsymbol{r}^{(N-2)}}{Q_N(V,T)}. \tag{1.12}$$

The normalization is provided by the configurational integral

$$Q_N(V,T) = \int e^{-\beta V_N(\boldsymbol{r}^N)}\, d\boldsymbol{r}^N \tag{1.13}$$

where we are using the notation [4] $\boldsymbol{r}^N = \{\boldsymbol{r}_1, \boldsymbol{r}_2, \ldots, \boldsymbol{r}_N\}$. $\rho_N^{(2)}(\boldsymbol{r}_1, \boldsymbol{r}_2)$ is the two-particle probability density, which for an ideal gas without interactions has the value $\rho^2(1 - 1/N)$. In the thermodynamic limit $N \to \infty$ this independent particle value equals ρ^2. For a homogeneous system the scaled (dimensionless) pair distribution function $g_N^{(2)}(\boldsymbol{r}_1, \boldsymbol{r}_2)$ is defined as

$$\rho^2 g_N^{(2)}(\boldsymbol{r}_1, \boldsymbol{r}_2) = \rho_N^{(2)}(\boldsymbol{r}_1, \boldsymbol{r}_2). \tag{1.14}$$

If the system is isotropic, $g_N^{(2)}(\boldsymbol{r}_1, \boldsymbol{r}_2) = g_N^{(2)}(|\boldsymbol{r}_1 - \boldsymbol{r}_2|)$, the pair distribution function is usually called the *radial distribution function* $g(r)$. For distances much larger than the range of the particle interactions, $g(r)$ approaches 1. At shorter distances, the deviations from this complete lack of structure is described by the *pair correlation function*

$$h(r) = g(r) - 1. \tag{1.15}$$

With pair interactions $V(\boldsymbol{r}^N) = \sum_{i<j}^N v(r_{ij})$ the internal energy per particle, excess to the ideal gas contribution, becomes

$$u \equiv \frac{U^{ex}}{N} = \frac{1}{2}\rho \int v(r) g(r)\, d\boldsymbol{r}. \tag{1.16}$$

This result is called *the energy equation.*

To study the correlations between the fluctuations $\delta\rho(\boldsymbol{r}) = \rho(\boldsymbol{r}) - \langle\rho(\boldsymbol{r})\rangle$ in the local particle densities $\rho(\boldsymbol{r}) = \sum_{i=1}^{N} \delta(\boldsymbol{r} - \boldsymbol{r}_i)$ at positions $\boldsymbol{r}$ and $\boldsymbol{r}'$, one has to use a grand canonical ensemble. They are measured by the density-density correlation function

$$\Gamma(\boldsymbol{r}, \boldsymbol{r}') = \langle\delta\rho(\boldsymbol{r})\delta\rho(\boldsymbol{r}')\rangle = \frac{\delta\langle\rho(\boldsymbol{r})\rangle}{\delta\beta\mu^*(\boldsymbol{r}')}, \tag{1.17}$$

which is the response of the equilibrium density at position $\boldsymbol{r}$, $\delta\langle\rho(\boldsymbol{r})\rangle$, to an external perturbation $\delta\phi_{ext}(\boldsymbol{r}')$ at position $\boldsymbol{r}'$–included in the chemical potential $\mu^*(\boldsymbol{r}') = \mu - \phi_{ext}(\boldsymbol{r}')$ (see section 2.1). In a homogeneous and isotropic system, $\Gamma(\boldsymbol{r}, \boldsymbol{r}') = \Gamma(|\boldsymbol{r} - \boldsymbol{r}'|)$. Writing

$$\Gamma(r) = \rho^2 h(r) + \rho\delta(r), \tag{1.18}$$

the density-density correlation function is expressed by pair correlations $h(r)$ and the particle correlations with themselves. The Fourier transform (denoted by tilde) $S(\boldsymbol{k}) = \tilde{\Gamma}(\boldsymbol{k})/\rho$ is the so called static structure factor, measured in elastic scattering experiments by the intensity of radiation scattered in the $\boldsymbol{k}$-direction:

$$S(\boldsymbol{k}) = 1 + \rho\tilde{h}(\boldsymbol{k}). \tag{1.19}$$

By neglecting surface effects we have

$$\tilde{\Gamma}(0) = \int \Gamma(r)\, d\boldsymbol{r} = \left(\frac{\partial\rho}{\partial\beta\mu}\right)_T = \rho\left(\frac{\partial\rho}{\partial\beta p}\right)_T, \tag{1.20}$$

or

$$S(0) = 1 + \rho\tilde{h}(0) = \left(\frac{\partial\rho}{\partial\beta p}\right)_T \tag{1.21}$$

in the macroscopic limit. Eq. (1.21), or equivalently Eq. (1.20), is known as *the fluctuation theorem* or *compressibility equation.* They give the equation of state from the pair correlation function $h(r)$, or equivalently, from the pair distribution function $g(r)$. Unlike the "energy route" (1.16), the "compressibility route" (1.21) is not restricted to pair interactions. The correlation length ξ is loosely defined as the range of $h(r)$. More specifically, in the limit $k \to 0$,

$$\frac{1}{S(k)} = \left(\frac{\partial\beta p}{\partial\rho}\right)_T (1 + \xi^2 k^2 + \cdots) \tag{1.22}$$

serves as a definition.

The Ornstein-Zernike integral equation [5] (here for a homogeneous system),

$$h(\boldsymbol{r}-\boldsymbol{r}') = c(\boldsymbol{r}-\boldsymbol{r}') + \rho \int c(\boldsymbol{r}-\boldsymbol{r}'')h(\boldsymbol{r}''-\boldsymbol{r}')\,d\boldsymbol{r}'', \tag{1.23}$$

defines the *direct correlation function* $c(\boldsymbol{r})$. In this way the total correlation is given by the direct correlation plus the indirect ones via other particles:

$$\begin{aligned} h(\boldsymbol{r}-\boldsymbol{r}') &= c(\boldsymbol{r}-\boldsymbol{r}') + \rho \int c(\boldsymbol{r}-\boldsymbol{r}'')c(\boldsymbol{r}''-\boldsymbol{r}')\,d\boldsymbol{r}'' + \\ &\quad \rho^2 \int\int c(\boldsymbol{r}-\boldsymbol{r}'')c(\boldsymbol{r}''-\boldsymbol{r}''')c(\boldsymbol{r}'''-\boldsymbol{r}')\,d\boldsymbol{r}''d\boldsymbol{r}''' + \cdots \end{aligned} \tag{1.24}$$

The infinitely long chains of c-bonds make it possible for the direct correlation function to have a finite range even when the pair correlation function has an infinite range at the critical point (where the reduced compressibility $(\partial\rho/\partial\beta p)_T$ in Eq. (1.21) diverges). Inserting the Fourier transform of (1.23)

$$1 + \rho\tilde{h}(\boldsymbol{k}) = \frac{1}{1-\rho\tilde{c}(\boldsymbol{k})} \tag{1.25}$$

into the fluctuation theorem, we obtain

$$1 - \rho\tilde{c}(0) = \left(\frac{\partial\beta p}{\partial\rho}\right)_T. \tag{1.26}$$

This shows that $\tilde{c}(0) = \int c(\boldsymbol{r})\,d\boldsymbol{r} \approx 1/\rho$ near the critical point. So $c(\boldsymbol{r})$ has to fall off at least as fast as r^{-3} for the integral to exist. The original assumption of Ornstein and Zernike [5] was that the range of $c(\boldsymbol{r})$ was the same as the range of the inter-particle potential, which for realistic pair potentials would correspond to something like $c(\boldsymbol{r}) \sim r^{-6}$. In this way the Ornstein-Zernike equation (1.23) is a useful tool for obtaining the pair distribution function $g(\boldsymbol{r})$, inferring the form of the direct correlation function $c(\boldsymbol{r})$ from the pair potential $v(\boldsymbol{r})$.

Chapter 2

Approximation methods

The equation of state for a pair-interacting spin model, Eq. (1.1), or lattice gas, Eq. (1.5), is obtained from the pair distribution function via the discrete versions of the internal energy equation (1.16) or the compressibility equation (1.21). But to calculate the pair distribution $g(r)$ from Eqs. (1.12) and (1.14) is a complicated many-particle problem, and some approximation scheme is called for. For a dilute gas it is convenient to expand $g(r)$ in the density. A systematic approximation scheme for studying long-range pair potentials consists of perturbing a known short-range repulsive system with an attractive tail interaction. To lowest order the tail is made infinitely long-ranged and infinitesimally weak, which produces a mean-field approximation. The mean spherical approximation includes the first-order correction to this mean-field approximation.

2.1 The virial expansion

The grand canonical partition function Ξ for a homogeneous one-component monoatomic gas with pair interactions $v(\boldsymbol{r})$ can be expressed as a diagrammatic expansion in the fugacity z, with coefficients Q_N being functionals of $v(\boldsymbol{r})$. The graphs consist of field points with an e-bond, $e(\boldsymbol{r}) = e^{-\beta v(\boldsymbol{r})}$, linking each pair of points:

$$\Xi = \sum_{N=0}^{\infty} \frac{z^N}{N!} \int e^{-\beta \sum_{i<j}^{N} v(\boldsymbol{r}_{ij})}\, d\boldsymbol{r}^N = 1 + \bullet\, z + \bullet\!\!-\!\!\bullet\, z^2 + \triangle\, z^3 + \boxtimes\, z^4 + \cdots \quad (2.1)$$

In the presence of an external field $\phi_{ext}(\boldsymbol{r}_i)$, the fugacity is considered to be a function $z^*(\boldsymbol{r}_i) = ze^{-\beta\phi_{ext}(\boldsymbol{r}_i)}$ attached to the field point $\boldsymbol{r}_i$. Therefore the

graphs will become functionals of $z^*(\boldsymbol{r})$ as well for the inhomogeneous gas. Functional differentiation of Eq. (2.1) with respect to a z^*-point gives the single-particle density

$$\rho^{(1)}(\boldsymbol{r}) = \frac{z^*(\boldsymbol{r})}{\Xi}\frac{\delta\Xi}{\delta z^*(\boldsymbol{r})} = \frac{\delta \ln \Xi}{\delta \ln z^*(\boldsymbol{r})}. \tag{2.2}$$

In the homogeneous case $z = z^*(\boldsymbol{r})$ and $\rho = \rho^{(1)}(\boldsymbol{r})$. By inverting the fugacity expansion of the single-particle density and eliminating the fugacity z in Eq. (2.1), the corresponding virial expansion is obtained. The excess part of Helmholtz free energy is then given by all simple[1] irreducible graphs (i. e. graphs who can not become disconnected by removal of a point):

$V\mathcal{A} \equiv -\beta F^{ex} =$ $+$ 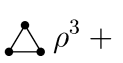 $+$ 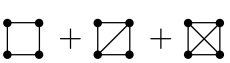 $+\cdots$ (2.3)

where the bonds here and below are f-bonds,

$$f(\boldsymbol{r}) = e^{-\beta v(\boldsymbol{r})} - 1. \tag{2.4}$$

$f(\boldsymbol{r})$ is called the Mayer function and has the same range as the potential $v(\boldsymbol{r})$. Helmholtz free energy gives the pressure p via

$$\beta p = \rho + (1 - \rho\frac{\partial}{\partial\rho})\mathcal{A} = \rho + \sum_{i=2}^{\infty} B_i(T)\rho^i \tag{2.5}$$

with virial coefficients

$$B_i(T) = -\frac{i-1}{i}\beta_{i-1}(T), \qquad i \geq 2 \tag{2.6}$$

in terms of the irreducible Mayer cluster graphs $\beta_i(T)$. These are the topologically distinct graphs given by (2.3), but with one field point replaced with a root point (in accordance with an intensive pressure p).

From Eqs. (1.14) and (1.12) the canonical pair distribution function is expressed as a functional derivative of the canonical excess Helmholtz free energy with respect to a v-bond

$$\rho^2 g_N(\boldsymbol{r}) = 2\frac{e(\boldsymbol{r})}{Q_N}\frac{\delta Q_N}{\delta e(\boldsymbol{r})} = 2\frac{\delta F_N^{ex}}{\delta v(\boldsymbol{r})} = 2e(\boldsymbol{r})\frac{\delta(-\beta F_N^{ex})}{\delta f(\boldsymbol{r})}. \tag{2.7}$$

[1] No pair of points is linked by more than one bond.

Weighting both sides of this equation with the probability of finding exactly N particles in a grand canonical ensemble and summing over all pair contributions $N \geq 2$ then yields

$$\rho^2 g(\boldsymbol{r}) = 2e(\boldsymbol{r})\frac{\delta V\mathcal{A}}{\delta f(\boldsymbol{r})} = \rho^2 e(\boldsymbol{r})\,[1 + \rho$$
$$+ (\quad + \quad + \quad + \quad + \quad)\,\rho^2 + \cdots\,] \tag{2.8}$$

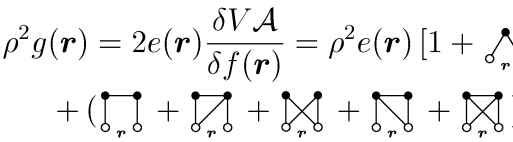

i. e. all graphs without connecting[2] field points and with an e-bond connecting the two root points labelled 0 and $\boldsymbol{r}$. (This e-bond prohibits hard spheres to overlap). Consistent with the Ornstein-Zernike equation (1.23) connecting $c(\boldsymbol{r})$ to $h(\boldsymbol{r}) = g(\boldsymbol{r}) - 1$ given by Eq. (2.8), the direct correlation function results from functional differentiating the excess Helmholtz free energy twice with respect to single particle densities

$$c(\boldsymbol{r}) = \frac{\delta^2 V\mathcal{A}}{\delta\rho^{(1)}(\boldsymbol{r})\delta\rho^{(1)}(0)} = \quad + \quad \rho$$
$$+ (\quad + \quad + \quad + \quad + \quad + \quad + \quad)\,\rho^2 + \cdots \tag{2.9}$$

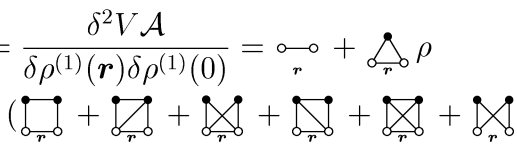

Irrespective of bond type, these graphs are the ones for $g(\boldsymbol{r})$, Eq. (2.8), plus those multiply connected[3] lacking the bond connecting the root points. Since all graphs apart from the single f-bond in Eq. (2.9) are at least doubly connected

$$c(\boldsymbol{r}) \underset{r\to\infty}{\simeq} f(\boldsymbol{r}) \approx -\beta v(\boldsymbol{r}) \tag{2.10}$$

to leading order in r. That the range of $c(\boldsymbol{r})$ is the same as for the pair potential $v(\boldsymbol{r})$, is in agreement with the Ornstein-Zernike approximation.

2.2 Mean-field theory

In absence of pair interactions $v(\boldsymbol{r})$, the virial expansions for the pressure and the pair distribution, Eqs. (2.5) and (2.8), reduce to the ideal gas results $\beta p = \rho$ and $g(\boldsymbol{r}) = 1$. To calculate the equation of state for a pair-interacting lattice gas via the virial expansion is in practice impossible beyond the first few terms. That means that the virial expansion is useful only for low densities.

[2] Removal of a connecting point causes the graph to become disconnected.

[3] A graph is multiply connected if there exists at least two independent paths between any pair of points.

When one tries to sum over all particle configurations $\{n\}$ in the partition function (1.6), the obstacle is the interaction term. With inhomogeneous chemical potentials μ_i, Eq. (1.6) in non-interacting form reads

$$\Xi = \sum_{\{n\}} e^{\beta \sum_i \mu_i(\{n\}) n_i}, \tag{2.11}$$

with a configuration-dependent chemical potential acting on particle no. i

$$\mu_i(\{n\}) = \mu_i - \sum_{j(\neq i)} \phi_{ij} n_j. \tag{2.12}$$

Since the term $\frac{1}{\beta}\ln(v_0/\Lambda^3)$ in Eq. (1.6) does not depend on density, and hence will not qualitatively alter the subsequent treatment, it is omitted here. In mean-field theory the configurations n_j are approximated by their averages ρ_j ($v_0 = 1$). Thus the configuration-dependent chemical potential seen by particle i is replaced with the effective chemical potential

$$\mu_i^e = \mu_i - \sum_{j(\neq i)} \phi_{ij} \rho_j, \tag{2.13}$$

causing the corresponding effective grand partition function to take the form of a hard-core lattice gas, i. e.

$$\Xi^e = \prod_i (1 + e^{\beta \mu_i^e}). \tag{2.14}$$

The particle densities ρ_j are unknown and are determined self-consistently from the coupled set of equations (2.13) and

$$\rho_i = \frac{\partial \ln \Xi^e}{\partial \beta \mu_i^e} = \frac{e^{\beta \mu_i^e}}{1 + e^{\beta \mu_i^e}}. \tag{2.15}$$

Here $\beta\mu_i^e$ as a function of ρ_i is antisymmetric around $\rho_i = 1/2$. This behavior reflects the spin up-spin down antisymmetry in the H-field of the Ising model. By switching to "Ising language", $\Delta\rho_i \equiv m_i = 2\rho_i - 1$, it is easy to uncover the qualitative aspects of the solution in the homogeneous case $\Delta\rho = \Delta\rho_i$. The set of Eqs. (2.15) and (2.13) is then reduced to

$$\Delta\rho = \tanh(\beta\mu^e/2) \tag{2.16}$$

$$\mu^e = \Delta\mu + a\Delta\rho, \tag{2.17}$$

where

$$a = -\frac{1}{2} \sum_{j(\neq i)} \phi_{ij} \tag{2.18}$$

is a positive constant for an attractive potential. With chemical potential $\mu_0 = -a$ along the coexistence line (Eq. (1.10) with the temperature dependent term dropped), $\Delta\mu = \mu - \mu_0$ subcritically gives the deviation from coexistence. For the system to be materially stable, $(\partial\mu/\partial\rho)_{V,T} \geq 0$. In phase equilibrium, $\Delta\mu = 0$, Eq. (2.16) has materially stable solutions $\Delta\rho = 0$ and $\Delta\rho = \pm\Delta\rho'$ for $T > T_c$ and $T = T' < T_c$, respectively. Hence the critical point is given by the density $\rho_c = 1/2$ and the temperature T_c as

$$k_B T_c = \frac{a}{2}. \tag{2.19}$$

With nearest-neighbor attractive interaction $-w < 0$ and coordination number[4] $q = 2d$ the critical temperature is

$$k_B T_c = \frac{qw}{4}. \tag{2.20}$$

Solved with respect to the chemical potential, Eq. (2.16) gives

$$\Delta\mu = \mu^{hc} - a\Delta\rho, \tag{2.21}$$

with hard core contribution

$$\beta\mu^{hc} = \ln\left(\frac{\rho}{1-\rho}\right). \tag{2.22}$$

This expression is diverging at close-packing $\rho = 1$, in agreement with the construction of the lattice-gas model, Eq. (1.4). Correspondingly the pressure is

$$p = p^{hc} - a\rho^2 \tag{2.23}$$

where

$$\beta p^{hc} = -\ln(1-\rho). \tag{2.24}$$

The mean-field approximation (2.13) treats the density fluctuations and hence the critical properties in a brutal and inaccurate way. By smoothing and infinitely stretching the interactions, collective effects are exaggerated

[4] on a hypercubic lattice

and disruptive fluctuations suppressed. For instance, Eq. (2.19) predicts incorrectly a phase transition in the one-dimensional ($d = 1$) lattice gas (or Ising model).

On the other hand the mean-field theory approximates the equation of state rather accurately *outside* the narrow critical region, where the isothermal compressibility $\sim (\partial\rho/\partial\beta p)_T$ is finite. See Fig. 1.1(b). At high densities, $1 - \rho \ll 1$, the fluctuation theorem (1.21) shows that the hard cores (2.24) provided by the lattice gas, "screen" the long-range mean-field correlations;

$$1 + \rho\tilde{h}(0) = (\partial\rho/\partial\beta p)_T = (1-\rho)[1 + 2\beta a\rho(1-\rho) + \cdots] \tag{2.25}$$

At sufficiently low densities, the ideal gas law, i. e. $(\partial\rho/\partial\beta p)_T = 1$, approximates the equation of state (2.23) well. Only in the critical region, where $(\partial\rho/\partial\beta p)_T$ becomes very large, the role of the long-range attractive forces is crucial. Therefore the mean-field approximation becomes less important with regard to producing a qualitatively correct phase diagram.

Beyond thermodynamical quantities, the mean-field equations (2.13) and (2.15) give the detailed correlations of the occupation number fluctuations $\delta n_i = n_i - \langle n_i \rangle$ (the discrete version of Eq. (1.17)), consistent with the compressibilty equation of state (1.21):

$$\Gamma_{ij} = \langle \delta n_i \delta n_j \rangle = \frac{\partial \rho_i}{\partial \beta \mu_j} = \rho_i(1-\rho_i)(\delta_{ij} - \beta \sum_{p(\neq i)} \phi_{ip}\Gamma_{pj}). \tag{2.26}$$

In a spatially homogenous phase, ρ_i and μ_i are replaced with ρ and μ. When one specializes to nearest-neighbor interaction on a hypercubic lattice (with lattice constant b), the long-range Fourier components

$$\tilde{\phi}_{\boldsymbol{k}} = 2(-w)\sum_{i=1}^{d} \cos(k_i b) \approx -w(q - b^2k^2) \tag{2.27}$$

inserted into the Fourier transform of Eq. (2.26),

$$\tilde{\Gamma}_{\boldsymbol{k}} = \frac{\rho(1-\rho)}{1 + \beta\rho(1-\rho)\tilde{\phi}_{\boldsymbol{k}}}, \tag{2.28}$$

give the asymptotic form

$$\tilde{\Gamma}_{\boldsymbol{k}} \propto \frac{1}{\varepsilon^2 + k^2} \tag{2.29}$$

close to the critical point. We have expanded in $kb \ll 1$. On the spinodal curve, and more specifically at the critical point (Eq. (2.20), we have

$$(\varepsilon b)^2 = \frac{1-\beta\rho(1-\rho)qw}{\beta\rho(1-\rho)w} = q\frac{T-T_c}{T_c} = 0. \tag{2.30}$$

This causes the range $1/\varepsilon$ of Γ_{ij} to diverge although the theory itself neglects all fluctuations. This result is consistent with smoothing and infinitially stretching all fluctuations, taken care of by the term $\sum_{p(\neq i)} \phi_{ip}\Gamma_{pj}$ in Eq. (2.26), and hence forcing a phase transition on the system.

Qualitatively the critical behavior is unchanged when the interaction is extended to n'th-nearest neighbors. But quantitatively the critical temperature and the correlation length are increased by factors n^d and n, respectively, for n large. With interaction strength $-w$ between each pair of interacting lattice sites, $k_B T_c \simeq \frac{1}{4}An^d w$ and Eqs. (2.30) now reads

$$(\varepsilon n b)^2 \simeq \frac{1-\beta\rho(1-\rho)An^d w}{\beta\rho(1-\rho)Bn^d w} = \frac{A}{B}\frac{T-T_c}{T_c} = 0, \tag{2.31}$$

where A and B are positive constants.

As we all know, the idea of representing a fluid as a system of hard spheres moving in a uniform, attractive potential stems from van der Waals and leads to his equation of state (2.23). But for continuum fluids only approximate expressions for the hard-core pressure p^{hc} are known in dimensions higher than one.

2.3 The γ-expansion

Due to the finite range of interaction there will be corrections to mean field or van der Waals theory. The work by Kac, Uhlenbeck, and Hemmer [6] on an exactly solvable one-dimensional model initiated a new method. They considered the Kac interaction $-\gamma a \exp(\gamma|x|)$, where the parameter γ is the inverse range of interaction. In the limit $\gamma \to 0$ van der Waals equation of state, Eq. (2.23), is obtained.

2.3.1 The expansion procedure

More generally, this method [7] consists of dividing the intermolecular potential,

$$v(\boldsymbol{r}) = v_0(\boldsymbol{r}) + w_\gamma(\boldsymbol{r}), \tag{2.32}$$

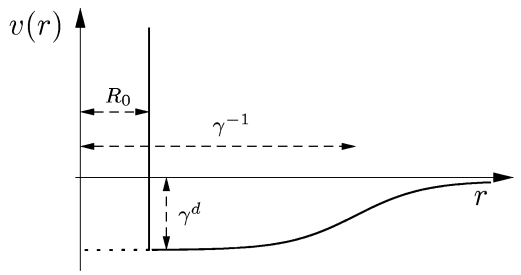

Figure 2.1: The pair interaction $v(r)$ for the γ-ordering as a function of distance r. Here a gas of hard d-dimensional spheres with diameter R_0 is chosen to be the reference system. The long-range perturbation has range γ^{-1} and strength γ^d.

into a short-range repulsion $v_0(\boldsymbol{r})$, the reference potential, whose properties are considered known, and a d-dimensional, weak, and long-ranged attraction

$$w_\gamma(\boldsymbol{r}) = -\gamma^d \phi(\gamma \boldsymbol{r}). \tag{2.33}$$

If R_0 is the range of the reference potential (for instance a hard core diameter), the dimensionless parameter of expansions is $\zeta = (\gamma R_0)^d$, roughly equal to the ratio of the reference interaction volume to the perturbation interaction volume. (See Fig. 2.1.). Next the virial expansion is rearranged such that contributions will appear in increasing order of ζ (i. e. to each order in ζ, graphs are summed to infinite order in density).

With the separation (2.32), the Mayer function (2.4) is represented by at most one reference Mayer function $f_0(\boldsymbol{r}) = e^{-\beta v_0(\boldsymbol{r})} - 1$ and any number of potential functions

$$\Phi(\boldsymbol{r}) = -\beta w_\gamma(\boldsymbol{r}) \tag{2.34}$$

in parallel, i. e.

$$f(\boldsymbol{r}) = e^{-\beta v_0(\boldsymbol{r}) + \Phi(\boldsymbol{r})} - 1 = f_0(\boldsymbol{r}) + [1 + f_0(\boldsymbol{r})] \sum_{n=1}^{\infty} \frac{1}{n!} [\Phi(\boldsymbol{r})]^n. \tag{2.35}$$

Inserting this Mayer expansion into the bonds of the Helmholtz free energy graphs, Eq. (2.3), the corresponding γ-ordering

$$\mathcal{A} = \mathcal{A}_0 + \sum_{i=0}^{\infty} \mathcal{A}_{(i)} \tag{2.36}$$

is given by the free energy of the reference system $\mathcal{A}_0$ whose graphs contain only reference bonds f_0, and contributions $\mathcal{A}_{(i)}$ of order $(\gamma^d)^i$. To lowest order $i = 0$ there is only one graph, namely

$$\mathcal{A}_{(0)} = \frac{1}{V} \bullet\!\!-\!\!\bullet\, \rho^2 = \frac{1}{2}\rho^2 \int \Phi(\boldsymbol{r})\, d\boldsymbol{r} = \frac{1}{2}\beta\rho^2 \int \gamma^d \phi(\gamma \boldsymbol{r})\, d\boldsymbol{r} = \beta a \rho^2, \qquad (2.37)$$

with a solid line denoting the Φ-bond and mean field constant (2.18) $a = -\frac{1}{2}\int w_\gamma(\boldsymbol{r})\, d\boldsymbol{r}$. From (2.5) we have to lowest order

$$\beta p = \rho + (1 - \rho\frac{\partial}{\partial\rho})(\mathcal{A}_0 + \mathcal{A}_{(0)}) = \beta p_0 - \beta a \rho^2, \qquad (2.38)$$

where the irreducible reference graphs $\mathcal{A}_0$ give exactly the pressure βp_0 of the reference system. So in the limit $\gamma \to 0$, van der Waals equation of state (2.23), together with the Maxwell construction to ensure non-negative compressibility, is exact.

The first-order contribution $i = 1$ is given by the ring graphs[5]

$V\mathcal{A}_{(1)} =$ 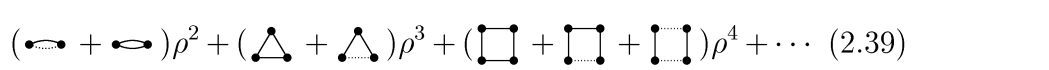 $\qquad (2.39)$

Due to topological reduction of the f_0-bonds in Eq. (2.36) in terms of reference pair correlation bonds h_0 (denoted by dotted lines), none of the rings contains two successive h_0-bonds. Only two of the graphs in (2.36) contain a single potential bond $\Phi(\boldsymbol{r}) \sim \beta$. Hence they give to lowest order the high temperature correction

$$a_{HT} = \frac{1}{V}\,(\bullet\!\!-\!\!\bullet\, + \bullet\!\!\frown\!\!\bullet\,)\,\rho^2 = -\frac{1}{2}\beta\rho^2 \int [1 + h_0(\boldsymbol{r})] w_\gamma(\boldsymbol{r})\, d\boldsymbol{r}, \qquad (2.40)$$

to the free energy $\mathcal{A}_0$, leaving the pair distribution (2.7) unaltered by the perturbation and equal to the reference pair distribution function;

$$g_{HT}(\boldsymbol{r}) = g_0(\boldsymbol{r}) = 1 + h_0(\boldsymbol{r}). \qquad (2.41)$$

[5] Topologically speaking the first graph is no ring because of its lack of bond symmetry. But what matters here is that they are the only graphs having one more Φ-bond of order γ^d, than "free" integrations over volumes γ^{-d}. I. e. the integrations are of the same kind as the one in the last integral of Eq. (2.37), not restricted by a short-range reference bond. Thus their contributions are of order $i = 1$ due to the excess Φ-bond. Otherwise the first graph does not cause any difficulties since it will be treated separately via the high temperature contribution a_{HT}. (See Eqs. (2.40), (2.43), and (2.44) below.).

In order to study structual influences from the attractive forces, the ring graphs are grouped with respect to the number of Φ-bonds. To each number $n \geq 2$, every possible combination of inserted h_0-bonds in the field points, will occur in Eq. (2.39). So with reference system hypervertices (drawn as big open circles with two terminals) representing

$$F_0(\boldsymbol{r}) = \rho\delta(\boldsymbol{r}) + \rho^2 h_0(\boldsymbol{r}), \tag{2.42}$$

we have

$$\mathcal{A} = \mathcal{A}_0 + a_{HT} + a_{ring} \tag{2.43}$$

to first order in γ^d. Using the convolution theorem, the contribution to the free energy from the ring graphs becomes

$$\begin{aligned} Va_{ring} &= \quad + \quad + \quad + \cdots \\ &= \frac{V}{(2\pi)^d} \int \sum_{n=2}^{\infty} \frac{1}{2n} [\tilde{F}_0(\boldsymbol{k})\tilde{\Phi}(\boldsymbol{k})]^n \, d\boldsymbol{k} \\ &= -\frac{1}{2}\frac{V}{(2\pi)^d} \int \{\tilde{F}_0(\boldsymbol{k})\tilde{\Phi}(\boldsymbol{k}) + \ln[1 - \tilde{F}_0(\boldsymbol{k})\tilde{\Phi}(\boldsymbol{k})]\} \, d\boldsymbol{k}. \end{aligned} \tag{2.44}$$

By removal of a Φ-bond, Eq. (2.8) gives the pair distribution function with its long-range part to first order included:

$$\rho^2 g(\boldsymbol{r}) = \rho^2 g_0(\boldsymbol{r}) + 2\frac{\delta V a_{ring}}{\delta\Phi(\boldsymbol{r})}, \tag{2.45}$$

i. e. the chain bonds

$$\rho^2 C(\boldsymbol{r}) = 2\frac{\delta V a_{ring}}{\delta\Phi(\boldsymbol{r})} = \quad + \quad + \quad + \cdots. \tag{2.46}$$

Fourier transforming and summing the chains gives the corresponding pair correlation function $\tilde{h}(\boldsymbol{k})$ via

$$\rho + \rho^2 \tilde{h}(\boldsymbol{k}) = \frac{\tilde{F}_0(\boldsymbol{k})}{1 - \tilde{F}_0(\boldsymbol{k})\tilde{\Phi}(\boldsymbol{k})}, \tag{2.47}$$

and the direct pair correlation function (Eqs. (1.25) and (2.34))

$$c(\boldsymbol{r}) = c_0(\boldsymbol{r}) - \beta w_\gamma(\boldsymbol{r}). \tag{2.48}$$

Since the perturbation contains the long-range part of the potential (Eqs. (2.32) and (2.33)), this first-order approximation is asymptotically correct at large distances, as shown by Eq. (2.10). But the perturbation has to be sufficiently weak (the temperature sufficiently high) or the density sufficiently low to ensure $\tilde{F}_0(\boldsymbol{k})\tilde{\Phi}(\boldsymbol{k}) < 1$ for all wave numbers. Without this condition fulfilled, the structure factor (1.19) becomes negative for some range of $\boldsymbol{k}$ [4].

Expressions (2.44) and (2.47) can be simplified [8] noting that the long-range potential picks out the Fourier transform $\tilde{\Phi}(\boldsymbol{k}) = \beta\tilde{\phi}(\boldsymbol{K})$ with $\boldsymbol{K} = \boldsymbol{k}/\gamma$. Thus to leading order in γ one can replace $\tilde{F}_0(\boldsymbol{k}) = \tilde{F}_0(\boldsymbol{K}\gamma)$ with $F_0 \equiv \tilde{F}_0(0)$. In this way the second graph of the high-temperature contribution (2.40) drops out from the free energy to $\mathcal{O}(\gamma^d)$, Eq. (2.43)[6]. For $r \gtrsim \mathcal{O}(R_0)$ the reference system correlations $\tilde{h}_0(\boldsymbol{k})$ will dominate the correlations, Eq. (2.47). But for distances of order of the range of the potential, $r = \mathcal{O}(\gamma^{-1})$, the $\tilde{h}_0(\boldsymbol{k})$ will fall off so much that the chain bond contribution dominates;

$$\rho^2\tilde{C}(\boldsymbol{k}) = \rho^2[\tilde{h}(\boldsymbol{k}) - \tilde{h}_0(\boldsymbol{k})] = \frac{F_0^2\beta\tilde{\phi}(\boldsymbol{K})}{1 - F_0\beta\tilde{\phi}(\boldsymbol{K})}. \tag{2.49}$$

Taking the inverse Fourier transform gives a contribution of order γ^d and range γ^{-1} since the right-hand side of (2.49) is a function of $\boldsymbol{K}$. Via the fluctuation theorem (1.21) the constant F_0 can be directly related to the compressibility of the reference system

$$\frac{1}{F_0} = \frac{1}{\rho + \rho^2\tilde{h}_0(0)} = \frac{1}{\rho}\frac{\partial(\beta p_0)}{\partial\rho}. \tag{2.50}$$

So by putting $\boldsymbol{k} = 0$ in Eq. (2.47) (or equivalently $\boldsymbol{K} = 0$ in Eq. (2.49)), the equation of state reduces to the van der Waals or mean field result (Eq. (2.38))

$$\frac{1}{\rho}\frac{\partial(\beta p)}{\partial\rho} = \frac{1}{F_0} - \tilde{\Phi}(0) = \frac{1}{\rho}\frac{\partial(\beta p_0)}{\partial\rho} - 2\beta a \tag{2.51}$$

to $\mathcal{O}(\gamma^0)$. At the critical point the pair correlation function (2.47) will diverge, since

$$1 - F_0\tilde{\Phi}(0) = 0. \tag{2.52}$$

[6] I. e. one simplifies by writing $\phi(0) = 0$. But this contribution is not crucial with respect to critical properties and is incorporated later. Besides it is obvious on physical grounds that the true properties of the fluid must be independent of the choice of perturbation for $r < R_0$.

Thus the main contribution to $h(\boldsymbol{k})$ near the critical point comes from $\boldsymbol{K} = 0$, and the denominator of Eq. (2.49) is expanded around $\boldsymbol{K} = 0$ through the spherically symmetric perturbation:

$$\begin{aligned}\tilde{\Phi}(\boldsymbol{k}) &= \beta\tilde{\phi}(\boldsymbol{K}) = \beta\int\left[1 + i\boldsymbol{K}\cdot\boldsymbol{R} - \frac{1}{2}(\boldsymbol{K}\cdot\boldsymbol{R})^2 + \cdots\right]\phi(R)\,d\boldsymbol{R} \\ &\approx \beta[\tilde{\phi}(0) + \frac{1}{2}K^2\tilde{\phi}''(0)] \end{aligned} \tag{2.53}$$

provided that $\tilde{\phi}''(0) = -\frac{1}{3}\int R^2\phi(R)\,d\boldsymbol{R}$ is finite ($\boldsymbol{R} = \gamma\boldsymbol{r}$). This holds for the Lennard-Jones potential, but the series expansion in K^2 can not be continued. Putting this expansion into Eq. (2.49) increases the range of $h(\boldsymbol{r})$ by a factor $1/\varepsilon$,

$$\rho^2[\tilde{h}(\boldsymbol{k}) - \tilde{h}_0(\boldsymbol{k})] = \frac{a}{\pi[-\tilde{\phi}''(0)]}\rho\frac{\partial\rho}{\partial(\beta p_0)}\frac{4\pi}{\varepsilon^2 + K^2} \tag{2.54}$$

with

$$\varepsilon^2 = \frac{2}{\beta[-\tilde{\phi}''(0)]}\frac{1 - F_0\tilde{\Phi}(0)}{F_0} = \frac{2}{[-\tilde{\phi}''(0)]}\frac{1}{\beta\rho}\frac{\partial(\beta p)}{\partial\rho} \tag{2.55}$$

vanishing at the critical point. Finally, in $d = 3$ dimensions (2.54) yields

$$h(\boldsymbol{r}) = h_0(\boldsymbol{r}) + \gamma^3\frac{a}{\pi[-\tilde{\phi}''(0)]}\frac{1}{\rho}\frac{\partial\rho}{\partial(\beta p_0)}\frac{e^{-\varepsilon\gamma r}}{\gamma r}. \tag{2.56}$$

The conclusion is that the first-order correction ($i = 1$) to mean-field theory is exponentially decaying except at the (mean-field) critical point $\varepsilon = 0$, where the correlation length $\xi = 1/(\varepsilon\gamma)$ and the fluctuation integral $\tilde{h}(0)$ diverge[7].

In one and two dimensions, however, the inverse Fourier transform of (2.54) diverges when $\varepsilon \to 0$. This first-order correction is therefore not meaningful in $d = 1$ and 2. In the lattice case $F_0 = \rho(1 - \rho)$ and with nearest neighbor interactions the first-order γ-expansion is equivalent to the Gaussian approximation [11] for the Ising model.

2.3.2 Thermodynamic inconsistency and critical renormalization

Including the ring graphs (2.44) to get the pressure (2.5) to order $i = 1$ (when dropping the second graph of a_{HT}, Eq. (2.40), from the free energy (2.43)),

[7] This form of the pair correlation function is exactly the same as the one predicted by the Ornstein-Zernike approximation, Eq. (1.25) with $c(r) \sim w_\gamma(r)$ at large separations.

one immediately faces the general problem of thermodynamical inconsistency for approximative liquid-state theories [4]. That is, the energy route adds the first-order correction beyond the mean field pressure (2.51) from the compressibility route:

$$\frac{1}{\rho}\frac{\partial(\beta p)}{\partial \rho} = \frac{1}{F_0} - \tilde{\Phi}(0) - \frac{\partial^2 a_{ring}}{\partial^2 \rho}, \tag{2.57}$$

where to dominating order

$$a_{ring} = \frac{1}{(2\pi)^d} \int \sum_{n=2}^{\infty} \frac{1}{2n} [F_0 \tilde{\Phi}(\boldsymbol{k})]^n \, d\boldsymbol{k}. \tag{2.58}$$

Differentiating once with respect to density (denoted by a prime),

$$\frac{\partial a_{ring}}{\partial \rho} = \frac{1}{2} F_0' K(0) \tag{2.59}$$

with

$$K(0) = \frac{1}{(2\pi)^d} \int \frac{F_0 [\tilde{\Phi}(\boldsymbol{k})]^2}{1 - F_0 \tilde{\Phi}(\boldsymbol{k})} \, d\boldsymbol{k}. \tag{2.60}$$

This is the chain bond

$K(\boldsymbol{r}) =$ 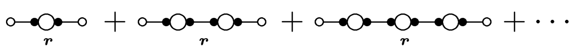 (2.61)

evaluated at $\boldsymbol{r} = 0$. Differentiating (2.58) once more gives

$$\frac{\partial^2 a_{ring}}{\partial^2 \rho} = \frac{1}{2} [F_0'' K(0) + F_0' K(0)']. \tag{2.62}$$

In principle the mismatch will be corrected by including higher-order terms. However, a more serious problem originates in the divergence of the integrals a_{ring} and $K(0)$. The divergence takes place at the mean-field critical point (2.52),

$$\tilde{\Phi}(0) = \beta_c \tilde{\phi}(0) = \frac{1}{F_0}, \tag{2.63}$$

where (2.62) adds a positive term to (2.51) since $K(0) > 0$, $F_0' = 0$, and $F_0'' < 0$. Here the last two relations follows from the conditions $\partial^2 p/\partial \rho^2 = 0$ and $\partial^3 p/\partial \rho^3 > 0$ on Eq. (2.51). Thus the added term (2.62) indicates a

lowering $\sim \gamma_r^d$ of the (mean-field) critical temperature T_c (2.63), as (2.57) gives

$$\tilde{\Phi}(0) = \beta_c \tilde{\phi}(0) = \frac{1}{F_0} - \frac{\partial^2 a_{ring}}{\partial^2 \rho}. \tag{2.64}$$

But the divergence makes the expressions invalid inside the mean-field spinodal curve. To partly remedy the divergence one can try to carry it along with the shift of the critical point. One then notes that at the (mean-field) critical point the last term of (2.62) vanishes where $F_0' = 0$ and $K(0)$ has its maximum. Thus adding (2.62) to (2.51) one obtains a renormalized hypervertex F_{0c} such that

$$\frac{1}{\rho}\frac{\partial(\beta p)}{\partial \rho} \approx \frac{1}{F_{0c}} - \tilde{\Phi}(0) \tag{2.65}$$

where (when deleting the last term of (2.62))

$$F_{0c} = F_0 + F_0'' F_0 F_{0c} K(0)/2. \tag{2.66}$$

The last expression takes the short-range part of the long-range pair correlations (the chain bonds (2.61) at $\boldsymbol{r} = 0$) into account. Chain bonds with endpoints F_0 and F_{0c} are attached to the two extra root points appearing when functional differentiating F_0 twice with respect to ρ [7, 9]. An exact treatment would involve four-body correlations [8]. Finally the range of the vertex is again regarded as a δ-function when integrating over these two root points. Consistent with the renormalization of F_0, $K(0)$ is replaced by

$$\begin{aligned} K(0) &= \frac{1}{(2\pi)^d} \int \frac{F_{0c}[\tilde{\Phi}(\boldsymbol{k})]^2}{1 - F_{0c}\tilde{\Phi}(\boldsymbol{k})}\, d\boldsymbol{k} \\ &= \frac{1}{(2\pi)^d} \int \frac{1}{F_{0c}^2} \left[\rho^2 \tilde{C}(\boldsymbol{k}) - F_{0c}^2 \tilde{\Phi}(\boldsymbol{k})\right] d\boldsymbol{k} = \left(\frac{\rho}{F_{0c}}\right)^2 C(0), \end{aligned} \tag{2.67}$$

where likewise

$$\rho^2 \tilde{C}(\boldsymbol{k}) = \frac{F_{0c}^2 \tilde{\Phi}(\boldsymbol{k})}{1 - F_{0c}\tilde{\Phi}(\boldsymbol{k})} \tag{2.68}$$

replaces the chain bonds (2.46). Note that the single Φ-bond (or literally the one with F_{0c}-endpoints) is subtracted in (2.67) as it will not contribute anyway when $\phi(0) = 0$, and this is consistent with the neglect of the second graph of a_{HT}, Eq. (2.40), in (2.57).

With (2.66), or actually using [8, 9]

$$F_{0c} = F_0 + F_0'' F_{0c}^2 K(0)/2, \tag{2.69}$$

the new critical point can be calculated directly from the divergence of the integrand in (2.67). Although the renormalized γ-ordering gives results valid in the critical region, things remain somewhat inconsistent, and isotherms become "irregular" such that for instance critical indices can not be defined. Nevertheless the singular behavior seen in real fluids is clearly reflected in a realistic interacting three dimensional continuum fluid [9]. For instance the coexistence curve is flattened on the top, relative to the mean-field result, due to the lowering of the critical point. Furthermore, using the fluctuation theorem to study the singularity of the integral $K(0)$ (Eq. (2.67)), Høye finds that [9]

$$\Delta(\beta F_{0c}) = \Big[\text{const}\Delta T + \text{const}(\Delta\rho)^2\Big]^2 \tag{2.70}$$

for deviations from critical values. Inserted in the equation of state (2.65), one obtains the asymptotic behavior

$$\Delta(\beta p) \sim (\Delta\rho)^5 \quad \text{and} \quad \frac{\partial(\beta p)}{\partial\rho} \sim (\Delta T)^2 \tag{2.71}$$

along the critical isotherm and isochor, respectively. This gives the critical exponents (to be defined in chapter 3) $\delta = 5$ and $\gamma = 2$. These values are also found in the mean spherical approximation, to be dealt with in the next section. From (2.70) Høye shows that the "irregular" isotherms originate from the last term of (2.62) not encountered by the critical renormalization. That is, near the critical point $F_0' \sim \Delta\rho$ and $K(0)' \sim \Delta\rho$ such that $-F_0'K(0)' \sim -(\Delta\rho)^2$. When added to (2.65), this is associated with a contribution $\Delta(\beta p) \sim -(\Delta\rho)^3$ in the pressure. For sufficiently small $\Delta\rho$ this term will dominate the fifth-order form in (2.71), and makes $\partial p/\partial\rho < 0$ on the critical isotherm. There is no easy way to remove this kind of inconsistency. With respect to nonuniversal critical properties, the high-temperature contribution a_{HT} is included via the reference system, to avoid interference with the critical renormalization. Formally a_{HT} is of higher order in γ, but due to correlations of hard particles at liquid densities it is of substantial magnitude. The main effect is a significant shift of the critical temperature, with a resulting T_c comparing favorably with the experimental value for Ar [8].

2.4 MSA

The mean spherical approximation (MSA) for continuum fluids [10] is the solution of the Ornstein-Zernike integral equation (1.23) with closure relations

$$\begin{aligned} h(r) &= -1 \qquad r < R_0 \\ c(r) &= -\beta v(r) \qquad r > R_0 \end{aligned} \tag{2.72}$$

for particles with a hard-core diameter R_0 and pair potential $v(r)$ outside R_0. The hard core condition on $h(r)$ is exact, while the condition on $c(r)$ is approximative although asymptotically correct (Eq. (2.10)) for large r. These relations are generalizations of the MSA closures for lattice gases with extended hard cores [10]. So with lattice vector $\boldsymbol{r}$, (2.72) applies to the lattice case as well. In fact the MSA originates from the spherical model for spin systems [11].

MSA is nothing but the first-order contribution in γ-ordering (2.47) with hypervertices

$$\tilde{F}_0(\boldsymbol{k}) = \frac{\rho}{1 - \rho\tilde{c}_0(\boldsymbol{k})} \tag{2.73}$$

and perturbation

$$\tilde{\Phi}(\boldsymbol{k}) = \tilde{c}(\boldsymbol{k}) - \tilde{c}_0(\boldsymbol{k}) \tag{2.74}$$

given by the solution $\tilde{c}_0(\boldsymbol{k})$ of the Percus-Yevick (PY) equation for hard spheres. PY is another solution of the Ornstein-Zernike equation, with closure relation $c(r) = [1 - e^{\beta v(r)}]g(r)$ in addition to the hard core condition. So $c_0(r > R_0) = 0$ and $h_0(r < R_0) = -1$ for hard spheres of diameter R_0. This solution is analytic [12], and it shows that the PY equation for hard spheres is the special case of MSA (2.72) with the potential tail $v(r)$ absent. If one identifies $-c_0(r)/\beta$, Eq. (2.48), as the potential inside hard cores satisfying the hard core condition, then

$$c(r) = -\beta[v(r) - c_0(r)/\beta] \tag{2.75}$$

is compatible with both MSA closure relations (2.72). Furthermore, from (2.34) and (2.48) we have identified the perturbation $\Phi(r) = -\beta w_\gamma(r)$ as $-\beta v(r)$ in (2.75), which leads to (2.74). Inserting (2.74) into the Ornstein-Zernike equation (1.25) immediately gives the pair correlation (2.47) with PY-hypervertices (2.73). By this identification MSA is the first-order contribution in the γ-expansion where the perturbating potential inside hard cores

is specified such that the hard core condition is fullfilled. MSA can therefore be regarded as an optimization of the first-order γ-expansion, in which the hard core reference system is treated exactly. Hence, MSA plays a crucial role as the leading correction to mean-field theory, Eq. (2.23).

In the lattice case, MSA and the renormalized γ-ordering share critical properties established in the previous section. This can be understood from Eq. (2.69) for the renormalized hypervertex F_{0c}. From the hard core pressure (2.24), the reference system hypervertex (2.50) equals

$$F_0 = \rho(1-\rho). \tag{2.76}$$

Thus $F_0'' = -2$ in (2.69), and together with Eq. (2.67) we have

$$F_0 = F_{0c} + \rho^2 C(0) = \frac{1}{(2\pi)^d} \int \frac{F_{0c}}{1 - F_{0c}\tilde{\Phi}(\boldsymbol{k})}\, d\boldsymbol{k}. \tag{2.77}$$

This is nothing but the MSA core condition, since from (2.47) with $\tilde{F}_0(\boldsymbol{k})$ replaced by F_{0c},

$$\begin{aligned} \frac{1}{(2\pi)^d} \int \frac{F_{0c}}{1 - F_{0c}\tilde{\Phi}(\boldsymbol{k})}\, d\boldsymbol{k} &= \frac{1}{(2\pi)^d} \int \rho[1 + \rho\tilde{h}(\boldsymbol{k})]\, d\boldsymbol{k} \\ &= \rho[1 + \rho h(0)] = \rho(1-\rho). \end{aligned} \tag{2.78}$$

But due to the remaining thermodynamic inconsistency associated with the critical renormalization, MSA is rather inaccurate for the nearest-neighbor Ising model: For instance on a simple cubic lattice $F_0 = 1.516\ldots F_{0c}$. Hence Eq. (2.63) with F_0 replaced by F_{0c} lowers T_c by as much as 34% compared to the mean-field result. According to series analyses of the Ising model [13] the actual lowering of T_c is about 25%, which shows the substantial perturbative influence of higher order terms in the γ-expansion.

Chapter 3

Critical properties

3.1 Critical exponents

At continuous phase transitions (Figs. 1.1 and 1.2) critical phenomena are observed. A characteristic feature of critical points is that asymptotically close to them a number of quantities show power-law behavior.

The critical exponent β describes how the order parameter vanishes as the critical point is approached from below along the curve of coexistence (Fig. 1.3). In the fluid case, the density difference $\Delta\rho = \rho_l(T) - \rho_g(T)$ between the liquid and gas phases, plays the role as order parameter. For a homogeneous lattice gas with unit cell volume $v_0 = 1$ and critical density $\rho_c = 1/2$, the asymptotic behavior

$$\Delta\rho \sim (-t)^\beta \tag{3.1}$$

defines β, where

$$t = \frac{T - T_c}{T_c} \tag{3.2}$$

$$\Delta\rho = \frac{\rho - \rho_c}{\rho_c} = 2\rho - 1 \tag{3.3}$$

are small relative density and temperature deviations from the critical point. Moreover, the sub- and supercritical divergences of the isothermal compressibility $\kappa_T = -\frac{1}{V}\left(\frac{\partial V}{\partial p}\right)_T$ seen in Fig. 1.1(b), are described by the exponents[1]

[1] To avoid confusion, the inverse range of interaction (Sec. 2.3) will from now on be denoted γ_r.

γ and γ', respectively. Above critical point, γ is defined along the critical isochor, while below, γ' is defined along the coexistence curve[2]. Thus

$$\kappa_T \sim \begin{cases} t^{-\gamma} & , \quad t > 0 \\ (-t)^{-\gamma'} & , \quad t < 0. \end{cases} \tag{3.4}$$

Similarly the specific heat exponents α and α' are defined by the relations

$$C_V \sim \begin{cases} t^{-\alpha} & , \quad t > 0 \\ (-t)^{-\alpha'} & , \quad t < 0 \end{cases} \tag{3.5}$$

along the critical isochor $\rho = 1/2$. Subcritically C_V is calculated as the mean value of the contributions from the symmetric branches of the coexistence curve in the lattice case[3]. The degree of flatness of the critical isotherm $T = T_c$, drawn in Fig. 1.1(b), is measured by an exponent δ, i. e.

$$p - p_c \sim |\Delta\rho|^{\delta} \mathrm{sgn}(\Delta\rho), \quad t = 0. \tag{3.6}$$

Finally the exponents ν, ν', and η refer to the behavior of the pair correlation function $h(r)$ in the critical region. The asymptotic behavior

$$\xi \sim \begin{cases} t^{-\nu} & , \quad t > 0 \\ (-t)^{-\nu'} & , \quad t < 0 \end{cases} \tag{3.7}$$

defines exponents ν and ν' for the correlation length (1.22) along the critical isochor and the coexistence curve, respectively, as before. At the critical point $T = T_c$ the correlations extend over all length scales, and the power-law decay of these correlations with respect to distance r, is given by η. In d dimensions

$$h(r) \sim \frac{\text{const}}{r^{d-2+\eta}}, \quad t = 0. \tag{3.8}$$

In case of the first-order result for the γ_r-expansion, Eqs. (2.54) and (2.55) shows that $\eta = 0$ and $\gamma = 2\nu = 1$.

[2]Both paths correspond to $H = 0$ (Fig. 1.2(b)) in the magnetic case.

[3]In the symmetric magnetic case $C_{M=0} = C_{H=0}(-M) = C_{H=0}(M)$. So definitions (3.4) and (3.5) both refer to the same situation with no external field or coupling, $H = 0$.

3.2 Classical fluctuations

Essentially all theories with an analytic equation of state give the same set of critical exponents. The mean-field theory, section 2.2, is an example of such a theory. The corresponding exponents are called classical. Averaging out the inhomogeneities in the occupation configurations $\{n\}$, leaves the deviation in chemical potential from coexistence $\Delta\mu$ an antisymmetric function of the spatially homogeneous order parameter $\Delta\rho$, Eqs. (2.16), (2.17), and (3.3). Equivalently the corresponding deviation in Helmholtz free energy $\Delta\mathcal{A}$, $\beta\Delta\mu = -2(\partial\Delta\mathcal{A}/\partial\Delta\rho)$, is symmetric in $\Delta\rho$. Thereby the qualitative influence of a fluctuating order parameter on a continuous phase transition, is neglected. Expanding $\Delta\mathcal{A}$ in even powers of $\Delta\rho$ yields the classical critical exponents $\alpha = \alpha' = 0$ (discontinuity), $\beta = 1/2$, $\gamma = \gamma' = 1$, and $\delta = 3$. Moreover, $\nu = \nu' = 1/2$ and $\eta = 0$ follow from Eqs. (2.29) and (2.30).

The phenomenological Landau theory [3] is based on constructing a free energy ΔF symmetric in the small order parameter $\Delta\rho$ near the critical point, taking the classical nature of the phase transition for granted. Minimization with respect to the order parameter gives the equilibrium state of the system. However, at the critical point, the stiffness against fluctuations in $\Delta\rho$, $\partial\Delta\mu/\partial\Delta\rho \sim \partial^2\Delta F/\partial\Delta\rho^2 \sim 1/\tilde{\Gamma}(0)$, determined by the fluctuations of long wavelength (Eq. (1.20)), disappears and makes the assumption of analyticity of ΔF in $\Delta\rho$ a suspect one. The Landau-Ginzburg theory represents a minimal extension of the classical theories, by allowing the order parameter to fluctuate. Landau free energy then becomes a functional, in which even powers of local densities $\Delta\rho(\boldsymbol{r})$ are integrated over space. Including the simplest possible free energy cost due to spatial inhomogeneities, we have [3]

$$\Delta F[\Delta\rho(\boldsymbol{r})] = \int_V \left\{ \frac{g}{2}[\nabla\Delta\rho(\boldsymbol{r})]^2 + \frac{r}{2}[\Delta\rho(\boldsymbol{r})]^2 + \frac{u}{4!}[\Delta\rho(\boldsymbol{r})]^4 + \cdots \right\} d\boldsymbol{r}, \quad (3.9)$$

for a finite lattice with an infinitesimal cell volume $v_0 = V/N$. g, c, and u are here positive constants while $r = ct$ to lowest order in the relative temperature deviation (3.2). The square gradient term immediately identifies the long-wavelength fluctuations as the energetically inexpensive and most important fluctuations. For the purpose of comparing the strengths of the different terms, it is convenient to measure the fluctuations $\Delta\rho(\boldsymbol{r})$ in units of $1/\sqrt{g}$ (Sec. 6.1. in [14]) by which $g \to 1$, $r \to r' = r/g$, and $u \to u' = u/g^2$ in (3.9). From a statistical mechanical point of view, the Landau-Ginzburg functional (3.9) can be regarded as an effective Hamiltonian for

these fluctuations. By prescribing the long-wavelength Fourier components of the configuration-dependent occupation numbers $\tilde{n}_{\boldsymbol{k}}(\{n\})$ to take the values $\tilde{\rho}_{\boldsymbol{k}}$ for all $\boldsymbol{k}$ with $|\boldsymbol{k}| < k_0$, they are singled out for careful treatment. Here k_0 is a cut-off parameter, small on the microscopic scale set by the lattice constant b, i. e., $k_0 b \ll 1$. For $T > T_c$ with $\Delta\mu = 0$, the spontaneous density difference or "magnetisation" vanishes, and $\Delta\rho(\boldsymbol{r})$ is itself the fluctuation $\delta\Delta\rho(\boldsymbol{r})$. To second order in the fluctuating quantities

$$H_{eff} = \frac{1}{2V}{\sum}'_{\boldsymbol{k}}(k^2 + r')\widetilde{\Delta\rho}_{-\boldsymbol{k}}\widetilde{\Delta\rho}_{\boldsymbol{k}}, \tag{3.10}$$

where the prime denotes summation over all $\boldsymbol{k}$ with $|\boldsymbol{k}| < k_0$. With this effective Hamiltonian, the long-wavelength correlation function $\Gamma^{\rho}(\boldsymbol{r}, \boldsymbol{r'}) = \langle\delta\Delta\rho(\boldsymbol{r})\delta\Delta\rho(\boldsymbol{r'})\rangle$ can be calculated:

$$\tilde{\Gamma}^{\rho}_{\boldsymbol{k},\boldsymbol{k'}} = V\delta_{\boldsymbol{k'},-\boldsymbol{k}}\tilde{\Gamma}^{\rho}_{\boldsymbol{k}} \tag{3.11}$$

with

$$\tilde{\Gamma}^{\rho}_{\boldsymbol{k}} = \frac{1}{r' + k^2}. \tag{3.12}$$

Thus the fluctuating modes are Gaussian and will behave independently of each other. This reproduces the classical result, Eqs. (2.29) and (2.30), with

$$\varepsilon^2 = r' = \frac{c}{g}t, \tag{3.13}$$

or, by identifying $\sqrt{g}$ being proportional to the range of interaction $nb \propto \gamma_r^{-1}$, Eq. (2.31). In order to have a sound Gaussian approximation, the relative strength of the second-order term $\int_V d\boldsymbol{r}\frac{r'}{2}[\Delta\rho(\boldsymbol{r})]^2$ has to be large compared to that of the neglected fourth order term $\int_V d\boldsymbol{r}\frac{u'}{4!}[\Delta\rho(\boldsymbol{r})]^4$ in Eq. (3.9). With spatial extent $\xi = 1/\varepsilon$, the integral over the spontaneous fluctuations yields that

$$\int_{r<\xi} d\boldsymbol{r}\langle\Delta\rho(0)\Delta\rho(\boldsymbol{r})\rangle \sim \tilde{\Gamma}^{\rho}_{k\sim\xi^{-1}} \sim \frac{1}{r'}, \tag{3.14}$$

must be considerable smaller than $\widehat{\Delta\rho}^2\xi^d$, where $\widehat{\Delta\rho}$ is the value of $\Delta\rho$ at which the two competing terms in (3.9) are equal:

$$\widehat{\Delta\rho}^2 = \frac{12r'}{u'} \tag{3.15}$$

This means that

$$\frac{1}{r'} \ll \frac{r'}{u'}(r')^{-d/2} \tag{3.16}$$

or

$$(r')^{(4-d)/2} \gg u'. \tag{3.17}$$

So in dimension $d \leq 3$, the *Ginzburg criterion* [15, 16] (3.17) delimits classical theories and fluctuations to a region not too close to criticality. I. e., the temperature region scales with the inverse range of interaction γ_r as

$$t \gg \frac{1}{c} u^{2/(4-d)} g^{d/(d-4)} = \text{const}\, \gamma_r^{2d/(4-d)}. \tag{3.18}$$

Similarily

$$\xi \ll u^{1/(d-4)} g^{2/(4-d)} = \text{const}\, \gamma_r^{-4/(4-d)}, \tag{3.19}$$

for the spatial extent $\xi = 1/\sqrt{r'}$ of the decoupled fluctuations.

Strictly speaking the Ginzburg criterion is only satisfied for long-range interactions $\gamma_r \ll 1$ in $d \leq 3$. For the sake of simplicity let us put const $= 1$ and $\gamma_r = 1$ in (3.18) to consider a short-range potential. With t defined by (3.2), $t = -1$ at $T = 0$, and according to (3.18) the whole two-phase region is obviously more or less "critical". I. e., in view of the γ_r-expansion, deviations from the mean-field equation of state are not negligible. And in some distance from the critical point, the effective critical behavior of such a system does not resemble the classical one ($\alpha = 0$, $\beta = 1/2$, etc.). However, at supercritical temperatures (3.2), the Ginzburg criterion (3.18) cannot unambiguously be utilized since $t \gg 1$ also for the "regular" high-temperature behavior of a short-range system. The reason for this is lack of scale; $t \to \infty$ when $T \to \infty$. A more natural definition of t should therefore be

$$t = \begin{cases} 1 - T_c/T & , \quad T > T_c \\ -(1 - T/T_c) & , \quad T < T_c \end{cases} \tag{3.20}$$

Close to the critical point $|t| \ll 1$, (3.2) and (3.20) are essentially equal.

Due to the configurational energy connected with the fluctuations (3.12) the specific heat diverges in accordance with

$$\alpha = \frac{4-d}{2}. \tag{3.21}$$

3.3 Relations among the critical exponents

3.3.1 Exact inequalities

The only rigorous relations between the critical exponents are a set of inequalities.

From the thermodynamic relation

$$C_H - C_M = T \left(\frac{\partial M}{\partial T}\right)_H^2 \left(\frac{\partial H}{\partial M}\right)_T \tag{3.22}$$

and the requirement of thermodynamic stability, $C_M \geq 0$, C_H has to be greater than or equal to the right hand side of Eq. (3.22). For subcritical temperatures $T < T_c$, and in the limit $H \to 0$, this implies

$$\alpha' + 2\beta + \gamma' \geq 2. \tag{3.23}$$

Here we have used the definitions (3.1), (3.4), and (3.5) of the critical exponents β, γ', and α', translated to magnetic quantities by Eqs. (1.9) and (1.11). Whenever C_H is dominant compared to C_M, the inequality (3.23) reduces to an equality. Another inequality based on pure thermodynamical arguments is

$$\alpha' + \beta(1 + \delta) \geq 2. \tag{3.24}$$

In addition a series of other inequalities appear when certain less fundamental assumptions are made [2].

3.3.2 Scaling laws

A natural generalization of the phenomenological Landau or classical theory, section 3.2, is due to Widom [17]. Rather than using the quasi-thermodynamic construction of Landau, he focused upon the *singular* part of the equilibrium free energy itself. By this, the exponents inequalities in the previous section turn into equalities, reducing the number of independent critical exponents to two. As a result, the equation of state in the critical region is a two-sided analytic function, expressed by scaled chemical potential and density. But the values of the two independent exponents are otherwise left unspecified.

In terms of reduced temperature t and chemical potential $\Delta\mu$, an arbitrary scaling factor λ, and constants a and b, Widom postulated that the singular part of the appropriate free energy obeys the homogeneity relation

$$F_s(\lambda^a t, \lambda^b \Delta\mu) = \lambda F_s(t, \Delta\mu) \tag{3.25}$$

close to the critical point $(t, \Delta\mu) = (0, 0)$. For our materially open system, F_s is the singular part of the grand canonical potential, $\Omega = F - \mu N$. Whence the number of particles $N = -(\partial\Omega/\partial\mu)_{V,T}$ and the specific heat in constant chemical potential is $C_\mu = -T(\partial^2\Omega/\partial T^2)_{V,\mu}$. By choosing the value $\lambda^a = 1/|t|$, one obtains

$$F_s(t, \Delta\mu) = |t|^{1/a} F_s(t/|t|, \Delta\mu/|t|^{b/a}) = |t|^{2-\alpha}\Phi_\pm(\Delta\mu/|t|^{b/a}), \tag{3.26}$$

since in zero external "field" (Eq. (3.5)) $C \sim \partial^2 F_s(t, 0)/\partial t^2 \sim |t|^{1/a-2}$. Thus we have

$$\alpha = \alpha' = 2 - 1/a. \tag{3.27}$$

Note that the first argument $t/|t|$ of F_s can only take the values ± 1 for $T \gtrless T_c$. Furthermore

$$\beta = 2 - \alpha - b/a \tag{3.28}$$

follows from a non-vanishing order parameter $\Delta\rho$ below the critical temperature:

$$\Delta\rho \sim \frac{\partial F_s}{\partial \Delta\mu} = |t|^{2-\alpha-b/a}\Phi'_\pm(\Delta\mu/|t|^{b/a}). \tag{3.29}$$

Similarly the isothermal compressibility in zero "field", $\Delta\mu = 0$,

$$\kappa_T = \frac{1}{\rho^2}\left(\frac{\partial\rho}{\partial\mu}\right)_T \sim \frac{\partial^2 F_s}{\partial\Delta\mu^2} = |t|^{2-\alpha-2b/a}\Phi''_\pm(0) \tag{3.30}$$

gives

$$\gamma = \gamma' = -2 + \alpha + 2b/a. \tag{3.31}$$

To extract the critical exponent δ, defined on the critical isotherm $t = 0$, one has to assume that $\Phi_\pm(x)$ has power-law behavior for large x. In order for $\Delta\rho$ to have a finite limit as $|t| \to 0$, one from Eq. (3.29) must have

$$\delta = \frac{b/a}{2 - \alpha - b/a}. \tag{3.32}$$

Eliminating b/a between (3.27), (3.28), (3.31), and (3.32), gives finally the scaling laws

$$\alpha + 2\beta + \gamma = 2 \tag{3.33}$$
$$\alpha + \beta(1+\delta) = 2, \tag{3.34}$$

reducing the number of independent critical exponents to two. We note that the classical exponents from section 3.2, obey the scaling laws.

If for instance β and δ are known, the equation of state (3.29) can be written

$$\frac{\Delta\rho}{|t|^\beta} = \Phi'_\pm\left(\frac{\Delta\mu}{|t|^{\beta\delta}}\right). \tag{3.35}$$

The density, $\Delta\rho(t, \Delta\mu)$, is in general a function of two variables. In the critical region, however, the scaled density difference $\Delta\rho/|t|^\beta$ can be represented by the two functions (3.35). They refer to each side of the critical temperature, $T \gtrless T_c$, and they depend on the scaled chemical potential $\Delta\mu/|t|^{\beta\delta}$ alone. Therefore different isotherms close to the critical point will fall onto two single universal curves, when properly scaled order parameters and respective conjugate thermodynamic variable are used when plotting. This is known as *data collapse*, and is experimentally demonstrated for five different fluids and a ferromagnet in Figs. 3.1 and 3.2, respectively.

In figure 3.1 Green *et al.* [18] have plotted a series of isotherms in a range of about $\pm 50\%$ of the critical densities and within 0.5% below to 3% above the critical temperatures. On each side of T_c, the nearest isotherms are as close as $|t| \simeq 10^{-5}$. To have the curves of the different fluids to coincide in the plot, dimensionless density $\Delta\rho$ (Eq. (3.3)) and chemical potential $\Delta\mu = [\mu(\rho, t) - \mu(\rho_c, t)]\rho_c/p_c$ are used in the scaled variables. With exponent values $\beta = 0.35$ and $\delta = 5$, the scaled isotherms fall somewhat scattered on two universal curves. In agreement with the scaling relation

$$\gamma = \beta(\delta - 1) \tag{3.36}$$

(which follows by subtracting (3.34) from (3.33)) and the values of β and δ used, Green *et al.* found $\gamma = \gamma' = 1.40$ to be not in conflict with the experimental data. While the value of β was taken from elsewhere, a separate analysis of isotherms close to the critical showed that $\delta = 5.06 \pm 0.06$.

The measurements of Kouvel and Comly [19] on the metallic ferromagnet Ni are plotted in Fig. 3.2 as the square of the scaled magnetisation,

m^2, versus the ratio h/m between the scaled magnetic field and the scaled magnetisation. From (1.9) and (1.11), with magnetisation m in (1.11) replaced by σ used by Kouvel and Comly, $m = \sigma/|t|^{\beta}$ and $h = H/|t|^{\beta\delta}$. Hence $h/m = (H/\sigma)/|t|^{\gamma}$, Eq. (3.36). The isotherms approximately cover a range of $\pm 35\%$ of the saturation magnetic moment (at zero temperature) and a temperature range within 2% above and below the critical temperature. But in this plot $|t| \simeq 10^{-2.4}$ for the isotherms nearest to T_c, shrinking the inaccessible temperature range on both sides ($T \gtrless T_c$) with about two and a half decade in comparison to Fig. (3.1) of Green *et al.* Kouvel and Comly found experimentally the critical exponents $\beta = 0.378 \pm 0.004$, $\gamma = 1.34 \pm 0.01$, and $\delta = 4.58 \pm 0.05$ for Ni. These values are consistent with (3.36).

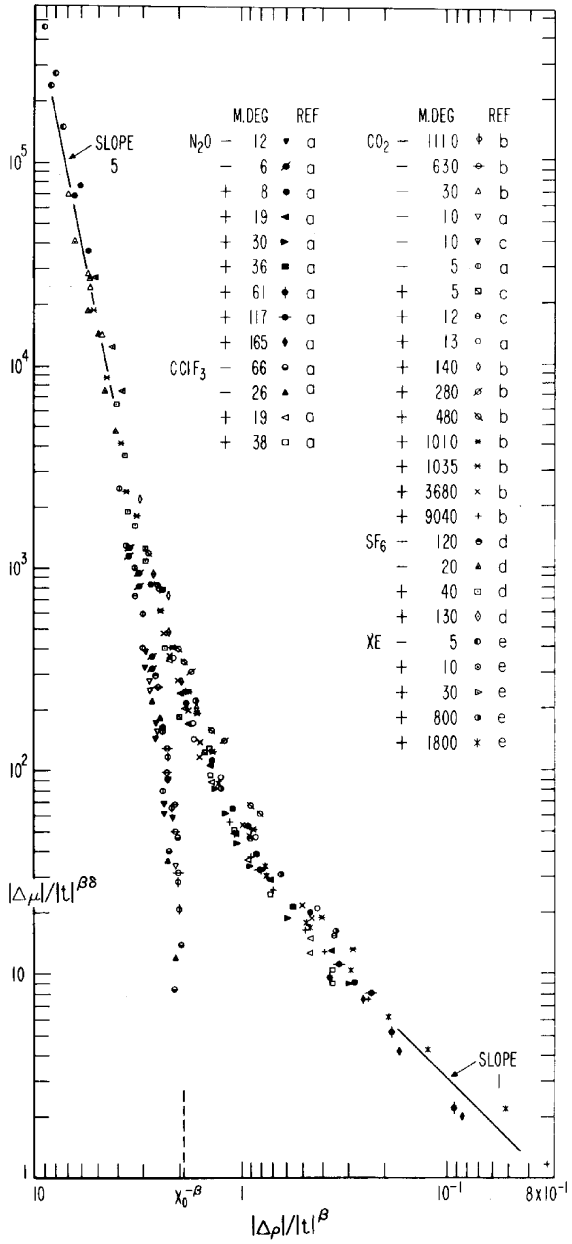

Figure 3.1: Scaled chemical potential $\Delta\mu/|t|^{\beta\delta}$ versus scaled density $\Delta\rho/|t|^{\beta}$ in the critcal region of several fluids, using $\beta = 0.35$ and $\delta = 5$. After Green *et al.* [18].

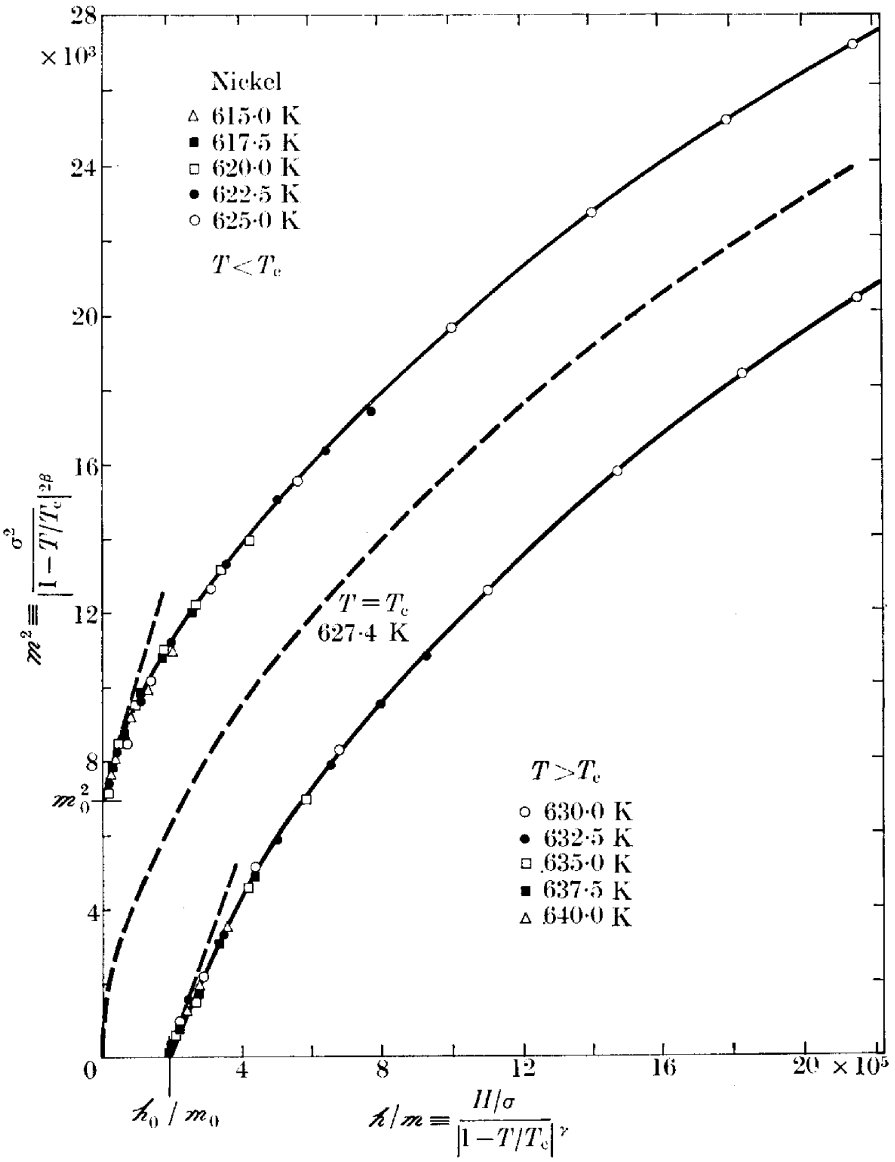

Figure 3.2: Plot of $m^2 = \sigma^2/|t|^{2\beta}$ versus $h/m = (H/\sigma)/|t|^{\gamma}$ in the critical region for the ferromagnet nickel, using $\beta = 0.378$ and $\gamma = 1.34$. m (emu/g) is the scaled magnetization and h (Oe) is the scaled magnetic field. After Kouvel and Comly [19].

Chapter 4

SCOZA

As demonstrated in subsection 2.3.2, in the critical region there is no obvious way to improve the equation of state beyond the renormalized γ_r-ordering or MSA (section 2.4). Høye and Stell proposed an *a priori* thermodynamically self-consistent theory building directly upon the MSA; the self-consistent Ornstein-Zernike approximation (SCOZA) [20]. With a pair potential composed of a hard core and a tail of Yukawa form, they derived equations necessary for solving the self-consistency problem for continuum fluids. Moreover, preliminary numerical studies of a simplified version for the 3-dimensional lattice gas shows supercritical behavior that mimics fairly well the expected exact critical behavior.

4.1 From MSA to SCOZA

In the simple form used here, SCOZA builds on the MSA-like closure scheme

$$\begin{aligned} h(r) &= -1 & r < R_0 \\ c(r) &= -\beta_e(\rho,\beta)w(r) & r > R_0 \end{aligned} \tag{4.1}$$

for the Ornstein-Zernike equation. With pair-potential tail $w(r)$ (compare Eq. (2.32)) outside the hard core, $w(r < R_0) = 0$, and direct pair correlation function $c_0(r)$ inside the core chosen in such a way that the exact core condition is fulfilled ($c_0(r > R_0) = 0$), Eq. (4.1) is equivalent to

$$c(r) = c_0(r) - \beta_e(\rho,\beta)w(r). \tag{4.2}$$

By choosing $\beta_e(\rho,\beta) \equiv \beta$ (4.2) embodies the mean-spherical approximation (2.75). More generally, however, the *effective* inverse temperature $\beta_e(\rho,\beta)$ can be a function of density ρ and inverse temperature β. This degree of freedom enables us to demand self-consistency between two independent routes for obtaining the equation of state. Both the inverse reduced compressibility $(\partial\beta p/\partial\rho)_T$ and the internal energy ρu, Eqs. (1.21) and (1.16), can be expressed in terms of the same pair correlation function $h(r)$. Using the Ornstein-Zernike equation (1.23), $h(r)$ is eliminated in favour of $c(r)$ in which β_e occurs more directly, Eq. (4.2). Thus the thermodynamic relation

$$\frac{\partial}{\partial\beta}\left(\frac{\partial\beta p}{\partial\rho}\right) = \rho\frac{\partial^2}{\partial\rho^2}\left(\rho u\right) \tag{4.3}$$

provides us with a closed partial differential equation for the adjustable "parameter" $\beta_e(\rho,\beta)$ whose solution will give the same thermodynamics via either the compressibility or energy routes. Together with the Ornstein-Zernike form (4.2), this is called SCOZA.

With the SCOZA approach one expects improvements compared to the MSA itself or, in the lattice case, the renormalized γ_r-ordering. This is easily seen from (4.3), which, with $\rho u = -\partial\mathcal{A}/\partial\beta$ ($\mathcal{A}$ given by (2.43)) and integration with respect to β, reduces to the first order result (2.57) for the compressibility. Thus the crucial term $-\frac{1}{2}F_0''K(0)$ incorporated via (2.62), will to leading order in γ_r correctly determine T_c, Eq. (2.66). In addition, the second term $-\frac{1}{2}F_0'K(0)'$ of (2.62) prevents SCOZA from developing first order "irregular" isotherms of the type described at the end of subsection 2.3.2. So in view of the γ_r-ordering, SCOZA gives higher order corrections to the thermodynamics. And to each order this is done self-consistently, e. g. all mismatches in the location of the spinodal, resulting from using the two different routes, disappear and all "irregularities" in the isotherms are "smoothened" out. Therefore SCOZA gives a well-defined thermodynamic description in the critical region superior to the one given by the MSA.

4.2 The basic PDE for the lattice gas

4.2.1 Deduction

For a lattice gas, the Ornstein-Zernike form (4.2) simplifies since the on-site direct correlation function is a constant c_0. Thus

$$\tilde{c}(\boldsymbol{k}) = c_0 + \beta_e \tilde{\psi}(\boldsymbol{k}), \tag{4.4}$$

where

$$\psi(\boldsymbol{r}) \equiv \frac{w(\boldsymbol{r})}{\tilde{w}(0)} \tag{4.5}$$

is positive, normalized to one ($\tilde{\psi}(0) = 1$), and has a vanishing on-site value ($\psi(0) = 0$, Eq. (4.2)). Here we have included the positive interaction strength $-\tilde{w}(0)$ as a multiplicative constant in β_e, and in the following energies and temperatures are measured in units of $-\tilde{w}(0)$ and $-\tilde{w}(0)/k_B$, respectively[1]. Together with the hard-core condition ($h(0) = -1$) and the Fourier transformed Ornstein-Zernike equation (1.25), (4.4) gives c_0's dependence on ρ and β, and provides us with a relation between c_0 and β_e :

$$\begin{aligned} 1-\rho &= \frac{1}{(2\pi)^d}\int [1+\rho\tilde{h}(\boldsymbol{k})]\, d\boldsymbol{k} = \frac{1}{(2\pi)^d}\int \frac{d\boldsymbol{k}}{1-\rho\tilde{c}(\boldsymbol{k})} \\ &= \frac{1}{1-\rho c_0} P(z), \end{aligned} \tag{4.6}$$

where the integral

$$P(z) = \frac{1}{(2\pi)^d}\int \frac{d\boldsymbol{k}}{1-z\tilde{\psi}(\boldsymbol{k})}, \tag{4.7}$$

for an infinite regular d-dimensional lattice, is evaluated over the first Brillouin zone and is a function of the variable

$$z = \frac{\rho\beta_e}{1-\rho c_0}. \tag{4.8}$$

We are now in position of expressing the partial differential equation (PDE) (4.3) in terms of the single state-dependent quantity $z(\rho, \beta)$. From Eq. (1.26)

[1] In Papers I and II energies are measured in units of the nearest neighbor interaction strength $w = -\tilde{w}(0)/q$. To compare with those used here, inverse temperature β and energies u in Papers I and II should be replaced by β/q and qu (q is the coordination number), respectively.

the inverse reduced compressibility equals

$$\frac{\partial\beta p}{\partial\rho} = 1 - \rho\tilde{c}(0) = (1-\rho c_0)(1-z) = \frac{(1-z)P(z)}{1-\rho}. \tag{4.9}$$

Next, Eqs. (1.16) and (1.15) give the excess internal energy per unit volume,

$$\rho u = -\frac{1}{2}\rho^2 \sum_{\boldsymbol{r}} \psi(\boldsymbol{r}) g(\boldsymbol{r}) = \rho u_0 + \rho u_1, \tag{4.10}$$

as the sum of the mean-field contribution ($-\partial\mathcal{A}_{(0)}/\partial\beta$ with $a = \frac{1}{2}[-\tilde{w}(0)]$, Eq. (2.37))

$$\rho u_0 = -\frac{1}{2}\rho^2, \tag{4.11}$$

plus the amount due to correlations, i. e.

$$\begin{aligned} \rho u_1 &= -\frac{1}{2}\rho^2 \sum_{\boldsymbol{r}} \psi(\boldsymbol{r}) h(\boldsymbol{r}) = -\frac{1}{2}\rho \sum_{\boldsymbol{r}} \psi(\boldsymbol{r})[\delta(\boldsymbol{r}) + \rho h(\boldsymbol{r})] \\ &= -\frac{1}{2}\rho \frac{1}{(2\pi)^d} \int \frac{\tilde{\psi}(\boldsymbol{k})}{1-\rho\tilde{c}(\boldsymbol{k})}\, d\boldsymbol{k} \\ &= -\frac{1}{2}\rho(1-\rho)\frac{P(z)-1}{zP(z)}. \end{aligned} \tag{4.12}$$

Inserting (4.9), (4.10), (4.11), and (4.12) into (4.3), the SCOZA PDE for the unknown function $z(\rho,\beta)$ is

$$\frac{\partial}{\partial\beta}\left[(1-z)P(z)\right] = -\rho(1-\rho)\left\{1 + \frac{\partial^2}{\partial\rho^2}\left[\frac{1}{2}\rho(1-\rho)\frac{P(z)-1}{zP(z)}\right]\right\}. \tag{4.13}$$

4.2.2 Boundary conditions

Via the structure factor (1.19) z is related to the correlation length ξ, Eq. (1.22). On a cubic lattice, Fourier transforming the potential gives the isotropic result

$$\tilde{\psi}(\boldsymbol{k}) = 1 + \frac{1}{2}\tilde{\psi}''(0)k^2 + \mathcal{O}(k^4) \tag{4.14}$$

with a negative[2] coefficient

$$\tilde{\psi}''(0) \propto -\sum_{\boldsymbol{r}} r^2 \psi(\boldsymbol{r}). \tag{4.15}$$

[2] assuming a predominantly ferromagnetic interaction $\psi(\boldsymbol{r})$.

Inserting for $\tilde{\psi}(k)$, the Ornstein-Zernike form (4.4) implies (via (1.25) and (1.19)) that the correlation length is equal to the range of the potential multiplied by the density and temperature dependent factor $\sqrt{z/(1-z)}$. I. e.,

$$\xi^2 = \frac{1}{2}[-\tilde{\psi}''(0)]\frac{z}{1-z}. \tag{4.16}$$

In the physically acceptable region $0 \leq z \leq 1$. Eqs. (4.6) and (4.8) combine to

$$zP(z) = \rho(1-\rho)\beta_e. \tag{4.17}$$

So $z = 0$ corresponds to the high temperature limit $\beta = 0$ and the density boundaries $\rho = 0$ and 1, where ξ vanishes. As z, for a possible finite value of β (via $\beta_e(\rho, \beta)$), grows toward 1 from below, ξ and the compressibility will diverge. That is, the inverse compressibility given by

$$\begin{aligned}(1-\rho)\frac{\partial\beta p}{\partial\rho} &= (1-z)P(z) = \frac{1}{(2\pi)^d}\int \frac{d\boldsymbol{k}}{1+\frac{z}{1-z}[1-\tilde{\psi}(\boldsymbol{k})]} \\ &\approx I(\xi),\ \ \xi \to \infty \end{aligned} \tag{4.18}$$

vanishes, which is seen from the approximative integral

$$I(\xi) \equiv \frac{1}{(2\pi)^d}\int \frac{d\boldsymbol{k}}{1+\xi^2 k^2}. \tag{4.19}$$

Since the integrand is isotropic, the integration is performed spherically symmetric over a finite d-dimensional sphere. Depending on the magnitude of the cut-off radius (k_0), the integrand of $I(\xi)$ does not necessarily approximate the exact integrand of $(1-z)P(z)$ very well over the whole range of integration ($k < k_0$). But for small k, i. e. $\xi^2 k^2 \ll 1$, the correct form for the integrand is kept. And for large ξ, i. e. $\xi k_0 \gg 1$, this region gives the dominant contribution to the integral. The asymptotic result for $\xi \to \infty$ is

$$I(\xi) \sim \begin{cases} \frac{1}{\xi^2}(1-\frac{A}{\xi}) \sim \frac{1}{\xi^2} & , \quad d=3 \\ \frac{1}{\xi^2}\ln\xi & , \quad d=2 \\ \frac{1}{\xi} & , \quad d=1 \end{cases} \tag{4.20}$$

with $A = \pi/2k_0$. But in one and two dimensions

$$zP(z) \approx \frac{2}{[-\tilde{\psi}''(0)]}\xi^2 I(\xi),\ \ \xi \to \infty \tag{4.21}$$

do not converge. In one dimension $T_c = 0$, i. e. β_c diverges when $\beta_e \sim \xi$ does, Eq. (4.17). So in view of the well-known phase transition for the two-dimensional Ising model, we have the strange situation with a diverging (although very slowly) $\beta_e \sim \ln \xi$. Hence, we are not guaranteed to get a non-zero critical temperature below three dimensions.

4.3 Calculations for the three-dimensional case

4.3.1 A simple asymptotic approximation

SCOZA gives corrections to MSA which are small outside the narrow critical region. Therefore we first concentrate on the asymptotic behavior close to the critical point to capture the essential features exhibited by SCOZA. From Eqs. (4.21) and (4.20)

$$P(z) \sim 1 - A/\xi \tag{4.22}$$

is finite at the divergence of ξ, and via (4.16)

$$1 - z \sim 1/\xi^2. \tag{4.23}$$

Hence $P(z)$ is no longer tied to the detailed interaction structure $\tilde{\psi}(\boldsymbol{k})$, Eq. (4.7), other than through multiplicative constants in front of equalities (4.22) and (4.23). This eliminates $P(z)$ and z in favour of the correlation length ξ in the PDE (4.13). With such a contracted asymptotic description Høye and Stell [21] expects the precise form of the function $P(z)$ to be of minor importance.

$P(z)$ and $1-z$ depend crucially on the range of interaction γ_r^{-1}, Eq. (2.33) with $w(\boldsymbol{r}) = w_{\gamma_r}(\boldsymbol{r})$. In the limit $\gamma_r \to 0$ the range of the potential extends over all length scales and the discrete Fourier transform of (4.5) equals the continuous transform

$$\tilde{\psi}(\boldsymbol{k}) = \frac{\tilde{\phi}(\boldsymbol{K})}{\tilde{\phi}(0)}, \tag{4.24}$$

a function of $\boldsymbol{K} = \boldsymbol{k}/\gamma_r$. Repeating the asymptotic analysis of the last section one gets

$$\begin{aligned} 1 - z\tilde{\psi}(\boldsymbol{k}) &\approx (1-z)(1+\xi_0^2 K^2), \quad K \to 0 \\ &= \frac{1}{2}\left[-\frac{\tilde{\phi}''(0)}{\tilde{\phi}(0)}\right] z(\epsilon_0^2 + K^2) \end{aligned} \tag{4.25}$$

for the denominator of $P(z)$, Eq. (4.7). Here we have included the γ_r-dependence of the correlation length (4.16) into K^2:

$$\xi^2 = \xi_0^2/\gamma_r^2 \tag{4.26}$$

where

$$\xi_0^2 = \frac{1}{2}\left[-\frac{\tilde{\phi}''(0)}{\tilde{\phi}(0)}\right]\frac{z}{1-z} \equiv \frac{1}{\epsilon_0^2}. \tag{4.27}$$

The exact integrand of $P(z)$ falls off towards a constant value 1 as K increases. I. e., when $\xi_0^2 K^2 \gg 1$. Therefore, as $z \to 1$, the dominant contribution to $P(1) - P(z)$ will come from small values of K, $\xi_0^2 K^2 \lesssim 1$, and the integration can be performed over the whole $\boldsymbol{K}$-space. Treating the important region correctly and having a negligible tail contribution, Eq. (4.25) yields for $\epsilon_0 \to 0$ the asymptotic result

$$\begin{aligned} P(1) - P(z) &\approx 2\left[-\frac{\tilde{\phi}(0)}{\tilde{\phi}''(0)}\right]\frac{4\pi\gamma_r^3}{(2\pi)^3}\int_0^\infty \left(\frac{1}{K^2} - \frac{1}{\epsilon_0^2 + K^2}\right) K^2 dK \\ &\propto \gamma_r^3 \epsilon_0 \int_0^\infty \frac{dx}{1+x^2} \quad \propto \quad \gamma_r^3 \epsilon_0. \end{aligned} \tag{4.28}$$

Finally, subtraction of the limiting level for the integrand of $P(1)$ again permits an infinite integration

$$\begin{aligned} P(1) - 1 &\approx \frac{1}{(2\pi)^3}\int_0^\infty \frac{\tilde{\psi}(\boldsymbol{k})}{1 - \tilde{\psi}(\boldsymbol{k})} 4\pi k^2 dk \\ &= \frac{\gamma_r^3}{(2\pi)^3}\int_0^\infty \frac{\tilde{\phi}(\boldsymbol{K})/\tilde{\phi}(0)}{1 - \tilde{\phi}(\boldsymbol{K})/\tilde{\phi}(0)} 4\pi K^2 dK \quad \propto \quad \gamma_r^3. \end{aligned} \tag{4.29}$$

This gives us the asymptotic expression

$$P(z) = 1 + B\gamma_r^3(1 - C\epsilon_0) \tag{4.30}$$

where B and C are positive constants.

Instead of performing the announced elimination we actually eliminate the internal energy function (Eq. (4.12))

$$F(z) = \frac{1}{2}\frac{P(z) - 1}{zP(z)}, \tag{4.31}$$

sitting on the right hand side of the PDE (4.13), in favour of its left hand side; the inverse compressibility function (Eq. (4.9))

$$\varepsilon^2 \equiv (1-\rho)\frac{\partial \beta p}{\partial \rho} = (1-z)P(z). \tag{4.32}$$

It is readily seen from Eqs. (4.27) and (4.30) that asymptotically $\epsilon_0 \to 0$, $\varepsilon \sim \epsilon_0 \sim \sqrt{1-z}$. Thus, with another constant D, we proceed with

$$P(z) = 1 + \gamma_r^3(1 - D\varepsilon). \tag{4.33}$$

The precise value of constant B in (4.30) is irrelevant as it will only rescale γ_r and is therefore put equal to one. As argued in the beginning of this subsection we now approximate $F(z)$ over the whole region $0 \leq z \leq 1$ by using the asymptotic expression (4.33). To lowest order in γ_r,

$$F(z) = \frac{1}{2}\gamma_r^3(1-\varepsilon) \tag{4.34}$$

will do, since the internal energy due to correlations, $\rho u_1 \sim F(z)$, vanishes exactly at $z = 0$ (i. e. by putting $D = 1$ in (4.33)). In the present approximation (4.34) the SCOZA PDE (4.13) for the unknown function $\varepsilon(\rho, \beta)$ reads

$$\frac{\partial \varepsilon^2}{\partial \beta} = -\rho(1-\rho)\left\{1 + \frac{1}{2}\gamma_r^3 \frac{\partial^2}{\partial \rho^2}\left[\rho(1-\rho)(1-\varepsilon)\right]\right\}. \tag{4.35}$$

From (4.32) $0 \leq \varepsilon \leq 1$, with boundary values $\varepsilon = 1$ at $\beta = 0$, $\rho = 0$, and $\rho = 1$, and $\varepsilon = 0$ along the spinodal curve. In addition (4.35) immediately incorporates the range of interaction γ_r^{-1}, the effect of which upon ε and thus upon the critical properties we have studied.

It is clear that SCOZA does not scale in agreement with the scaling laws of subsection 3.3.2. The asymptotic behavior of the compressibility and the internal energy close to the critical point, given by Eqs. (4.32) and (4.34), implies that $\varepsilon \sim t^{\gamma/2} \sim t^{1-\alpha}$ as $t \to 0^+$. This follows from the definitions of the critical exponents γ and α on the critical isochor (Eqs. (3.4) and (3.5)) where the mean-field internal energy (4.11) does not contribute to the specific heat above T_c. I. e.

$$\gamma = 2(1-\alpha), \tag{4.36}$$

which is in conflict with relations (3.33) and (3.34).

4.3.2 The MSA solution

In view of the γ_r-ordering it is now of interest to establish the MSA solution and to consider its critical properties using the procedure in the previous subsection.

With $\beta_e(\rho,\beta)=\beta$, Eqs. (4.31), (4.32), and (4.34) give the solution

$$\varepsilon=-\frac{1}{2}\gamma_r^3 x+\sqrt{\left(\frac{1}{2}\gamma_r^3 x\right)^2-(1-\gamma_r^3)x+1}, \tag{4.37}$$

where from (4.17)

$$x=\rho(1-\rho)\beta. \tag{4.38}$$

The critical temperature

$$T_c=\frac{1}{4}(1-\gamma_r^3), \tag{4.39}$$

given by $\varepsilon=0$, incorporates the first order correction to the mean-field result (2.20). By use of the scaled temperature deviation

$$t=\frac{T-T_c}{T} \tag{4.40}$$

instead of (3.2), t and $(\Delta\rho)^2$ (Eq. (3.3)) will appear in a symmetric way in the variable

$$\Delta x=\frac{x_c-x}{x_c}=1-[1-(\Delta\rho)^2](1-t)=\begin{cases} t & , \quad \Delta\rho=0 \\ (\Delta\rho)^2 & , \quad t=0 \end{cases}. \tag{4.41}$$

So the solution (4.37) is the same function of $\Delta x=t$ $(t>0)$ along the critical isochor as of $\Delta x=(\Delta\rho)^2$ along the critical isotherm. To lowest order in γ_r^3 (4.37) is the function

$$\bar{\varepsilon}=\frac{1}{2}\left(\sqrt{1+4\bar{\Delta x}}-1\right), \tag{4.42}$$

given in terms of scaled quantities

$$\bar{\varepsilon}=\varepsilon/\gamma_r^3 \tag{4.43}$$

and

$$\bar{\Delta x}=\Delta x/(\gamma_r^3)^2. \tag{4.44}$$

Close to the critical point $(t, (\Delta\rho)^2 \ll 1)$ $\bar{\Delta x} = [t + (\Delta\rho)^2]/(\gamma_r^3)^2 \equiv \bar{t} + (\bar{\Delta\rho})^2$ to lowest order in γ_r. The solution (4.42) has a qualitatively different behavior for large and small $\bar{\Delta x}$:

$$\bar{\varepsilon} = \begin{cases} \sqrt{\bar{\Delta x}}\left(1 - \frac{1}{2}\frac{1}{\sqrt{\bar{\Delta x}}} + \cdots\right), & \bar{\Delta x} \gg 1 \\ \bar{\Delta x}\left(1 - \bar{\Delta x} + \cdots\right), & \bar{\Delta x} \ll 1 \end{cases} \tag{4.45}$$

Hence the MSA critical exponents γ and δ, given by the inverse compressibility ($\sim \varepsilon^2$) along the critical isochor ($\Delta x = t$) and the critical isotherm ($\Delta x = (\Delta\rho)^2$), respectively, take the values 2 and 5. Outside the critical region ($\bar{\Delta x} \gg 1$) the mean-field approximation $\varepsilon^2 = \Delta x$ (Eqs. (2.23) and (2.24)) is reproduced. In this region apparent or "effective" exponents $\gamma = 1$ and $\delta = 3$ is observed. Indeed this behavior is in agreement with the Ginzburg criterion (3.18) that the temperature region with classical fluctuations is limited to the region $t \gg (\gamma_r^3)^2$.

Effective critical exponents we define (although not uniquely) by the logarithmic derivative of the quantity in question. Here we will use $\gamma = \partial \ln \varepsilon^2 / \partial \ln t$ and $\delta = 1 + \partial \ln \varepsilon^2 / \partial \ln \Delta\rho$, which relate directly to the solution (4.37).In figure 4.1 the function $f(\Delta x) = d \ln \varepsilon / d \ln \Delta x$, capturing values of γ_r^3 up to 0.34 (see the next subsection), is plotted versus $\log_{10} \bar{\Delta x}$. Thus the effective exponents γ and δ are given by $2f(t)$ and $1+4f[(\Delta\rho)^2]$, respectively. When $\gamma_r^3 \to 0$ the curves approach the asymptotic solution given by (4.42). (See the dashed curve.) The "crossover" situation from mean-field to critical MSA behavior, described by (4.45), is clearly seen. With larger values of γ_r^3 no clear mean-field region is seen.

By (4.36) the effective exponent α is given by $\alpha = 1 - \gamma/2 = 1 - f(t)$. Hence $\alpha = 0$ at the critical point. But outside the critical region for small γ_r^3 the effective α takes the Gaussian value 1/2, Eq. (3.21), instead of the classical value 0. The reason is that the mean-field internal energy (4.11) does not contribute to the specific heat above T_c. I. e.,

$$\rho u = -\frac{1}{8}(1 + \gamma_r^3) + \frac{1}{8}(\gamma_r^3)^2 \bar{\varepsilon}, \tag{4.46}$$

along the critical isochor $\rho = 1/2$ (as follows from Eqs. (4.10)–(4.12), (4.31), (4.34), and (4.43)). Therefore

$$C_V = \frac{\partial(\rho u)}{\partial T} = \frac{1}{2}\frac{[1 - (\gamma_r^3)^2 \bar{t}\,]^2}{1 - \gamma_r^3}\frac{\partial \bar{\varepsilon}}{\partial \bar{t}} \simeq \frac{1}{2\sqrt{1 + 4\bar{t}}} \simeq \frac{1}{4\sqrt{\bar{t}}}, \quad \bar{t} \gg 1, \tag{4.47}$$

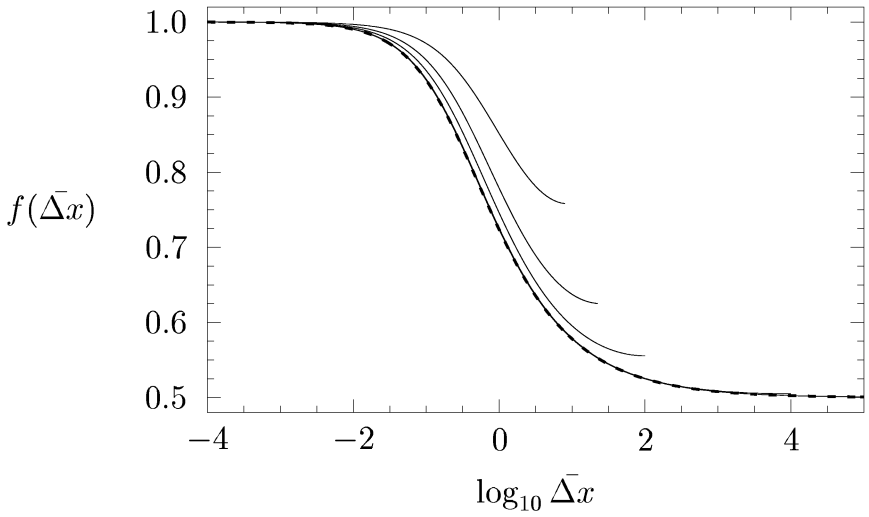

Figure 4.1: The effective exponent function $f(\bar{\Delta}x) = d\ln\bar{\varepsilon}/d\ln\bar{\Delta}x$ plotted versus $\log_{10}\bar{\Delta}x$. From right to left the different curves correspond to γ_r^3 values 0.34, 0.2, 10^{-1}, 10^{-2}, and 10^{-3}, respectively. The dashed graph is the asymptote in the limit $\gamma_r \to 0$. The supercritical effective indices are given by $\alpha = 1 - f(\bar{t})$ and $\gamma = 2f(\bar{t})$ along the critical isochor $\bar{\Delta}x = \bar{t}$, and $\delta = 1 + 4f[(\bar{\Delta}\rho)^2]$ along the critical isotherm $\bar{\Delta}x = (\bar{\Delta}\rho)^2$.

for the specific heat per cell (or unit volume) to zeroth order in γ_r^3, Eq. (4.42). At the critical point $\bar{t} = 0$ the specific heat reaches the maximal value $1/[2(1-\gamma_r^3)]$ corresponding to $\alpha = 0$. And $\rho u_c = -\frac{1}{8}(1+\gamma_r^3)$ is the same as for the SCOZA.

For $t > c(\gamma_r^3)^2$ (c a constant) we expect the MSA behavior to approximate the exact result well. But when $t \lesssim c(\gamma_r^3)^2$ the MSA will be too inconsistent and modifications from higher order terms ($i > 1$ in Eq. (2.36)) become important. The irregular thermodynamic behavior caused by these inconsistencies is clearly seen in figure 4.2. Here the equation of state, represented by chemical potential isotherms, is calculated via the internal energy. For the MSA in the lattice case one generally has $F = F(x)$ (Eqs. (4.31) and (4.38)) and

$$\beta\Delta\mu = \beta\mu^{hc} + \beta\mu_0\,[1 - 2F(x)]\,, \tag{4.48}$$

where $\beta\mu_0 = -\frac{1}{2}\beta\Delta\rho$ is the mean-field term. Inserting for the solution (4.42)

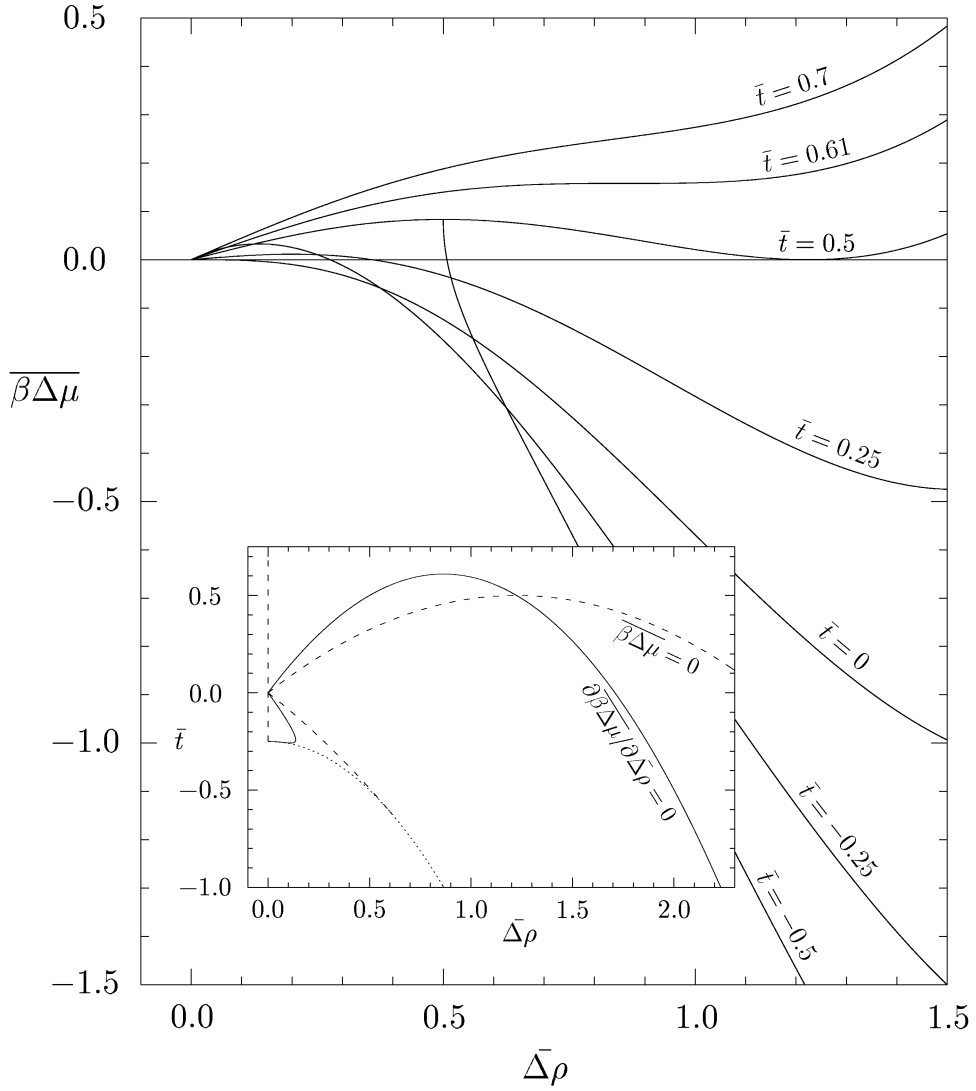

Figure 4.2: Isotherms for the chemical potential $\overline{\beta\Delta\mu}$ plotted as function of density $\bar{\Delta}\rho$, close to the critical temperature $\bar{t} = 0$ (Eq. (4.49)). The inset shows the locus of the zeroes of $\overline{\beta\Delta\mu}$ (dashed lines) and $\partial\overline{\beta\Delta\mu}/\partial\bar{\Delta}\rho$ (solid lines), respectively. The dotted line bounds the region $\bar{t} < -1/4 - \bar{\Delta}\rho^2$ where $\overline{\beta\Delta\mu}$ is complex.

via (4.34) gives the asymptotic result

$$\begin{aligned}\overline{\beta\Delta\mu} &= 2\bar{\Delta}\rho\left[\bar{t}+\frac{1}{3}(\bar{\Delta}\rho)^2-\bar{\varepsilon}\right]\\ &= \bar{\Delta}\rho\left[1+2\bar{t}+\frac{2}{3}(\bar{\Delta}\rho)^2-\sqrt{1+4\bar{t}+4(\bar{\Delta}\rho)^2}\right],\end{aligned}\qquad(4.49)$$

for the scaled chemical potential $\overline{\beta\Delta\mu}=\beta\Delta\mu/(\gamma_r^3)^3$ ($\partial(\beta\Delta\mu)\simeq 2\varepsilon^2\partial\Delta\rho = 2(\gamma_r^3)^3\bar{\varepsilon}^2\partial\bar{\Delta}\rho$, $(\Delta\rho)^2\ll 1$) in the limit $\gamma_r\to 0$. With respect to the inverse compressibility $\bar{\varepsilon}^2=\frac{1}{2}\partial\overline{\beta\Delta\mu}/\partial\bar{\Delta}\rho$, (4.49) is identical to (4.42) along the critical isochor $\bar{\Delta}\rho=0$. But along the critical isotherm $\bar{t}=0$, the consistency with the compressibility route (4.45) only holds outside the critical region to leading order in $\bar{\Delta}\rho$. I.e., $\overline{\beta\Delta\mu}=\frac{2}{3}\bar{\Delta}\rho^3-2\bar{\Delta}\rho^2+\cdots$ or $\bar{\varepsilon}^2=\bar{\Delta}\rho^2-2\bar{\Delta}\rho+\cdots$ when $|\bar{\Delta}\rho|\gg 1$. Inside the critical region, $|\bar{\Delta}\rho|\ll 1$, $\overline{\beta\Delta\mu}=-\frac{4}{3}\bar{\Delta}\rho^3+2\bar{\Delta}\rho^5+\cdots$ in agreement with Høye's description of the "irregular" critical isotherm (Sec. 2.3.2). Furthermore the nontrivial ($\bar{\Delta}\rho\neq 0$) solution for $\overline{\beta\Delta\mu}=0$ splits up in two solutions, instead of giving a regular subcritical solution of the type (3.1). I. e., with $\bar{\Delta}\rho>0$, $\bar{t}=\frac{1}{3}(\pm\sqrt{6}\bar{\Delta}\rho-\bar{\Delta}\rho^2)$ for $\bar{t}\leq 1/2$ and $0\geq\bar{t}\geq -5/8$, respectively ($\pm$). See the inset in Fig. 4.2 where also the solution for $\partial\overline{\beta\Delta\mu}/\partial\bar{\Delta}\rho=0$ is drawn. Above the critical temperature these cross-sections explain the extra "loop" for the isotherms in the main plot. The onset of this irregular behavior occurs at $\bar{t}\approx 0.61$ where the tangent becomes horisontal at $\bar{\Delta}\rho\approx 0.86$.

Alternatively one may obtain the chemical potential by integrating the compressibilty with respect to the density. Of course there will be no "irregularities" at supercritical temperatures ($\varepsilon^2>0$). But it is impossible to match the high and low density branches for the isotherms without violating the high and low density behavior. As checked numerically this effect grows rapidly close to the critical point. So with respect to thermodynamic consistency the situation is even worse for the compressibility route.

Sufficiently below the critical temperature the energy-route (4.49) yields a well-defined two-phase region. To leading order $-\bar{t}\gg 1$, corrections due to correlations (the $\bar{\varepsilon}$ term) do not contribute to the (mean-field) coexistence and spinodal curves. I. e., $(\bar{\Delta}\rho)^2=-3\bar{t}$ ($\overline{\beta\Delta\mu}=0$) and $(\bar{\Delta}\rho)^2=-\bar{t}$ ($\partial\overline{\beta\Delta\mu}/\partial\bar{\Delta}\rho=0$), respectively. Including the corrections due to a finite range of interaction leads to mean-field/Gaussian effective critical properties analogous to the supercritical ones. To lowest order this is accomplished by simply using the mean-field approximation $\bar{\varepsilon}^2=\bar{\Delta}x=\bar{t}+(\bar{\Delta}\rho)^2=-2\bar{t}$ or

$\frac{2}{3}(\bar{\Delta}\rho)^2$. From the full form (4.49)

$$-2\bar{t} = \frac{2}{3}\bar{\Delta}\rho^2 - 2\left(\frac{2}{3}\bar{\Delta}\rho^2\right)^{1/2} \tag{4.50}$$

gives the locus for $\overline{\beta\Delta\mu} = 0$. The outer branch matching the mean-field coexistence curve is the solution

$$\bar{\Delta}\rho = \sqrt{\frac{3}{2}}\left(1+\sqrt{1-2\bar{t}}\right) = \sqrt{-3\bar{t}} + \sqrt{\frac{3}{2}} + \mathcal{O}(-\bar{t})^{-1/2}. \tag{4.51}$$

By insertion into (4.42)

$$\bar{\varepsilon} = 1+\sqrt{1-2\bar{t}} = \sqrt{-2\bar{t}}\left[1+(-2\bar{t})^{-1/2}+\mathcal{O}(-2\bar{t})^{-1}\right]. \tag{4.52}$$

In equilibrium between the symmetric high and low density branches $\pm\bar{\Delta}\rho$ the mean-field internal energy (4.11) becomes $\rho u_0 = -\frac{1}{8}[1+(\Delta\rho)^2]$. To zeroth order in γ_r^3 this gives a contribution $C_{V0} = -\frac{1}{2}d(\bar{\Delta}\rho)^2/d\bar{t} = \frac{3}{2}(1+1/\sqrt{1-2\bar{t}}\,)$ to the specific heat. Likewise the correlation part $\rho u_1 = -\frac{1}{8}[1-(\Delta\rho)^2]\gamma_r^3(1-\varepsilon)$ gives $C_{V1} = \frac{1}{2}d\bar{\varepsilon}/d\bar{t} = -1/(2\sqrt{1-2\bar{t}}\,)$. In sum

$$C_V = \frac{3}{2} + \frac{1}{\sqrt{1-2\bar{t}}} = \frac{3}{2} + \frac{1}{\sqrt{-2\bar{t}}} + \mathcal{O}(-2\bar{t})^{-3/2}. \tag{4.53}$$

Outside the critical region, $-\bar{t} \gg 1$, (4.53) gives a Gaussian correction (3.21) to the plain mean-field value 3/2. With the irregular thermodynamic behavior in mind we observe that $C_V = 5/2 - (-\bar{t}) + \cdots$ close to the critical temperature $\bar{t} = 0$.

4.3.3 Nearest neighbor interaction

Recently Dickman and Stell [22] were the first to develop a method for solving SCOZA numerically below T_c and to obtain the prescribed well-defined phase transition. With an iterative procedure for β_e (Eq. (4.1)) they were able to integrate the consistency relation (4.3) for the three various types of cubic lattice gases with nearest-neighbor attractive interactions. Compared to analytic and numerical estimates for the Ising model, they obtained remarkably accurate thermodynamic and structural predictions. E. g. critical

temperatures were within 0.2% of the numerically exact values and the general behavior in the critical region described by effective critical exponents was close to such estimates.

For a lattice gas with attractive nearest-neighbor interactions the potential (4.5) is

$$\psi(\boldsymbol{r}) = \begin{cases} 0 & , \quad \boldsymbol{r} = 0 \\ 1/q & , \quad \boldsymbol{r} \text{ a nearest-neighbor lattice vector} \\ 0 & , \quad \text{otherwise} \end{cases} . \tag{4.54}$$

The coordination number q for the specific type of cubic lattice is the number of nearest neighbors to a lattice site. Fourier transforming (4.54) and inserting into $P(z)$ (Eq. (4.7)) gives the Green's function for the Helmholtz equation on the lattice. In case of the simple cubic lattice ($q = 6$)

$$\tilde{\psi}(\boldsymbol{k}) = \frac{1}{3}(\cos k_x + \cos k_y + \cos k_z), \tag{4.55}$$

which leads to the product formula [23]

$$P(z) = \frac{\sqrt{1 - \frac{3}{4}x_1}}{1 - x_1} \left(\frac{2}{\pi}\right)^2 K(k_+)K(k_-). \tag{4.56}$$

Here

$$\begin{aligned} k_\pm^2 &= \frac{1}{2} \pm \frac{1}{4}x_2\sqrt{4 - x_2} - \frac{1}{4}(2 - x_2)\sqrt{1 - x_2} \\ x_1 &= \frac{1}{2} + \frac{1}{6}z^2 - \frac{1}{2}\sqrt{1 - z^2}\sqrt{1 - \frac{1}{9}z^2} \\ x_2 &= x_1/(x_1 - 1) \end{aligned} \tag{4.57}$$

and

$$K(k) = \int_0^{\pi/2} \frac{d\theta}{\sqrt{1 - k^2 \sin^2 \theta}} \tag{4.58}$$

is the complete elliptic integral of first kind. Indeed the cusp singularity at $z = 1$,

$$P(z) = P(1) - \frac{3\sqrt{3}}{\pi}\sqrt{1 - z} + \mathcal{O}(1 - z), \tag{4.59}$$

with

$$P(1) = 1.516\ldots, \tag{4.60}$$

confirms the asymptotic treatment of the subsection 4.3.1, Eqs. (4.22) and (4.23), or equivalently, (4.32) and (4.33). In order to follow the recipe of Dickman and Stell, the exact PDE (4.13) is solved with respect to the internal energy due to fluctuations, Eq. (4.12). Therefore one has to tabulate the function (4.31) (given by (4.56) for the simple cubic lattice gas) numerically.

The inverse range of interaction, γ_r, the free parameter of the simplified PDE (4.35), can in principle be adjusted to give the same critical point as the exact one (4.13) for the three cubic types of nearest-neighbor interacting lattice gases. If the expectation in subsection 4.3.1 is fulfilled, that the precise form of $P(z)$ is of minor importance except its asymptotic behavior close to the critical point, the two solutions should differ insignificantly over the whole region $0 \leq \varepsilon \leq 1$. By choosing γ_r in such a way that the approximate internal energy equals the exact value at criticality, one gets less than 0.7% deviation in T_c for the three cases. That is, from (4.31) and (4.34),

$$2F(1) = 1 - \frac{1}{P(1)} = \gamma_r^3 \tag{4.61}$$

is chosen. So for the SC lattice (4.60) $\gamma_r^3 = 0.3405\ldots$ which we just will refer to as 0.34 in subsection 4.3.5.

Eq. (4.13), as well as (4.35), was first solved with an implicit and thus unconditionally stable finite-difference method developed by Pini, Stell, and Dickman [24]. With less computational effort their method offered accurate computations close to criticality and results in fully agreement with those previously reported by Dickman and Stell. Furthermore they found excellent overall agreement between the approximated version (4.35) and (4.13) for the SC lattice with γ_r^3 chosen as mentioned above.

4.3.4 Numerical method

In this part I will first review the numerical integration of the PDE (4.35) developed by D. Pini. This method is described in detail in Ref. [24] for the exactly treated nearest-neighbor interaction for Eq. (4.13).

First Eq. (4.35) is rewritten as a nonlinear diffusion equation, with ρ and β corresponding to position and time in a diffusion process, respectively. To remove "convection" terms proportional to $\partial\varepsilon/\partial\rho$, Pini combines the factor $\rho(1-\rho)$ with ε by introducing the new unknown function $\varphi(\rho, \beta)$:

$$\varphi = \rho(1-\rho)\varepsilon. \tag{4.62}$$

In terms of φ, (4.35) reads

$$\frac{1}{2}\gamma_r^3[\rho(1-\rho)]^3\frac{\partial^2\varphi}{\partial\rho^2} = 2\varphi\frac{\partial\varphi}{\partial\beta} + (1-\gamma_r^3)[\rho(1-\rho)]^3. \tag{4.63}$$

With "coefficients" depending on ρ only via $\rho(1-\rho)$ besides φ itself, one immediately realizes that φ preserves particle-hole symmetry:

$$\varphi(\rho) = \varphi(1-\rho). \tag{4.64}$$

(Which also is the case for z in the original equation (4.13)). This is used to restrict the range of integration for (4.63) to $0 \le \rho \le \frac{1}{2}$, with boundary conditions $\varphi(\rho = 0, \beta) = 0$ and $\varphi(\frac{1}{2} + \Delta\rho, \beta) = \varphi(\frac{1}{2} - \Delta\rho, \beta)$. $\Delta\rho$ is here the constant grid spacing in the ρ-direction. The initial condition is $\varphi(0 \le \rho \le 1, \beta = 0) = \rho(1-\rho)$.

The primitive way to solve a diffusion equation numerically is just to integrate the time derivative of the solution stepwise forward in time, for every position grid. As is well known, with a diffusion constant D, this explicit method is not stable unless the time steps are made smaller than a certain value proportional to $(\Delta\rho)^2/D$. But as one bumps into the spinodal curve $\varphi = 0$ for $T \le T_c$, the diffusion "constant"

$$D = \frac{\gamma_r^3[\rho(1-\rho)]^3}{4\varphi} \tag{4.65}$$

of (4.63) will diverge. This causes difficulties. Dickman and Stell [22] had to be careful to avoid oscillations, using very small steps $\Delta\beta$ and an unusual difference formula when calculating the second derivative with respect to ρ. The more advanced implicit methods take the backward time derivative of the solution into account. They lead to a coupled set of equations, involving all position grid points, to be solved simultaneously at each new time step. This is an unconditionally stable procedure. If the original PDE is nonlinear, the equation set will be nonlinear as well. However, (4.63) is quasilinear. That is, the "coefficients" are functions of the variable ρ in addition to the unknown function φ itself. A predictor-corrector scheme specially adapted to this kind of PDE [25], first predicts the solution and thus the coefficients in the middle of two consecutive time steps. These coefficients are finally used to correct the solution at the new step. With $\partial^2\varphi/\partial\rho^2$ approximated by the standard central difference, Eq. (4.63) is solved by a linear tridiagonal

set of equations at a computationally low cost. The accuracy is of second order both in density and temperature.

The critical point terminates the critical isochor $\rho_c = 1/2$ at the temperature $T = T_c$ where the isothermal compressibility diverges. Numerically we find the inverse critical temperature β_c by gradually decreasing $\Delta\beta$ until the reduced inverse isothermal compressibility

$$\frac{\partial\beta p}{\partial\rho} = \frac{\varphi^2}{\rho^2(1-\rho)^3}, \tag{4.66}$$

reaches a small prescribed minimum value along the critical isochor. Below the critical temperature, the broadening spinodal curve $\rho_{spin}(\beta)$ at which $\varphi(\rho_{spin}, \beta) = 0$, gives the location of diverging compressibility. Thus the non-negative compressibility region of integration is reduced to the ρ-interval $(0, \rho_{spin})$. Wherever the solution φ at the high-density boundary becomes negative gives the spinodal within the accuracy of the grid, and the ρ-interval is reduced by one grid point in the next β-step.

The pressure is found by integrating the reduced inverse isothermal compressibility (4.66) with respect to density. At the high-density side, $\frac{1}{2} < \rho \leq 1$, the integration is achieved by exploiting the particle-hole symmetry of $(\partial\beta\mu/\partial\rho) = (\partial\beta p/\partial\rho)/\rho$. To avoid possible loss of accuracy while summing, we only integrate the part excess to the hard-core contribution $1/(1-\rho)$ which dominates at close-packing $\rho \to 1$. Finally the exact hard-core pressure (2.24) is added. Above the critical temperature the integration can be done straight-forward from $\rho = 0$. But subcritically the spinodal makes this impossible. Therefore one integrates on the high-density branch from $\rho = 1$ where the mean-field or van der Waals result, Eq. (2.23) with $a = 1/2$, applies. This follows from the Helmholtz free energy containing the mean-field term plus a particle-hole symmetric term due to correlations, analogous to the internal energy equations (4.11) and (4.12). As the hard-core pressure diverges at $\rho = 1$, we have to integrate from the penultimate grid point $1 - \Delta\rho$. Corrections to the mean-field result are obtained from expanding the excess part of $(\partial\beta p/\partial\rho)$ in powers of ρ. That is, from the virial expansion (2.5) and the corresponding expansion for the hard cores (2.24),

$$\frac{\partial\beta p}{\partial\rho} = \frac{\partial\beta p^{hc}}{\partial\rho} + 2B_2'\rho + 3B_3'\rho^2 + \ldots \tag{4.67}$$

in the "excess" virial coefficients

$$B_i' = B_i - B_i^{hc} = B_i - 1/i. \tag{4.68}$$

By using the particle-hole symmetry argument for $(\partial\beta p/\partial\rho)/\rho$ again, we end up with the high-density expansion

$$\beta p = -\ln(1-\rho) - \frac{1}{2}\beta - 2B_2'(1-\rho) + (B_2' - \frac{3}{2}B_3')(1-\rho)^2 + \mathcal{O}\left((1-\rho)^3\right). \quad (4.69)$$

The coefficients B_i' are found by solving the self-consistency relation (4.3) successively in orders of ρ. By calculating the limiting $\rho \to 1$ pressure (4.69) to second order in $1-\rho$, this procedure gives

$$\begin{aligned} B_2' &= -f \\ B_3' &= \frac{1}{3}\gamma_r^3 f^2[6 + (2\gamma_r^3 - 1)f] \end{aligned} \quad (4.70)$$

where $f = \frac{1}{\gamma_r^3}(e^{\frac{1}{2}\gamma_r^3\beta} - 1)$. As checked numerically by Pini [24], the pressure obtained from this (compressibility) route is the same as the one from the energy route, that is, the pressure obtained by integrating $\partial\beta p/\partial\beta = \rho^2\partial u/\partial\rho$ with respect to β. Finally the phase equilibrium can be found from the low- and high-density pressure branches with a Maxwell construction. Due to the particle-hole symmetric coexistence curve $\rho_{coex}(\beta)$, this reduces to finding the density ρ_{coex} such that the pressures at each branch coincide, i. e. $p(\rho_{coex}, \beta) = p(1 - \rho_{coex}, \beta)$.

With regard to the determination of the phase coexistence, some details of the numerical integration have to be mentioned. We use the Simpson rule to obtain the pressure at every other grid point in the ρ-direction, with an accuracy of order $(\Delta\rho)^4$. Furthermore, the high-density boundary value (4.69) is calculated with an accuracy of order $(\Delta\rho)^2$. Due to the resulting inaccuracy, the pressure at $\rho = 1/2$ would differ slightly for $T > T_c$ when integrating from both sides; $p_{high}(\frac{1}{2}, \beta) - p_{low}(\frac{1}{2}, \beta) = \Delta p(\beta)$. In order to calculate $\Delta p(\beta)$ we have to have an even number of grid spaces $\Delta\rho$ on the interval $0 \le \rho \le \frac{1}{2}$ and to start the high-density integration from the third largest density grid point $1 - 2\Delta\rho$. To eliminate the mismatch $\Delta p(\beta)$, to which the determination of the phase equilibrium is very sensitive close to T_c, we simply subtracted $\Delta p(\beta)$ from the high-density branch $p_{high}(\rho, \beta)$. Below T_c we use the constant $\Delta p(\beta_c)$ since the integrand (4.66), the boundary value (4.69), and hence the mismatch $\Delta p(\beta)$, will essentially stay constant under small changes in temperature near T_c where this is important.

4.3.5 Numerical results

Section IV of Paper I[3] mainly deals with the critical properties of the numerical solution of Eq. (4.35). One of the main points of the present subsection is to go more deeply into the general thermodynamic properties of the SCOZA PDE (4.35). Another is to give a more precise description of items only mentioned briefly, left out, or calculated less accurately in Secs. IV and V of I.

In Fig. 4.3 the inverse compressibility ε^2 (4.32) along the critical isochor ($T > T_c$) is plotted for $\gamma_r^3 = 10^{-3}, 10^{-2}, 0.1, 0.2$, and 0.34. For $\gamma_r^3 \leq 10^{-2}$ the curves are apparently linear in $\beta - \beta_c$ and they vanish close to the mean-field critical point (2.20). For larger γ_r^3 values the isochores curve and the curvature is strongest close to the critical point β_c. Fig. 4.4 shows that the SCOZA critical temperature T_c^{SC} is higher than the MSA value T_c^M (Eq. (4.39)) and that the ratio between the two increases approximately linearly with $(\gamma_r^3)^2$ for $\gamma_r^3 \lesssim 0.5$. Numerically we find $T_c^{SC}/T_c^M \approx 1 + 1.2(\gamma_r^3)^2$ for $\gamma_r^3 \leq 0.5$. The deviation in chemical potential from its critical value, $\beta\Delta\mu$, along the critical isotherm ($T = T_c$), is shown in Fig. 4.5. For this plot the values of γ_r^3 are $10^{-6}, 10^{-2}, 0.1, 0.2, 0.3, 0.34, 0.4, 0.5, 0.6, 0.7$, and 0.8, which span the whole range for which we could get reliable results. Similar to the isochors of Fig. 4.3 we see that for $\gamma_r^3 \leq 10^{-2}$ the isotherms lie very close to a single cubic curve, viz. the mean-field critical isotherm. And by increasing γ_r^3 the curves flatten around the critical density $\rho_c = 1/2$.

The observed behavior in Figs. 4.3 and 4.5 for small γ_r^3 is qualitatively similar to the corresponding critical isochors and isotherms given by the MSA solution (4.37). This is easily seen by comparing the plots of the effective critical exponents γ and δ, Figs. 1 and 2 in I, with the MSA plot Fig. 4.1. First Figs. 1 and 2 in I show that SCOZA has critical exponents $\gamma = 2$ and $\delta = 5$. Next the range of the critical region scales as function of γ_r^3 in the same way that the asymptotic MSA solution (4.42) does. I. e., for $t \ll (\gamma_r^3)^2$ and $\Delta\rho \ll \gamma_r^3$ the effective exponents γ and δ approach their asymptotic values, analogous to the limiting MSA behavior, Eq. (4.45) with $\bar{\Delta x} \ll 1$. Outside this region mean-field behavior with effective exponents $\gamma = 1$ and $\delta = 3$ is observed, as Eq. (4.45) with $\bar{\Delta x} \gg 1$. So the curves in Figs. 4.3 and 4.5 are, respectively, linear and cubic functions of the deviations $\Delta\beta$ and $\Delta\rho$ from their critical values, except within a narrow critical region where they flatten and become quadratic and fifth-order functions, respectively. In

[3]Hereafter Paper I and II are referred to as I and II, respectively

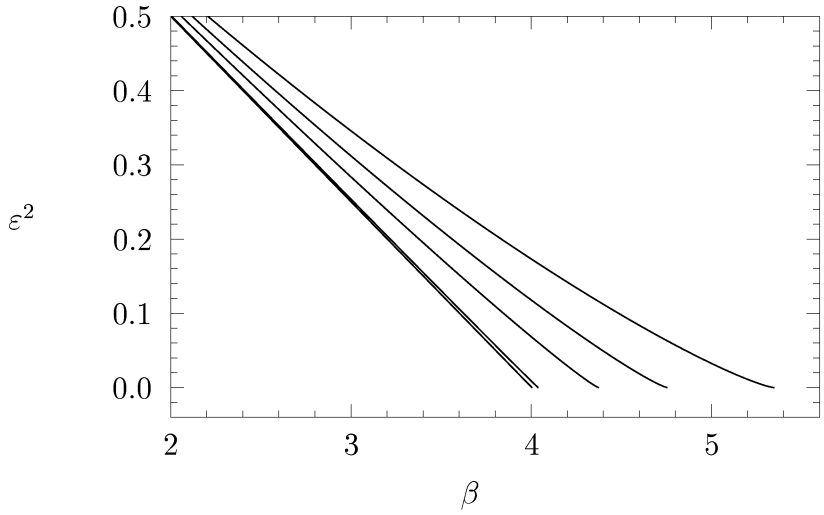

Figure 4.3: Reduced inverse compressibility ε^2 along the critical isochor ($T > T_c$) as function of inverse temperature β. The curves correspond to γ_r^3 values 10^{-3}, 10^{-2}, 0.1, 0.2, and 0.34, respectively, starting with the lower curve for 10^{-3}.

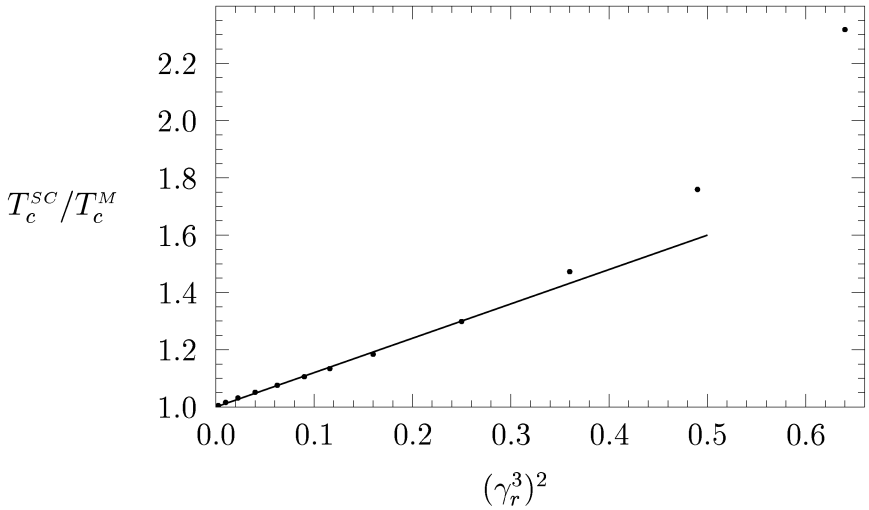

Figure 4.4: The ratio between the SCOZA and the MSA critical temperature T_c^{SC}/T_c^M plotted versus $(\gamma_r^3)^2$. For $\gamma_r^3 \lesssim 0.5$ the ratio is approximately linear in $(\gamma_r^3)^2$ and the line $T_c^{SC}/T_c^M = 1 + 1.2(\gamma_r^3)^2$ gives a good fit in this interval.

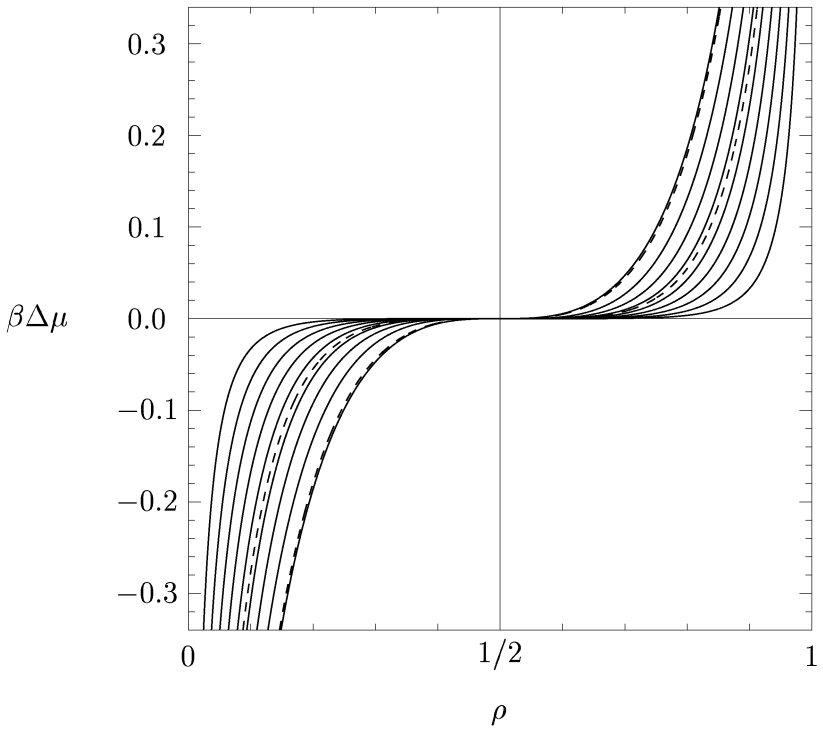

Figure 4.5: The deviation $\beta\Delta\mu$ in chemical potential from its critical value along the critical isotherm ($T = T_c$) as a function of density ρ. Here $\gamma_r^3 = 10^{-6}, 10^{-2}, 0.1, 0.2, 0.3, 0.34, 0.4, 0.5, 0.6, 0.7$, and 0.8, respectively, starting with the lower left curve. The two dashed curves correspond to values $\gamma_r^3 = 10^{-2}$ and 0.34.

addition we observe in Fig. 1 that with respect to t the range of the critical region is reduced considerably compared to MSA, with about two decades or a factor 100. A striking feature is that the band of curves in Fig. 1 seem to approach a single curve for $\gamma_r^3 \to 0$ analogous to the MSA curves in Fig. 4.1. This is also the case for the corresponding effective δ curves. But due to the results for δ shown in Fig. 2 of I this feature is somewhat modified at larger densities since the curves diverge at saturation $\Delta\rho = 1$. δ is found from the non-symmetric pressure (Eq. (3.6)), for which the curves will be lifted compared to using the compressibility directly (as in Fig. 4.7 below). More conspicuously the characteristic behavior along the t and $\Delta\rho$ axis is gathered in Figs. 4.6 and 4.7. In Fig. 4.6 the scaled solution (4.43) is shown as a function of the scaled variable

$$\bar{\Delta x} = \Delta x/(\gamma_r^3)^2 \tag{4.71}$$

along the critical isochor and isotherm, i. e.,

$$\Delta x \equiv \begin{cases} t & , \quad \Delta\rho = 0 \\ (\Delta\rho)^2 & , \quad t = 0 \end{cases} . \tag{4.72}$$

The MSA solution is the same in either direction (Eqs. (4.37) and (4.41)). As $\gamma_r^3 \to 0$ the MSA solution approaches the asymptotic solution (4.42) drawn as a single dashed curve in the correctly scaled plots Figs. 4.6 and 4.7, Eqs. (4.43) and (4.44). Analogously the SCOZA curves approach distinct solutions in either direction when $\gamma_r^3 \to 0$. Along the critical isotherm ($\bar{\Delta x} = (\bar{\Delta\rho})^2$) and asymptotically for small and large $\bar{\Delta\rho}$ SCOZA coincides with the asymptotic MSA (4.45). This is also the case for large $\bar{t}$ along the critical isochor ($\bar{\Delta x} = \bar{t}$). But for small $\bar{t}$ SCOZA is shifted in comparison to the universal MSA and approaches $\bar{\varepsilon} \simeq 7\,\bar{t}$. The critical amplitude (i. e. 7) is found with a relative numerical accuracy of about 10^{-3}. Using a similar technique to that used below for finding effective exponents, the corresponding effective amplitudes would converge to well-defined values in the limit $\gamma_r^3 \to 0$. In Fig. 4.7 the slopes of the curves in Fig. 4.6, or the effective exponent function $f(\bar{\Delta x}) = d\ln\bar{\varepsilon}/d\ln\bar{\Delta x}$, are calculated. The effective critical exponents α, γ, and δ (Figs. 1, 2, and 3 of I) are given by $1 - f(\bar{t})$, $2f(\bar{t})$, and $1 + 4f[(\bar{\Delta\rho})^2]$, respectively (with $\bar{t} = t/(\gamma_r^3)^2$ and $\bar{\Delta\rho} = \Delta\rho/\gamma_r^3$). This plot also offers better resolution and shows that the curves with $\gamma_r^3 = 10^{-3}$ and 10^{-2} are barely distinguishable for $\bar{\Delta x} \gtrsim 10^{3.2}$. Compared to the asymptotic MSA solution both the critical and the mean-field region are slightly reduced with respect

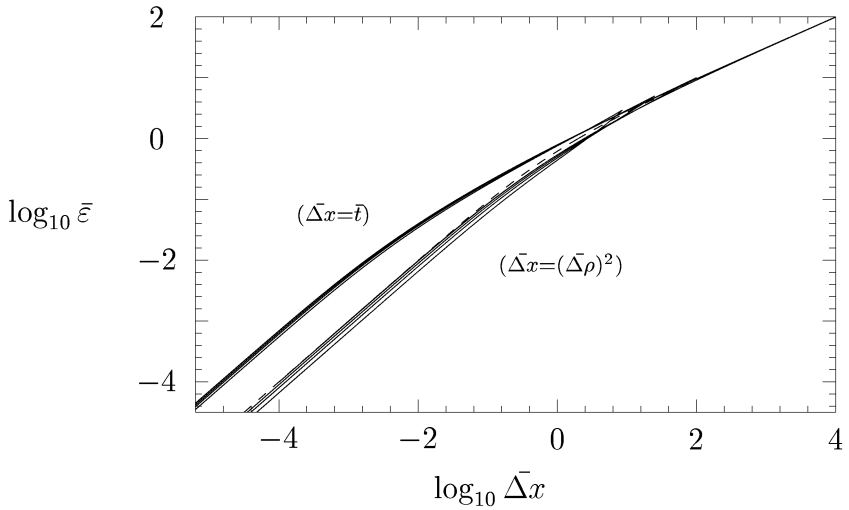

Figure 4.6: The scaled solution $\bar{\varepsilon}$ plotted as a function of the scaled variable $\bar{\Delta x}$ (see Eqs. (4.43) and (4.71)) along the critical isochor ($\bar{\Delta x} = \bar{t}$) and the critical isotherm ($\bar{\Delta x} = (\bar{\Delta\rho})^2$). The curves correspond to $\gamma_r^3 = 10^{-3}, 10^{-2}, 0.1, 0.2$ and 0.34, respectively, starting with the upper curves at the lower left ends. The dashed curve is the universal MSA solution (4.42).

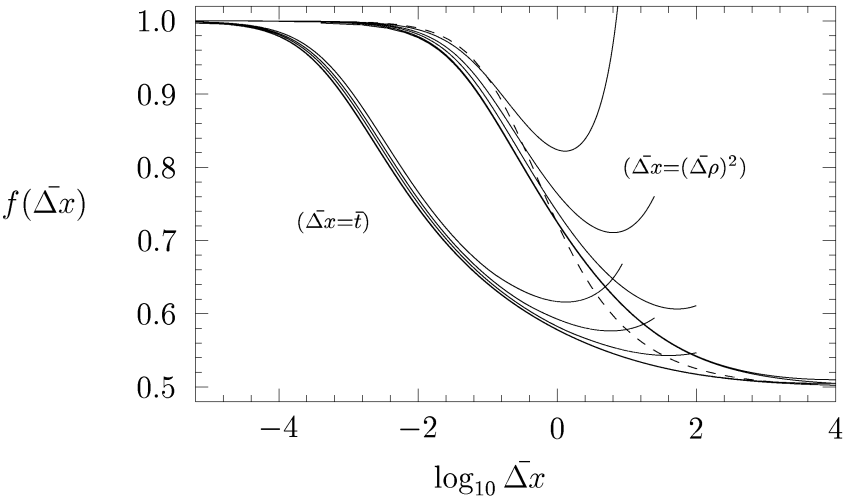

Figure 4.7: The slopes $f(\bar{\Delta x})$ of the curves in Fig. 4.6 above, plotted versus $\log_{10}\bar{\Delta x}$. Notation as in Fig. 4.6. The curves are systematically lowered as γ_r^3 decreases.

to $\Delta\rho$. E. g. the crossover region is enlarged by a factor of about 2. But along the t axis a more dramatic change is seen. The critical region is reduced by as much as a factor 230 such that the cross-over into the mean-field region is much slower. In Fig. 3 of I a similar effect to that of δ in Fig. 2 of I results when calculating α from the heat capacity (Eq. (3.5)), giving curves that diverge in the high-temperature limit.

The spinodal and coexistence curves are shown in Fig. 4.8 for a wide range of values of γ_r^3. Again, for $\gamma_r^3 \leq 10^{-2}$, results close to the corresponding mean-field behavior are obtained. I. e., the curves are parabolic close to the critical point in accordance with (2.31) ($\varepsilon = 0$) and phase equilibrium $\Delta\mu = 0$, Eqs. (2.21) and (2.22). Increasing γ_r^3 makes the spinodals sharper at the top and the coexistence curves flatter, compared to the parabolic ones. In Fig. 4.9 the scaled deviations, i. e. $\bar{\Delta}\rho$ as a function of $\bar{t}$, are shown for the same curves in a log-log plot. As in I we use $t = (T_c - T)/T_c > 0$ for subcritical temperatures. One finds that the curves fall on single limiting curves for small γ_r^3 ($\to 0$). For larger γ_r^3 one starts to see some deviations as especially the coexistence curves become broader. Also for larger $\bar{t}$ (further away from the critical point) the curves start to separate as one should expect since then $\rho \to 1$ (or 0). (Due to the scaling used, decreasing γ_r^3 moves the endpoints of the curves drawn to the right.) For small γ_r^3 and outside the critical region ($\bar{t} \gg 1$ and $\bar{\Delta}\rho \gg 1$) both sets of curves approach the mean-field result: straight lines with slope 1/2. More precisely, using values of γ_r^3 as small as 10^{-6}, shows that the asymptotic curves are given by $\bar{\Delta}\rho_{spin} \simeq \bar{t}^{1/2}$ and $\bar{\Delta}\rho_{coex} \simeq \sqrt{3}\,\bar{t}^{1/2}$, within a relative accuracy of about 1×10^{-4} and 5×10^{-4}, respectively. These curves are in agreement with the MSA result $\bar{\varepsilon} = 0$ (Eq. (4.42)) and with the mean-field coexistence curve (Eqs. (2.21) and (2.22)). In Fig. 4 of I the effective exponent β for the coexistence curves is shown. As $t \to 0$, the limiting value $\beta = 0.35$ is independent of γ_r^3. Actually Pini, Stell, and Dickmann [24] and Høye [8] have recently shown analytically that $\beta_{spin} = 3/4$ and $\beta_{coex} = 7/20$. Straight lines with slopes $3/4 = 0.75$ and $7/20 = 0.35$ have been drawn in Fig. 4.9 (dashed) to indicate the asymptotic behavior close to the critical point. With an accuracy of about 3% in the amplitudes, the corresponding curves are found to be $\bar{\Delta}\rho_{spin} \simeq 3.5\,\bar{t}^{3/4}$ and $\bar{\Delta}\rho_{coex} \simeq 1.6\,\bar{t}^{7/20}$ as $\gamma_r^3 \to 0$. Due to the greatly reduced extent of the critical region for decreasing γ_r^3, the spinodal and coexistence curves would easily deviate from the regular pattern shown in Fig. 4.9 for large values of γ_r^3, since close to the critical point the numerical solution becomes inaccurate. For instance, the curves with $\gamma_r^3 = 10^{-2}$ have been cut at $\bar{t} \simeq 10^{-1.6}$ and $\bar{t} \simeq 10^{-3.0}$, respectively. But

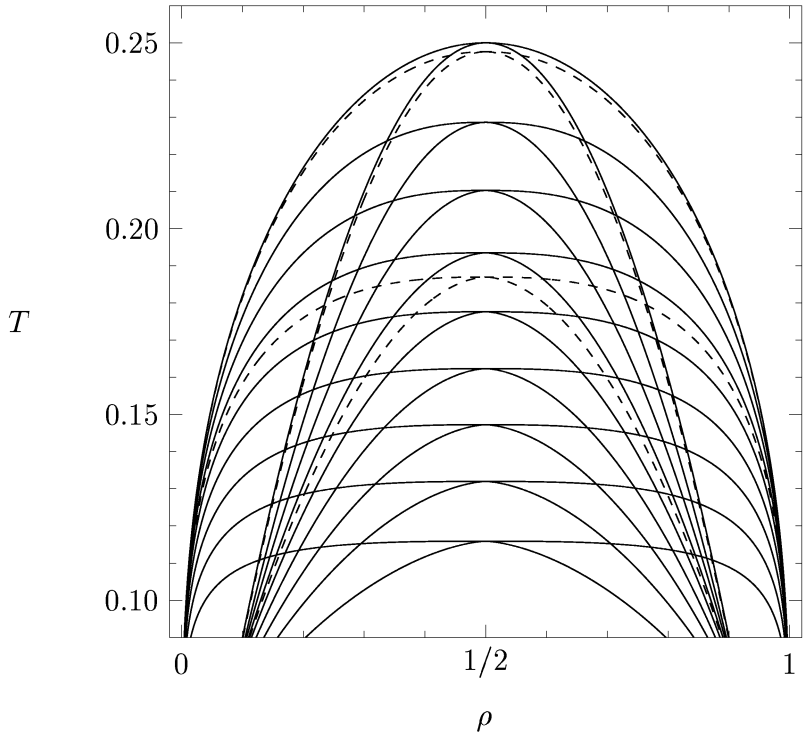

Figure 4.8: Temperature T versus density ρ for the coexistence and spinodal curves. Here $\gamma_r^3 = 10^{-6}, 10^{-2}, 0.1, 0.2, 0.3, 0.34, 0.4, 0.5, 0.6, 0.7$, and 0.8, respectively, starting with the upper curves. For each value of γ_r^3 the broad branches of the coexistence curve envelop the spinodal curve. The dashed curves correspond to values $\gamma_r^3 = 10^{-2}$ and 0.34.

thanks to the regular behavior and strong convergence (when $\gamma_r^3 \to 0$) close to the critical point, the remaining parts can be extrapolated with the aid of the curves with larger γ_r^3.

The value of $\bar{\varepsilon}$ (Eq. (4.43)) along the coexistence curve as function of temperature $\bar{t}$ is shown in Fig. 4.10. These subcritical curves are like the supercritical ones shown in Fig. 4.6 on the right-hand side while different slopes on the left-hand side reflect different indices γ and γ'. Analogous to the value of the critical exponent β the subcritical slope is found from Fig. 5 in I to be $\gamma'/2 = 0.70$ (while $\gamma/2 = 1$ in Fig. 4.6). Therefore $\gamma \neq \gamma'$, in disagreement with the scaling hypothesis, Eq. (3.31). On the other hand $\bar{\varepsilon}$ encounters no spurious singularity when passing the critical isotherm $T = T_c$. See Fig. 4.11 where isotherms both above and below the critical one are drawn for the case $\gamma_r^3 = 10^{-2}$. (As indicated by the previous figures this case should represent the universal limiting behavior $\gamma_r^3 \to 0$ well.) Indeed the "subcritical" scaling relation $\gamma' = \beta(\delta - 1)$ (Eq. (3.36) with γ replaced by γ') is fulfilled with the critical exponent values found above [24]. I. e., close to the critical point, $\bar{\varepsilon}$ goes like $(\bar{\Delta}\rho)^2$ along the critical isotherm as well as $(\bar{\Delta}\rho)^2 \sim \bar{t}^{2\beta}$ along the coexistence curve. Moreover $\bar{\varepsilon}$ approaches $(2.5 \pm 0.1)\,\bar{t}^{7/10}$ in the limit $\gamma_r^3 \to 0$. Within the numerical accuracy of the limiting ($\gamma_r^3 \to 0$) critical amplitudes along the critical isotherm ($\bar{\varepsilon} \equiv D\,(\bar{\Delta}\rho)^{(\delta-1)/2}$, $D \simeq 1 \pm 10^{-3}$) and the coexistence curve ($\bar{\Delta}\rho \equiv B\,\bar{t}^{\beta}$ and $\bar{\varepsilon} \equiv \Gamma'\,\bar{t}^{\gamma'/2}$), this means that also the coefficients of the $(\bar{\Delta}\rho)^2$ terms for $\bar{\varepsilon}$ are the same. I. e., they obey the amplitude relation

$$DB^{(\delta-1)/2} = \Gamma'. \tag{4.73}$$

In Fig. 4.11 the intersections of the subcritical isotherms with the coexistence curve have been marked with circles. And for $\bar{t} \leq 10^{-1}$ these points approach the limiting critical ($\gamma_r^3 \to 0$ and $\bar{t} \ll 1$) expression indicated by crosses. (One may conjecture $\Gamma' = B^2 = 5/2$ for which the crosses have been drawn.) As noted above serious numerical inaccuracy is encountered for $\bar{t} \leq 10^{-3}$ and significant deviations from the crosses are seen. Outside the critical region $\bar{\varepsilon}$ approaches the mean-field result $\sqrt{2}\,\bar{t}^{1/2} = \sqrt{2/3}\,\bar{\Delta}\rho$ (Eqs. (2.21) and (2.22)) in the limit $\gamma_r^3 \to 0$. This relation is shown as a dashed-dotted straight line with crosses matching the actual temperatures plotted in Fig. 4.11.

The specific heat C_V along the coexistence curve is plotted as function of $\bar{t}$ in Fig. 4.12. As we see from the figure C_V has a maximum at a temperature close to T_c, not at T_c itself. This temperature is approximately given by $\bar{t} \approx 10^{-2.7}$ for the values of γ_r^3 plotted. In the limit $\gamma_r^3 \to 0$, C_V converges

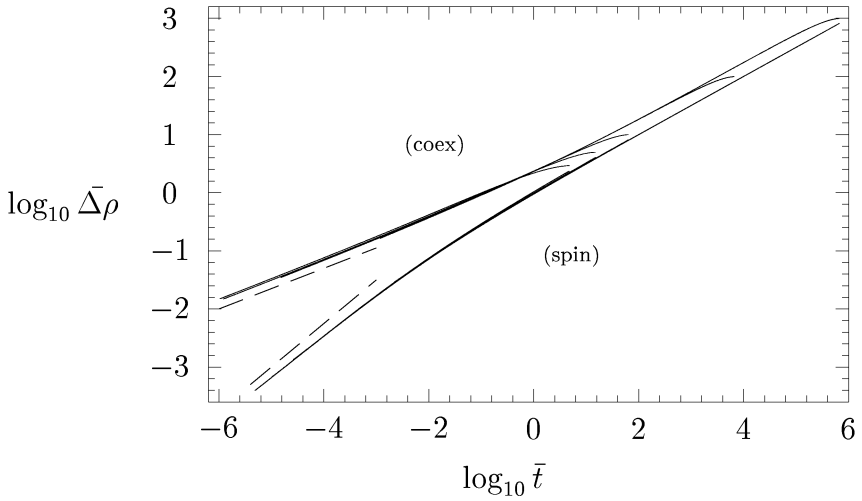

Figure 4.9: The scaled spinodal and coexistence curves, plotted as $\log_{10} \bar{\Delta}\rho$ versus $\log_{10} \bar{t}$. The curves correspond to $\gamma_r^3 = 10^{-3}, 10^{-2}, 0.1, 0.2$ and 0.34. Dashed straight lines with slopes 0.75 and 0.35 indicate the critical behaviour.

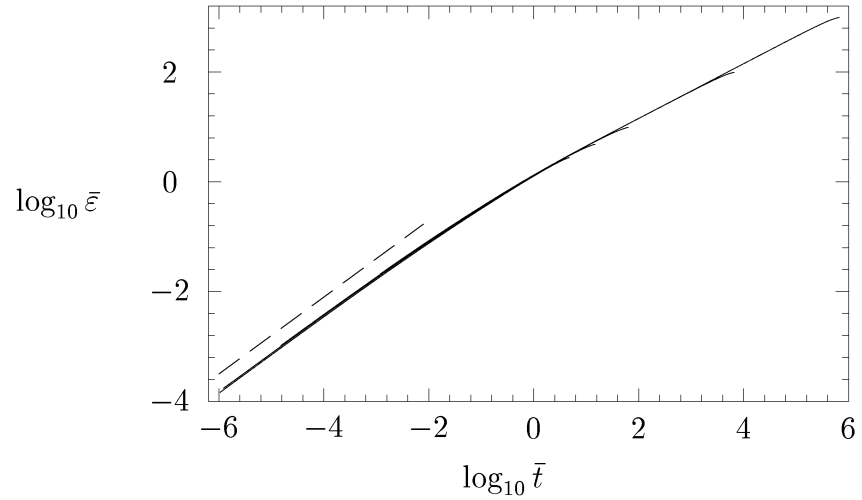

Figure 4.10: The scaled solution $\bar{\varepsilon}$ along the coexistence curve, plotted as function of the scaled temperature $\bar{t}$. The values of γ_r^3 are the same as in Fig. 4.9. The dashed straight line has slope 0.70.

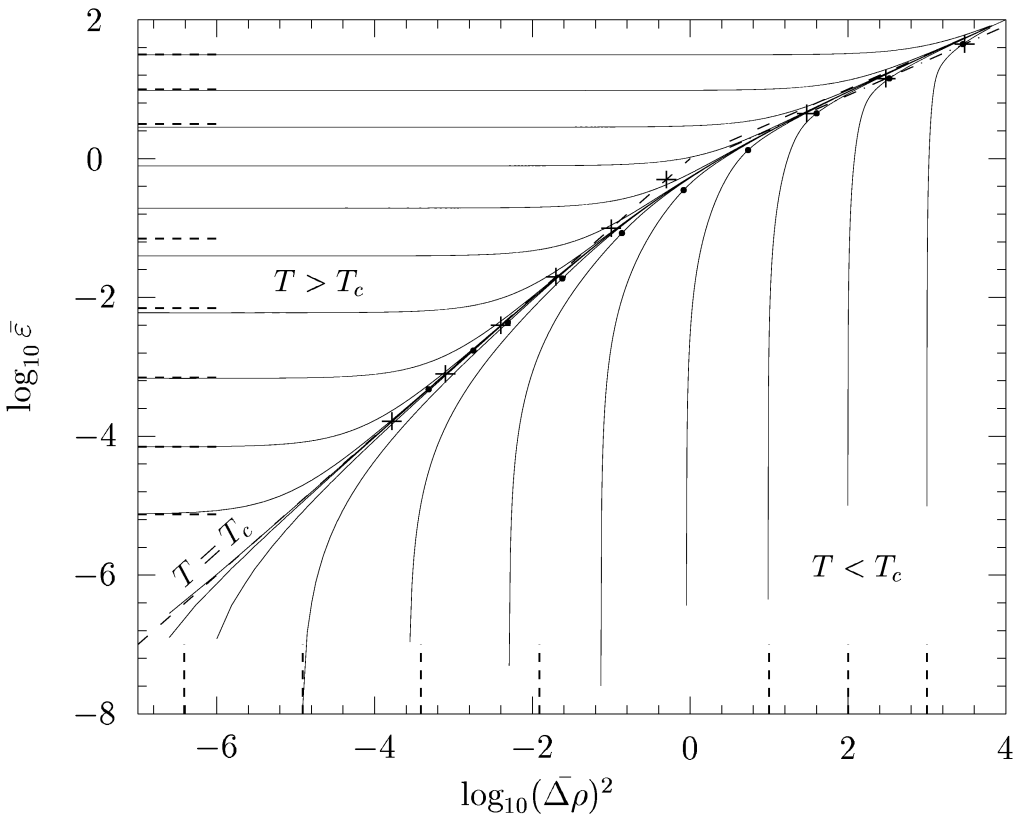

Figure 4.11: Log-log plot showing isotherms for the scaled solution $\bar{\varepsilon}$ as a function of the square of the scaled density $\bar{\Delta}\rho$. Here $\gamma_r^3 = 10^{-2}$ and the scaled temperatures used both above and below critical are $\bar{t} = 10^3, 10^2, \ldots, 10^{-6}$. The critical isotherm $T = T_c$ is "squeezed" continuously between supercritical and subcritical isotherms as $\bar{t}$ decreases. Crosses and various dashed lines indicate the limiting ($\gamma_r^3 \to 0$) asymptotic behaviour for small and large $\bar{\Delta}x$ (Eqs. (4.71) and (4.72)). See the text. E. g., the intersections of the isotherms with the critical isochor ($\bar{\Delta}\rho = 0$, $T > T_c$) and the spinodal ($\bar{\varepsilon} = 0$, $T < T_c$) have been marked for $\bar{t} \leq 10^{-2}$ and $\bar{t} \geq 10^1$. Circles mark the intersections with the coexistence curve.

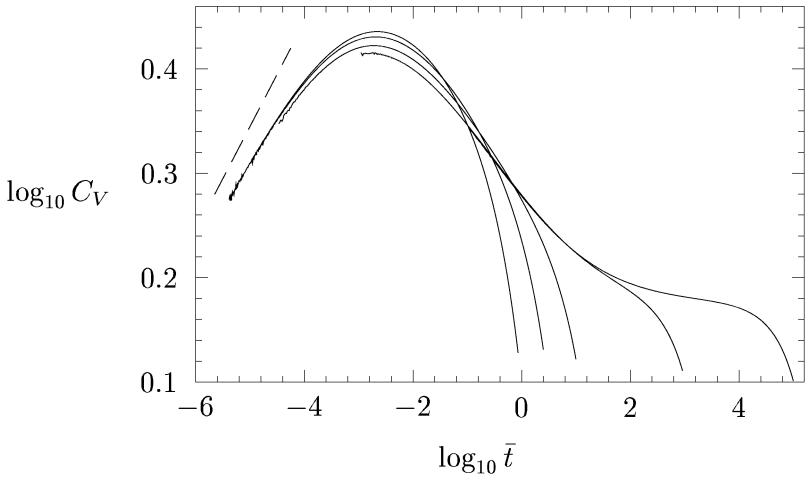

Figure 4.12: Log-log plot of the specific heat C_V along the coexistence curve as a function of the scaled reduced temperature $\bar{t}$. The values of γ_r^3 are the same as in Fig. 4.9. For increasing γ_r^3 the curves are systematically shifted to the left. After reaching a maximum, C_V vanishes as $\bar{t}^{-\alpha'}$ with $\alpha' = -0.10$ as $\bar{t} \to 0$. This is indicated by the dashed straight line.

to a value close to 2.60. Very close to the critical point (i. e. for $\bar{t} \lesssim 10^{-4}$) the C_V curves in the log-log plot come close to straight lines with slopes approaching 0.10. As in Fig. 6 of I Fig. 4.12 shows that the asymptotic ($t \to 0$) value $\alpha' = -0.10$ is independent of γ_r^3. Although $\alpha \neq \alpha'$ the value of α' is in agreement with the "subcritical" scaling relation $\alpha' + 2\beta + \gamma' = 2$, Eq. (3.33). According to Refs. [24] and [8] the analytic values for α' and γ' are indeed $-1/10$ and $7/5$, respectively. Hence the configurational specific heat along the coexistence curve vanishes when $T \to T_c^-$ since in our evaluation no constant has been subtracted from C_V. However, it is only in the immediate vicinity of the critical point that C_V drops sharply (but $C_V \geq 0$). E. g., with $\gamma_r^3 = 0.34$ the maximum of C_V is at the reduced subcritical temperature $t \approx 10^{-3.6}$. Outside the critical region mean-field behavior is seen for small γ_r^3. I. e., consistent with $\bar{\Delta\rho}$ and $\bar{\varepsilon}$ found numerically to lowest order in $\bar{t}$ along the coexistence curve, curves in Fig. 4.12 would intermediately reach a plateau $C_V \simeq 3/2$ before they vanish at $T = 0$. See also Fig. 4.13. For $T > T_c$ the specific heat along the critical isochor encounters the MSA-like cusp at the critical point ($\alpha = 0$ corresponds to a maximum). As $\gamma_r^3 \to 0$ this

cusp becomes infinitely sharp and its height approaches 3.5 consistent with (4.47) and $\bar{\varepsilon}$ found numerically along the critical isochor. Therefore C_V will undergo a jump discontinuity when passing through the critical point. This is shown in Fig. 4.13 where C_V is plotted versus T both below and above the critical point T_c. The supercritical specific heat does not describe the asymptotic critical behavior very well either, as the true $\alpha \simeq 0.1$ [24]. But as noted in Ref. [24] the supercritical saturation of C_V is not seen until $t \sim 10^{-4}$ for the nearest neighbor interaction. Compare this with Fig. 4.7 for $\gamma_r^3 = 0.34$ and $\bar{\Delta x} = \bar{t}$. Disregarding the tiny critical region, the variation of C_V with T has the λ shape characteristic for both fluids and magnets. In Fig. 4.14 SCOZA results are compared with specific heat measurements for argon [26] in the interval from the melting point to well above the critical point. To make the comparison we have subtracted the ideal gas contribution from the experimental points and rescaled the axes for SCOZA. I. e., for each value of γ_r^3, T is scaled to get the critical point T_c to coincide with $T_c^{\mathrm{Ar}} = 150\,K$. And C_V is scaled such that the curves intersect the rightmost experimental point. Apart from a nearly constant difference below T_c the curve for $\gamma_r^3 = 0.34$ seems to qualitatively describe the Ar data fairly well. Quantitatively the curve for $\gamma_r^3 = 0.2$ gives the best over-all agreement.

For large values of γ_r^3 (i. e. $\gamma_r^3 \gtrsim 0.1$) the solution no more embraces a mean-field region outside the critical region. For example the curves in Fig. 4.7 (or Fig. 1 in I) for the effective exponent γ flatten towards a minimum whose value gradually rises as γ_r^3 increases. This minimal value of γ very well describes the t dependence of the inverse reduced compressibility ($\sim \varepsilon^2 \sim t^\gamma$) in a wide temperature interval outside the critical. Due to the logarithmic t axis the narrow critical region is emphasized in Fig. 4.7. Hence a small increase of the effective γ above the minimal strongly reduces the temperature interval for which the effective γ is of relevance. This is illustrated in Fig. 4.15 where $\varepsilon^{2/\gamma}$ is plotted as a function of β, for the solution with $\gamma_r^3 = 0.34$ ($\beta_c = 5.3484$). In this case the minimal effective $\gamma \approx 1.23$, corresponding to $t \approx 10^{-0.82}$ ($\beta \approx 4.53$) in Fig. 4.7, for which the lower curve in Fig. 4.15 is plotted. The upper curve is plotted for $\gamma = 1.30$ which is the effective value at $t \approx 10^{-1.72}$ ($\beta \approx 5.25$). A dashed straight line has been drawn through the critical point and the one corresponding to the minimum of the effective γ (marked by a circle). Only within a region $t \lesssim 10^{-2}$ (for which the inset has been drawn) the lower curve deviates from the line, where the upper curve gives a better description (linearity). The situation is similar for the other effective exponents, see Figs. 1–6 in I. Subcritically the curve

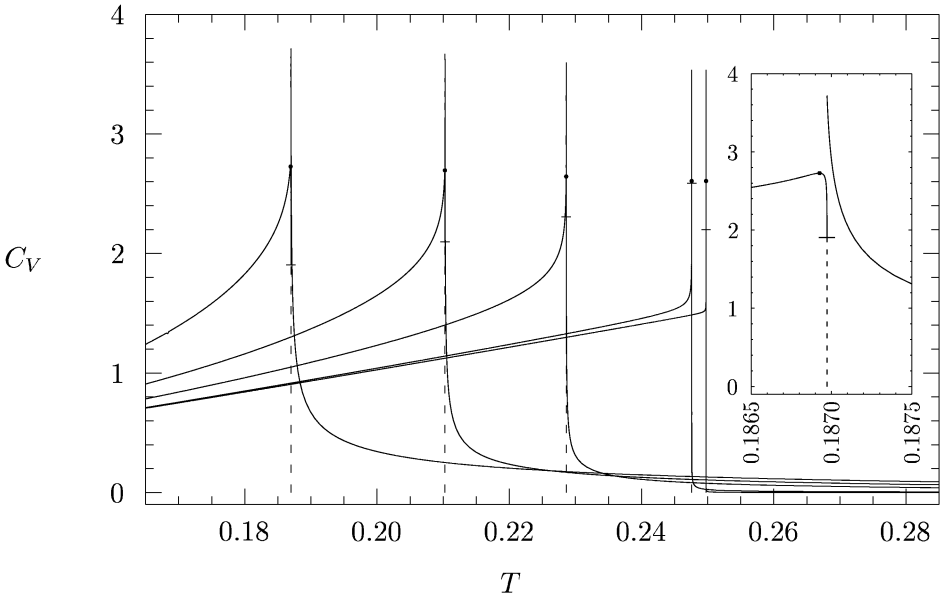

Figure 4.13: The specific heat along the critical isochor C_V as a function of the temperature T. The values of γ_r^3 are the same as in Fig. 4.9. All the curves undergo a jump discontinuity when T passes their respective critical point T_c, from a maximum on the supercritical side to zero at the subcritical side. However, C_V reaches a subcritical maximum close to T_c. See the inset of the curve with $\gamma_r^3 = 0.34$ shown for temperatures within about $\pm 10^{-2.6}$ relative to T_c. The subcritical maximum points have been marked with points to distinguish them from the supercritical branches of the curves. Horisontal bars mark the endpoints of our numerical results $T \to T_c^-$. Compare Fig. 4.12. And dashed lines have been added to indicate the extrapolations of the subcritical branches into the critical points. In the calculation with $\gamma_r^3 = 10^{-3}$ we could not reach the subcritical maximum of C_V ($\bar{t}_{min} \approx 10^{-1}$). Due to the coincidence shown in Fig. 4.12 we have just plotted the corresponding ordinate for $\gamma_r^3 = 10^{-2}$ onto this curve.

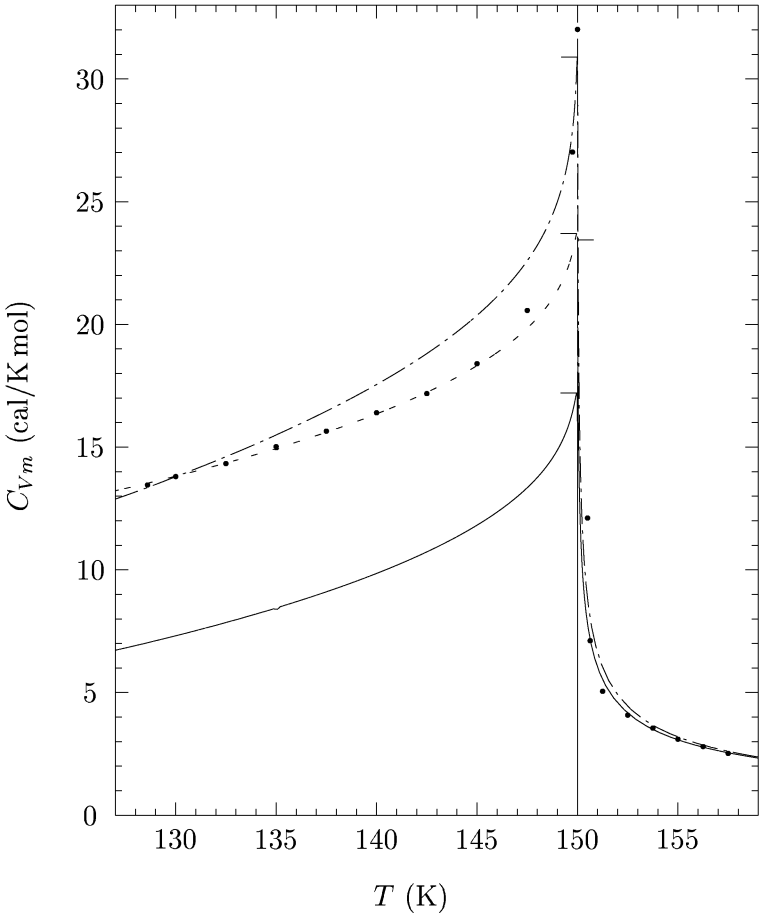

Figure 4.14: The excess molar specific heat C_{Vm} of Ar along the critical isochor versus absolute temperature T [26] (circles). These experimental data are compared with our rescaled numerical results. Solid curve: $\gamma_r^3 = 0.34$. Dash-dotted curve: $\gamma_r^3 = 0.2$. Dashed curve: $\gamma_r^3 = 0.34$ lifted subcritically. The horisontal bars indicate the maximal SCOZA values on each side of the critical point.

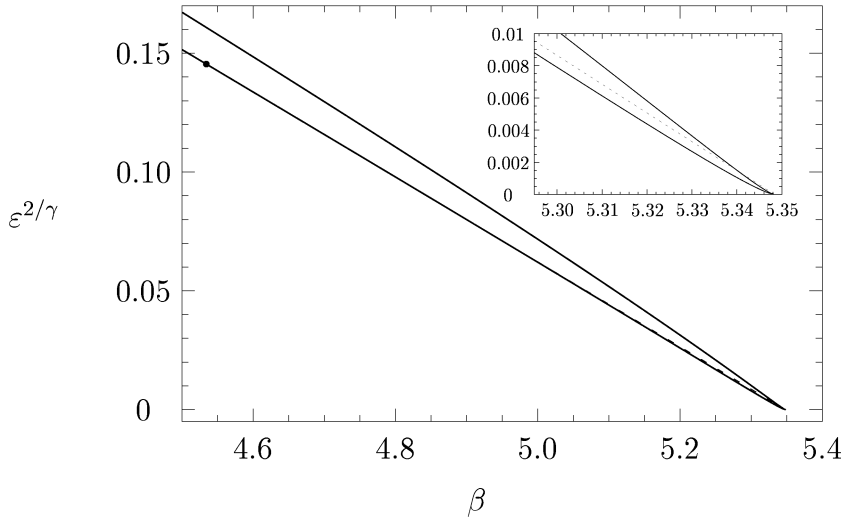

Figure 4.15: $\varepsilon^{2/\gamma}$ along the critical isochor as a function of inverse temperature β. Here $\gamma_r^3 = 0.34$, and effective values of γ are 1.23 (lower curve) and 1.30 (upper curve). Compare Fig. 4.4. The almost linear lower curve is compared with the dashed straight line.

for the effective exponent β flattens (in a maximum, see Fig. 4 in I and thus serves as a definition of the subcritical "effective" temperature region. I. e., for $t \approx 10^{-2.64}$ ($\beta \approx 5.36$) $\alpha' \approx 0.06$, $\beta \approx 0.378$, and $\gamma' \approx 1.27$. And along the critical isotherm δ is minimally 4.29 at $\Delta\rho \approx 0.4$. With these values for the critical exponents, it is clear that SCOZA ($\gamma_r^3 = 0.34$) gives a close-to-scaling solution in a region much larger than the critical region [4]. E. g., compare $\gamma = \gamma'$ (Eq. (3.31)) and the inequalities $\gamma' \geq \beta(\delta - 1) \simeq 1.24$ (Eqs. (3.23) and (3.24)) and $\alpha' + 2\beta + \gamma' \simeq 2.09 \geq 2$. Furthermore, with "exact" values $\alpha \simeq 0.1$, $\beta \simeq 0.33$, $\gamma \simeq 1.24$, and $\delta \simeq 4.8$ [27] estimated for the Ising model, the accuracy with regard to exponent values α and γ is much better within the effective region than close to the critical point. Generally, reducing the range of interaction (increasing γ_r^3) reduces the effective temperature and density regions and brings the corresponding exponents closer to their critical values. Conversely, extending the range of interaction infinitely ($\gamma_r^3 \to 0$) makes the effective solution approach the mean-field solution which scales

[4] Here γ' and δ are calculated from the particle-hole symmetric solution ε in order to compare with scaling relations outside the critical region.

perfectly outside an infinitely narrow critical region.

In Fig. 8 in I we compare the scaled equation of state (Eq. (3.35)) for SCOZA ($\gamma_r^3 = 0.34$) with the experimental results for CO_2 taken from Fig. 3.1 after Green *et al.* [18]. To correct for a miscalculated pressure $\Delta p = (p_2 - p_1)/2p_c$ (Eq. (17) in I) this figure is here redrawn as Fig. 4.16, using the same exponents $\beta = 0.38$ and $\delta = 5$ for the SCOZA results (while Ref. [18] used $\beta = 0.35$ and $\delta = 5$). Instead of using the critical pressure p_c in the denominator of Δp, we in I incorrectly used the pressures along the critical isochor ($T > T_c$) and along the coexistence curve ($T < T_c$). As a result the isotherms most far away from the critical point were shifted vertically by a small amount compared with the corrected ones in Fig. 4.16. Apart from the isotherms closest to the critical point, left out in Fig. 4.16, an even better coincidence between the SCOZA and the CO_2 curves is now obtained. Like SCOZA one notes that the CO_2 results, contrary to the assumption in Ref. [18], do not scale as they do not fall on a single curve in the region covered. Thus we find reason to believe that standard scaling must be limited to a more narrow region for real systems. For the temperatures left out, Refs. a and c in Fig. 3.1 (i. e. 3 supercritical and 2 subcritical in Fig. 8 in I), the experimental results wiggles more around the SCOZA solution. It should also be noticed that the isotherms kept are all taken from the same reference [28] (Ref. b in Fig. 3.1) and that Green *et al.* in their subsequent article [29] used exclusively the same data when analyzing CO_2 separately. (Due to systematically deviating results when including all data sources they in [29] omitted Refs. a and c in Fig. 3.1, suspecting systematic experimental errors.) The most striking coincidence displayed in Fig. 4.16 refers to the linear regime in the lower left corner $x \lesssim 0.4$, i. e. for data close to the critical isochor away from the critical temperature. With variables x and y along the axes (Eq. (16) in I) we from defenition (3.4) have

$$y \sim x\ t^{\Delta\gamma}, \tag{4.74}$$

where $\Delta\gamma = \gamma - \beta(\delta - 1)$ is the difference between the temperature dependent effective γ and the one given by the scaling relation (3.36) in terms of the values β and δ used for plotting. If $\Delta\gamma = const < 0$, the prefactor $t^{\Delta\gamma}$ increases as t decreases. For SCOZA $t^{\Delta\gamma}$ reaches a maximum at $t \approx 10^{-1.6}$ whereas the shift of the curves in the figure (including a t-dependent amplitude in (4.74)) is connected to the sign of $\Delta\gamma$. I. e. $\Delta\gamma < 0$ for $t \gtrsim 10^{-3}$. (Compare Fig. 7 in I.) Finally one should note that the original CO_2 curves are shifted -0.013 decade horizontally and -0.16 decade vertically in order to optimalize the

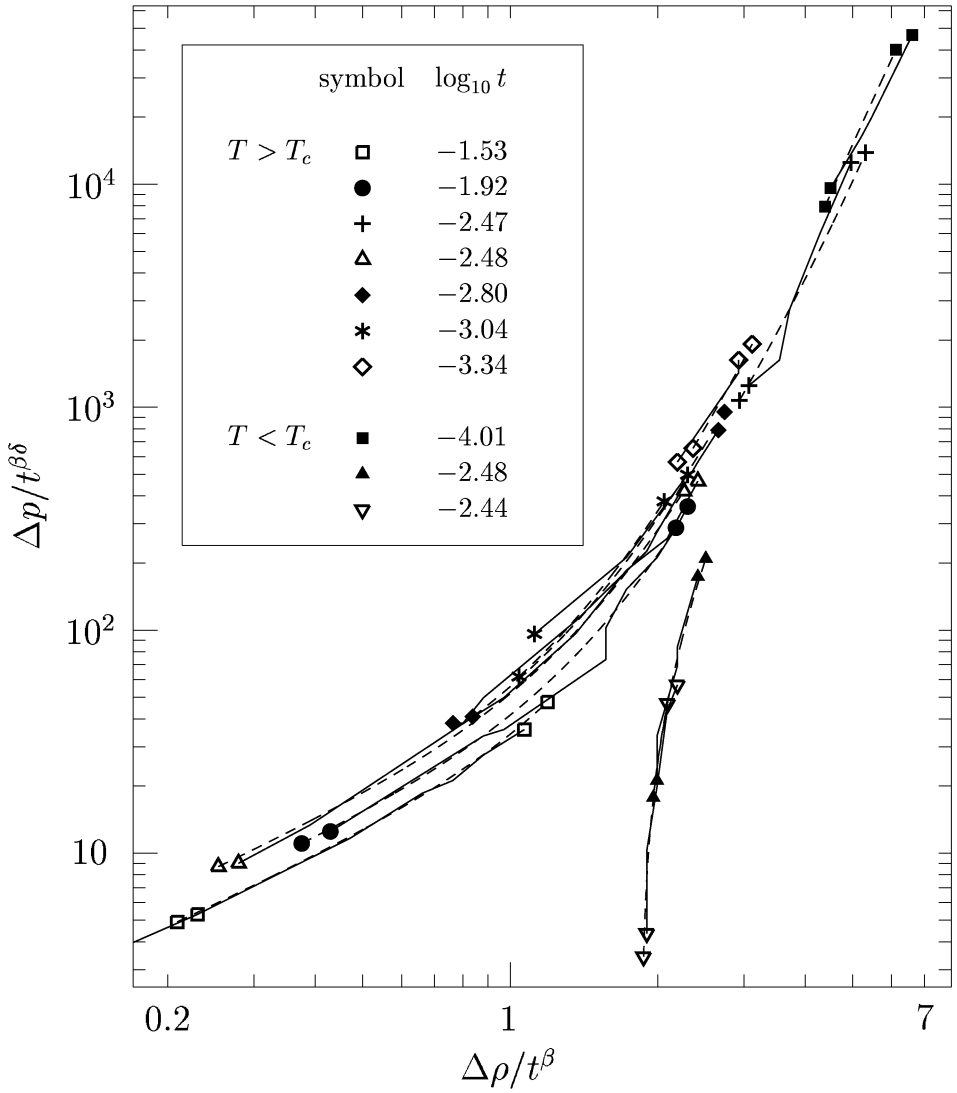

Figure 4.16: The scaled equation of state for SCOZA with $\gamma_r^3 = 0.34$ (dashed curves) compared to the experimental results for CO_2 (solid curves) taken from Ref. b [28] in Fig. 3.1. Start and endpoints for both sets of curves are indicated with symbols corresponding to the temperatures (given in the inset).

coincidence. In scaling language this corresponds to adjusting two system dependent critical amplitudes. I. e., in analogy to the scaling relations for the critical exponents by which two exponents can be chosen independently, the scaling hypothesis implies relations (ratios) between the corresponding critical amplitudes [30] defined by the coefficients in front of proportionality relations (3.1), (3.4), (3.5), and (3.6). But as we in fact are comparing a lattice-gas with a continuum fluid such a shift should be expected anyway.

4.4 Calculations for the two-dimensional case

As shown in II for the two-dimensional lattice gas, SCOZA does not give a critical point at a non-zero temperature. Nevertheless major improvements of MSA are achieved especially at low temperatures where the MSA fails severely. E. g., in case of nearest neighbor interactions on the square lattice, the internal energy along the critical isochor follows the exact solution in zero magnetic field very closely. Only near the critical point of the exact solution there is a small deviation. The corresponding maximum of the specific heat was located less than 0.3 % above the exact critical temperature. And near this maximum thermodynamic quantities show effective critical behavior which seems to mimic the exact critical behavior fairly well. In this section new and more accurate results for long-range interactions are given. A comparison with some recently reported Monte Carlo simulations is made.

4.4.1 Variable interaction range

In order to study long-range interactions on a square lattice we use the method due to Høye and Stell [31]. By this prescription the exact nearest neighbor interaction $\psi(\boldsymbol{r})$, Eq. (4.54), is replaced by a new interaction, parametrized with respect to the range of interaction. With a parameter α analogous to the density in the convolution (1.25), the new interaction is

$$\tilde{\varphi}(\boldsymbol{k}) = A\left[\frac{1}{1-\alpha\tilde{\psi}(\boldsymbol{k})} - I_\alpha\right] = 1 + \frac{1}{2}\tilde{\varphi}''(0)k^2 + \cdots. \tag{4.75}$$

The constants A and I_α ensure that $\tilde{\varphi}(0) = 1$ and $\varphi(0) = 0$, respectively, such that the new integral $P(z)$ can be calculated from (4.7) with $\tilde{\varphi}(\boldsymbol{k})$ replacing $\tilde{\psi}(\boldsymbol{k})$. (See Eqs. (21) and (22) in Sec. III of II.) The second moment $\tilde{\varphi}''(0)$ in

(4.75) determines the range of interaction, γ_r^{-1}. I. e., defined in units of the range for the nearest neighbor interaction, γ_r^{-1} is given by

$$\gamma_r^2 \equiv \frac{\tilde{\psi}''(0)}{\tilde{\varphi}''(0)} = \frac{1-\alpha}{\alpha}\left[1-(1-\alpha)I_\alpha\right]. \tag{4.76}$$

From (4.18) and (4.20) it follows that $\gamma_r^2 \simeq 1-\alpha$ as $\alpha \to 1$. In the opposite limit, $\alpha \to 0$, $I_\alpha = 1 + \frac{1}{q}\alpha^2 + \mathcal{O}(\alpha^4)$ shows that $\tilde{\varphi}(\boldsymbol{k}) \to \tilde{\psi}(\boldsymbol{k})$ and $\gamma_r^2 \to 1$. Thus $\alpha = 0$ yields the nearest neighbor interaction while $\alpha = 1$ corresponds to an infinitely long-ranged and weak potential.

4.4.2 Asymptotic relations

In this section we will study the asymptotic behavior at low and high temperatures, and near the extreme densities $\rho = 0$ and 1. Furthermore we derive the equation of state for small γ_r.

The $P(z)$, given by Eq. (22) in II, diverges weakly as $z \to 1$. It can be shown that

$$P(z) = \frac{1}{\pi}\gamma_r^2 \ln\left[\frac{8}{\gamma_r^2(1-z)}\right] + B + \mathcal{O}\left((1-z)\ln(1-z)\right), \tag{4.77}$$

where

$$B = 1-(1-\alpha)I_\alpha. \tag{4.78}$$

(4.77) generalizes (15) in II[5]. We now relate the compressibility to the internal energy (4.12), or, more specifically, to the internal energy function

$$y = \frac{P(z)-1}{zP(z)} = -\frac{2}{\rho(1-\rho)}\rho u_1. \tag{4.79}$$

As $z \to 1$, $y \to 1$, and by inverting the series expansion for $1-y$ one obtains

$$1-z \simeq \frac{8}{\gamma_r^2}\exp\left[\frac{\pi}{\gamma_r^2}\left(B-\frac{1}{1-y}\right)\right] \tag{4.80}$$

to leading order. At the same time the inverse compressibility function (4.32) behaves as

$$\varepsilon^2 \simeq \frac{8}{\gamma_r^2(1-y)}\exp\left[\frac{\pi}{\gamma_r^2}\left(B-\frac{1}{1-y}\right)\right] \overset{\alpha\to 1}{\simeq} \frac{1}{1-y}\exp\left(-\frac{\pi}{\gamma_r^2}\frac{y}{1-y}\right). \tag{4.81}$$

[5]where the correction term should be the same as in (4.77)

In the limit $\gamma_r \to 0$ ($\alpha \to 1$) we have used

$$B = 1 - \frac{1}{\pi}\gamma_r^2 \ln\left(\frac{8}{\gamma_r^2}\right) + \cdots . \tag{4.82}$$

$z \to 1$ at low temperatures and densities not too far from the "critical" isochor $\Delta\rho = 0$. The (implicit) temperature and density dependence become more evident by noting that[6]

$$x = zP(z) = \frac{1}{4}(1 - \Delta\rho^2)\beta_e \simeq \frac{1}{1-y} \tag{4.83}$$

extracts the leading dependence upon $\Delta\rho$ (Eq. (4.17)). I. e., the relation $1 - y = (1 - \varepsilon^2)/x$ gives an exponentially small correction to $1 - y \simeq 1/x$. One may therefore replace $1 - y$ by $1/x$ in (4.81) to obtain

$$1 - y \simeq \frac{1}{x} - \frac{8}{\gamma_r^2} \exp\left[\frac{\pi}{\gamma_r^2}(B - x)\right] . \tag{4.84}$$

In case of nearest neighbor interactions, the exact low-temperature behavior for the internal energy (4.79) along $\rho = 1/2$ follows from Onsager's solution (see Eq. (18) in II):

$$1 - y = 4e^{-\frac{1}{2}\beta} + \mathcal{O}\left(e^{-\frac{3}{4}\beta}\right) . \tag{4.85}$$

The corresponding exact coexistence curve $\Delta\rho(\beta)$ [32] obeys

$$1 - \Delta\rho^2 = 4e^{-\frac{1}{2}\beta} + \mathcal{O}\left(e^{-\frac{3}{4}\beta}\right) \tag{4.86}$$

at low temperatures. To leading order (4.85) and (4.86) also hold for the mean-field phase equilibrium $\Delta\mu = 0$, Eqs. (2.21) and (2.22), with y replaced by $\Delta\rho^2$ in (4.85) (symmetric mean-field term (4.11)).

At high temperatures or near the limiting densities $\rho = 0$ and 1, z is small and

$$P(z) = 1 + Cz^2 + \mathcal{O}(z^3). \tag{4.87}$$

We find

$$C = \left[\frac{1-\alpha}{1-(1-\alpha)I_\alpha}\right]^2 \left[\frac{2}{\pi}\frac{E(\alpha)}{1-\alpha^2} - I_\alpha^2\right] , \tag{4.88}$$

[6] For simplicity we write $\Delta\rho^2$ instead of $(\Delta\rho)^2$.

where I_α is defined in Eq. (21) of II, and

$$E(\alpha) = \int_0^{\pi/2} \sqrt{1 - \alpha^2 \sin^2\theta}\; d\theta \tag{4.89}$$

is the complete elliptic integral of second kind. For the nearest neighbor interaction $C = 1/4$ while $C \simeq \gamma_r^2/\pi$ when $\gamma_r \to 0$. (4.87) relates y to $1 - \varepsilon^2$ via the definitions (4.79) and (4.81). To lowest order in $1 - \varepsilon^2$,

$$y \simeq C(1 - \varepsilon^2). \tag{4.90}$$

Insertion of (4.90) into the self-consistency relation (4.3) eliminates the internal energy in favor of the inverse compressibility. Solving to first order in the density (or $1 - \rho$) then yields

$$B_2' = \frac{1}{2C}(1 - e^{C\beta}) \tag{4.91}$$

for the second "excess" virial coefficient (4.68). The mean field value $B_2' = -\beta/2$ is obtained for high temperatures or small values of γ_r^2, $C\beta \ll 1$, and corresponds to putting $z = \rho(1-\rho)\beta$.

Globally the mean-field equation of state is obtained by letting $\gamma_r \to 0$ and putting $z = \rho(1-\rho)\beta$. I. e., as long as $1 - z \gg e^{-\pi/\gamma_r^2}$, say $1 - z \sim \gamma_r^p$ with $p > 0$,

$$P(z) = 1 - \frac{1}{\pi}\left[z \ln(1-z)\right]\gamma_r^2 + \cdots, \tag{4.92}$$

for which $\varepsilon^2 \simeq 1 - z$, $x \simeq z$, and

$$y \simeq -\frac{1}{\pi}\gamma_r^2 \ln(1-z) \tag{4.93}$$

to lowest order in γ_r. The last expression gives the first order γ-correction to the absent mean-field value and with $z = \rho(1-\rho)\beta$ this is the Gaussian approximation. Furthermore $x \simeq z$ shows that the leading corrections given by the MSA ($\beta_e = \beta$ in (4.83)) are negligible outside the mean-field spinodal curve $1 - \rho(1-\rho)\beta = 0$. Beyond the Gaussian approximation, $z = \rho(1-\rho)\beta$, (4.93) relates the compressibility to the internal energy $y \sim \gamma_r^2 |\ln \gamma_r^p| \ll 1$ as follows

$$\varepsilon^2 \simeq e^{-\pi y/\gamma_r^2}. \tag{4.94}$$

One checks that the expressions (4.77) and (4.87), valid in the limits $z \to 1$ and $z \to 0$, respectively, are consistent with (4.92) when $\gamma_r \to 0$. Consequently (4.81) relates ε^2 and y correctly to lowest order in γ_r for all temperatures and densities.

In conclusion, MSA approximates the SCOZA solution well at high temperatures. The exact asymptote (4.85) provides via (4.83) an explicit behavior at low temperatures near the critical isochor. In view of the accuracy obtained for the nearest neighbor interaction in zero magnetic field, this gives us a hint what to look for in the numerical results.

4.4.3 Numerical results

In analogy to Fig. 4.3 for the three-dimensional case, Fig. 4.17 shows the inverse compressibility function ε^2 along the critical isochor $\rho = 1/2$ as a function of the inverse temperature β. The values of α used to calculate the curves in the figure are 0 (nearest neighbor interaction), 0.3, 0.6, 0.9, 0.99, and 0.999, respectively. Despite the absence of a critical point, the situation looks qualitatively much the same as for the three-dimensional case (Fig. 4.3). In both cases the graphs start out linearly for small β and curve before they apparently vanish at finite values of β. The crosses mark the point on each curve for which the corresponding specific heat along the critical isochor reaches its maximal value. See Fig. 4.19 below. Compared to the MSA a much faster decay of ε^2 is obtained for large β. While $\varepsilon^2 \simeq \frac{1}{4} e^{\pi/\gamma_r^2} \beta \exp(-\frac{\pi}{4\gamma_r^2}\beta)$ for the MSA, the SCOZA results for ε^2 seem to fall off approximately like $\exp[-\frac{k_1}{\gamma_r^2}\exp(k_2\beta)]$ (k_1 and k_2 positive constants). In fact we have used $k_1 = \pi/4$ and $k_2 = 1/2$ when plotting the dotted straight line $-\ln(-\gamma_r^2 \ln \varepsilon^2) = -\ln k_1 - k_2\beta$ (graph (a) in Fig. 4.17). This corresponds to dropping the prefactor $8\exp(\pi B/\gamma_r^2)/[\gamma_r^2(1-y)]$ in (4.81) and using (4.85) for the internal energy difference $1-y$ in the remaining exponential. Equivalently the same expression is obtained from the effective MSA-exponential $\exp(-\frac{\pi}{4\gamma_r^2}\beta_e)$ with $\beta_e = e^{\frac{1}{2}\beta}$, Eq. (4.83). The prefactor omitted above represents a weakly γ_r-dependent logarithmic correction to the straight line (a) in Fig. 4.17. But using (4.85) the full asymptote (4.81) gives only a limited improvement whereas the one for MSA ($\beta_e = \beta$, Eq. (4.83)) matches the solution perfectly at large β. See graphs (b) and (c) in Fig. 4.17 which both have been calculated with $\alpha = 0$. A separate numerical analysis shows that ε^2 and y are related by (4.81) including values ε^2 at least up to the specific heat

maximum (crosses in Fig. 4.17). In particular this relationship is demonstrated by the curves for the long-range interactions. As $\alpha \to 1$, SCOZA approaches the asymptotic solution $-\ln(-\gamma_r^2 \ln \varepsilon^2) = -\ln[\pi y/(1-y)]$ (compare (4.81)) given by the mean-field phase equilibrium $y = \Delta\rho(\beta)^2$. (See the dashed graph in the lower plot.) Along the critical isochor, Figs. 4.18 and 4.19 show the normalized internal energy $y = -8\rho u_1$ and the specific heat per particle (spin) $C_V = -(1/8)\partial y/\partial T$, respectively. Here also the exact results for the nearest neighbor interacting lattice gas, Eq. (18) in II, are shown. Apart from the MSA result, all the curves seem to coincide at low temperatures. The inset of the lower plot in Fig. 4.18 clearly shows how the mean-field and the exact nearest neighbor solution approach the low-temperature asymptote (4.85) drawn as a dotted straight line. For small γ_r the SCOZA curves practically overlap the mean-field result. As γ_r increases, the convergence towards the asymptote gradually slows down compared to the convergence of the exact nearest neighbor solution. Above the mean-field critical point ($\beta < 4$) the Gaussian approximation gives the asymptotic behavior in the limit $\alpha \to 1$. See the lower plot in Fig. 4.18 where (4.93) with $z = \beta/4$ is the dashed graph. Furthermore the over-all agreement between SCOZA (for $\alpha = 0$) and the exact result for nearest neighbor interactions is good. As in II the "critical point" for SCOZA is defined by the maximum of the specific heat and the corresponding "critical" quantities are denoted by the subscript c. In case of nearest neighbor interactions we find $\beta_c = 7.033$ and $y_c = 0.7097$, as compared with the exact values $\beta_c = 7.05098\ldots$ and $y_c = \sqrt{2}/2 = 0.707106\ldots$ (Eqs. (18) and (19) in II).

Fig. 4.20 shows a whole range of isotherms for the nearest neighbor interaction ($\alpha = 0$). The inverse compressibility ε^2 and the "magnetic" internal energy[7] $\Delta\rho^2 + (1 - \Delta\rho^2)y$ are plotted as functions of the density difference $\Delta\rho = (\rho - \rho_c)/\rho_c$. For "subcritical" temperatures both sets of curves become extremely flat in a region around the critical density $\Delta\rho = 0$. The flat regions correspond to regions where the asymptotic relation (4.81) applies. This is illustrated in Fig. 4.21 where isotherms for $-\ln(-\gamma_r^2 \ln \varepsilon^2)$ and $-\ln(1-y)$ are plotted as functions of $\ln(1-\Delta\rho^2)$. For each temperature covered ($\beta = 9, 11.5$, and 14) curves calculated with $\alpha = 0, 0.3, 0.6, 0.9$, and 0.99 have been drawn. From the lower plot in Fig. 4.21 the highly linear behavior (slope 1) around $\Delta\rho = 0$ shows that β_e is more or less independent of density

[7] equal contributions from the high and low density side, subtracted a constant, and normalized

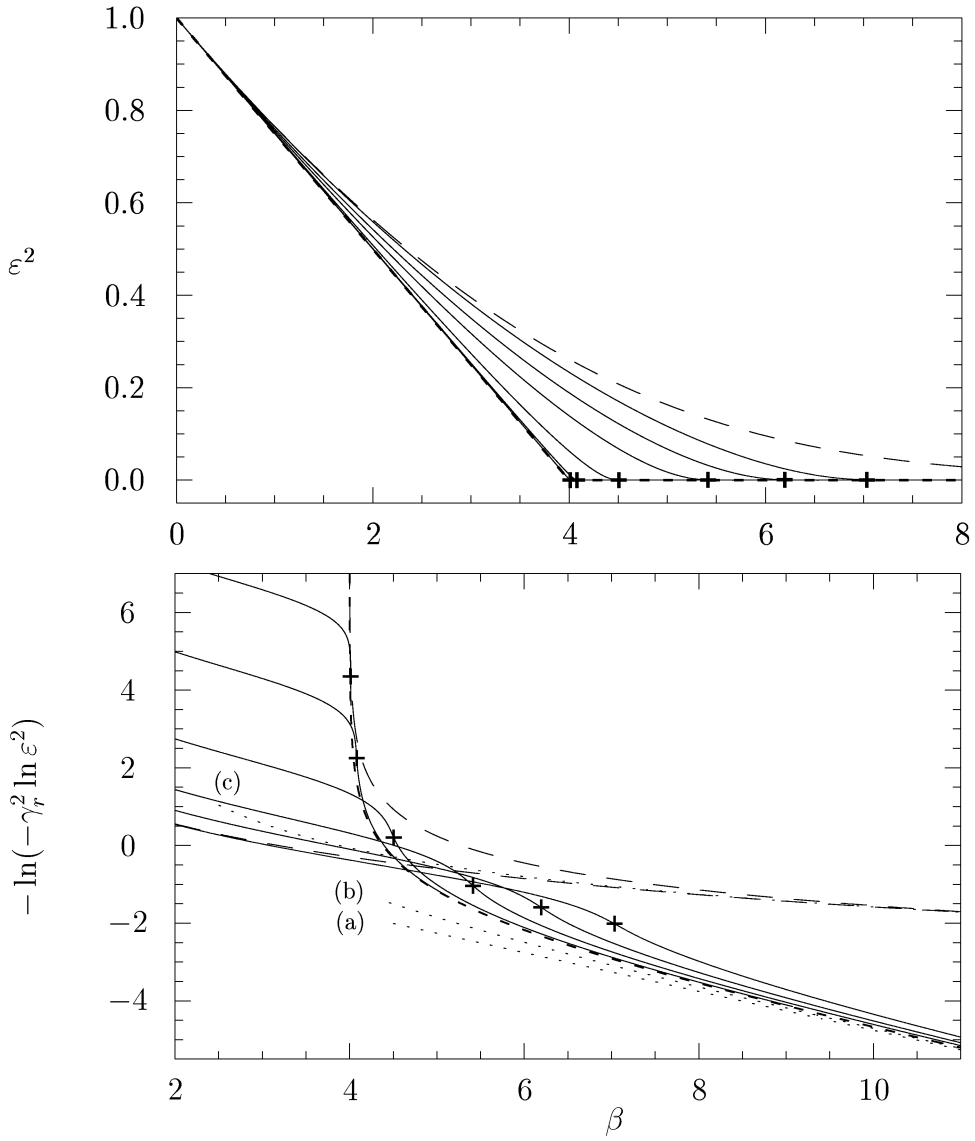

Figure 4.17: Normalized inverse compressibility ε^2 along the critical isochor as function of inverse temperature β. Solid curves: SCOZA corresponding to α values 0, 0.3, 0.6, 0.9, 0.99, and 0.999. Short dashes: Asymptotic solution $\alpha \to 1$. Crosses: Points corresponding to the maximum for the specific heat, running from right to left for increasing α. Long dashes: MSA with $\alpha = 0$ and $\alpha \to 1$ (only $\alpha = 0$ in the upper plot). Dotted lines (b) and (c): Low-temperature expression (4.81) for $\alpha = 0$ using $1-y = 4e^{-\beta/2}$ and $1-y = 4/\beta$, respectively. The straight line (a) is tangent to (b) when $\beta \to \infty$.

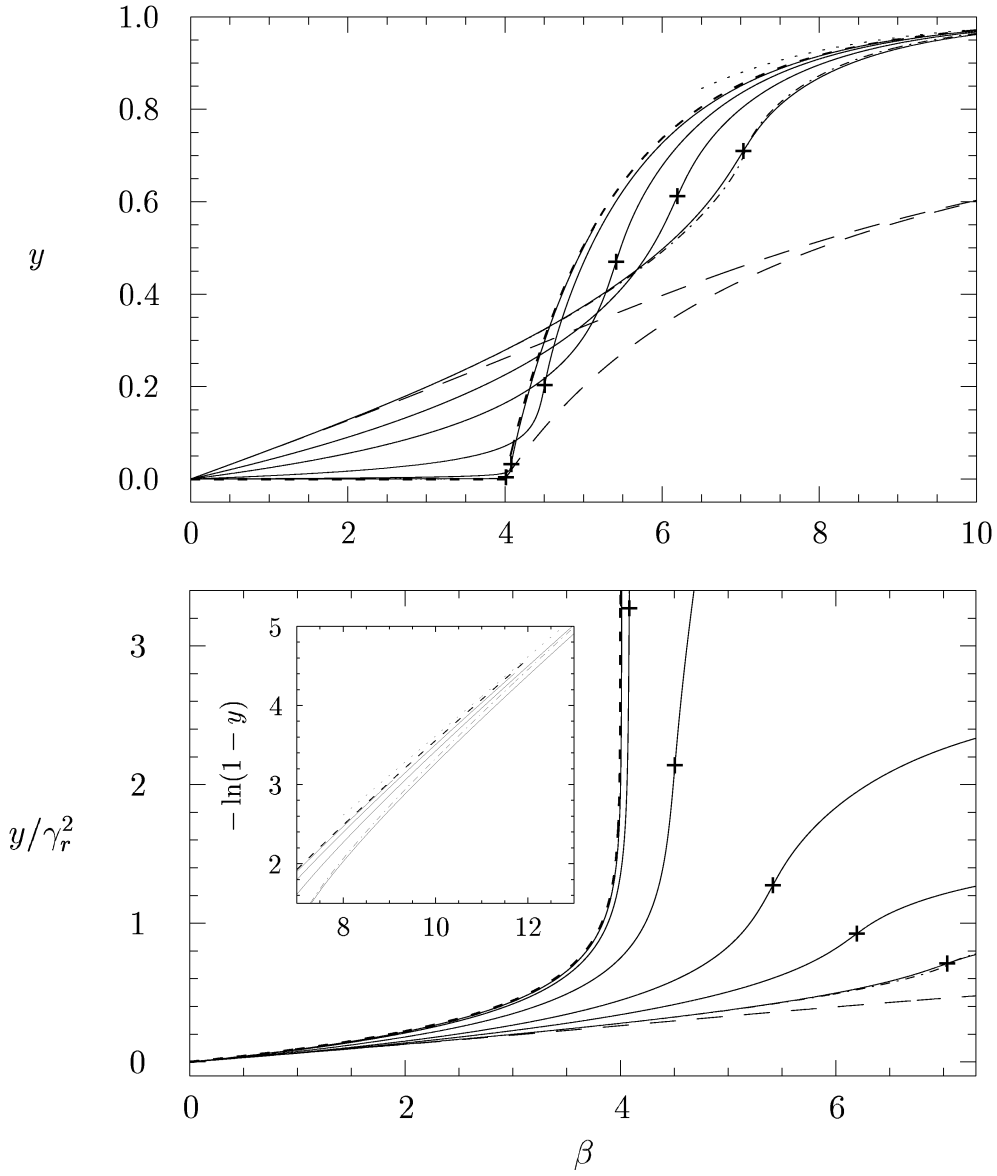

Figure 4.18: Internal energy y (4.79) along the critical isochor shown as function of inverse temperature β. Dash-dotted curve: Exact solution for two-dimensional Ising model with nearest neighbour interactions. Dotted line: Low-temperature asymptote (4.85) for the exact and the mean-field solution. Notation otherwise as in Fig. 4.17.

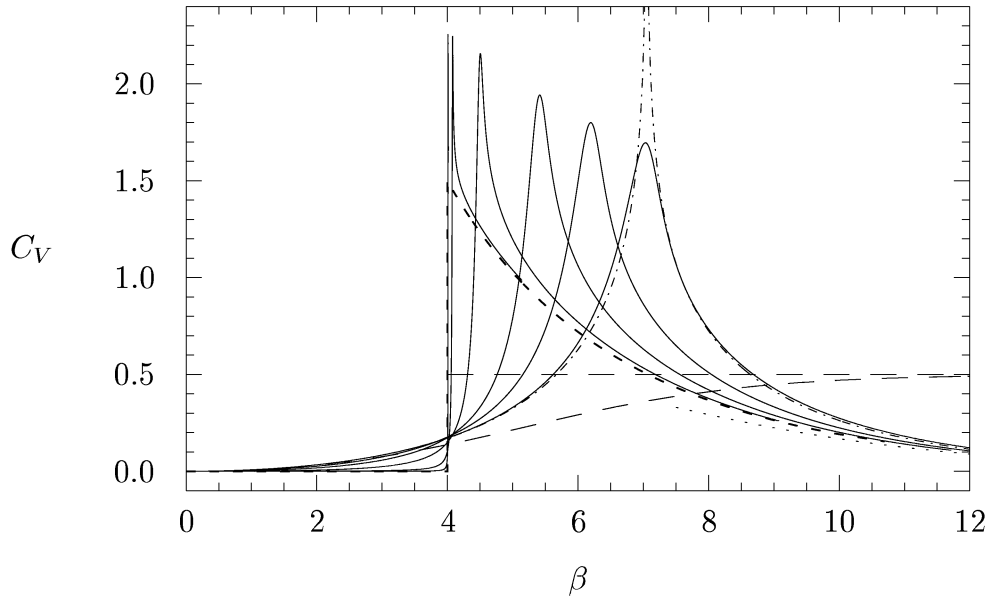

Figure 4.19: Specific heat per cell/spin C_V shown as a function of inverse temperature β along the critical isochor. Notation as in Figs. 4.17 and 4.18.

in this linear region. I. e., with $y_0 \equiv y(\Delta\rho = 0)$, $1 - y \simeq (1 - y_0)/(1 - \Delta\rho^2)$ when $1 - \Delta\rho^2 \gg 1 - y_0$, such that $\beta_e \simeq 4/(1 - y_0)$, Eq. (4.83). Hence the internal energy $\Delta\rho^2 + (1 - \Delta\rho^2)y \simeq y_0$ stays nearly constant inside the region bounded by the exact coexistence curve, Eqs. (4.85) and (4.86), $1 - \Delta\rho^2 \simeq 1 - y_0 \simeq 4e^{-\frac{1}{2}\beta}$. With $x = (1 - \Delta\rho^2)/(1 - y_0)$ and numerical constants y_0 we have plotted the asymptotes (4.81) and (4.84) for $\alpha = 0$ and $\alpha \to 1$ in Fig. 4.21. (See curves (a) and (b) for $\beta = 14$.) Only close to the intersections with their respective exact coexistence curves will there be visible deviations from the SCOZA solution. (See the vertical lines (c) and (d) for $\beta = 14$, which have been placed at values $\Delta\rho$ calculated from the mean-field and nearest neighbor phase equilibrium, respectively.) As β and/or α increases, SCOZA resembles the mean-field phase equilibrium more and more. In particular, ε^2 and y vanish at the mean-field coexistence curve. Close to the boundaries $\Delta\rho^2 = 1$ the truncated virial expansion $\varepsilon^2 = 1 + \frac{1}{2}B_2'(1 - \Delta\rho^2)$ applies, consistent with the linear graphs in the upper plot of Fig. 4.21. In the limit $\alpha \to 1$ this linear graph is the mean field solution and it extends all the way to the exact mean-field coexistence curve. At the same time the

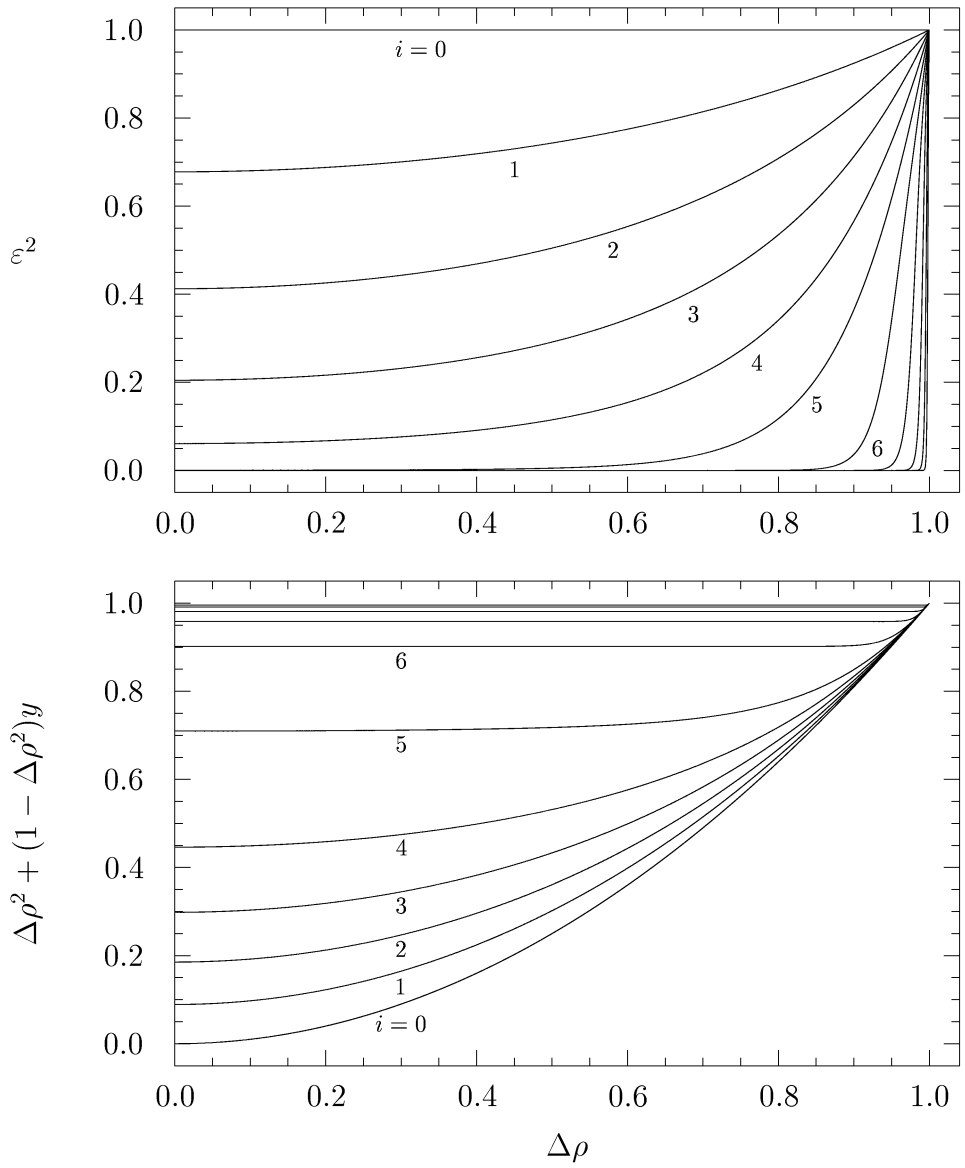

Figure 4.20: Isotherms for the nearest neighbour interaction ($\alpha = 0$) showing the inverse compressibilty ε^2 and the internal energy $\Delta\rho^2 + (1 - \Delta\rho^2)y$ as functions of the density difference $\Delta\rho$. The inverse temperatures are $\beta_i = \frac{i}{5}\beta_c$ with $i = 0, 1, \ldots, 10$.

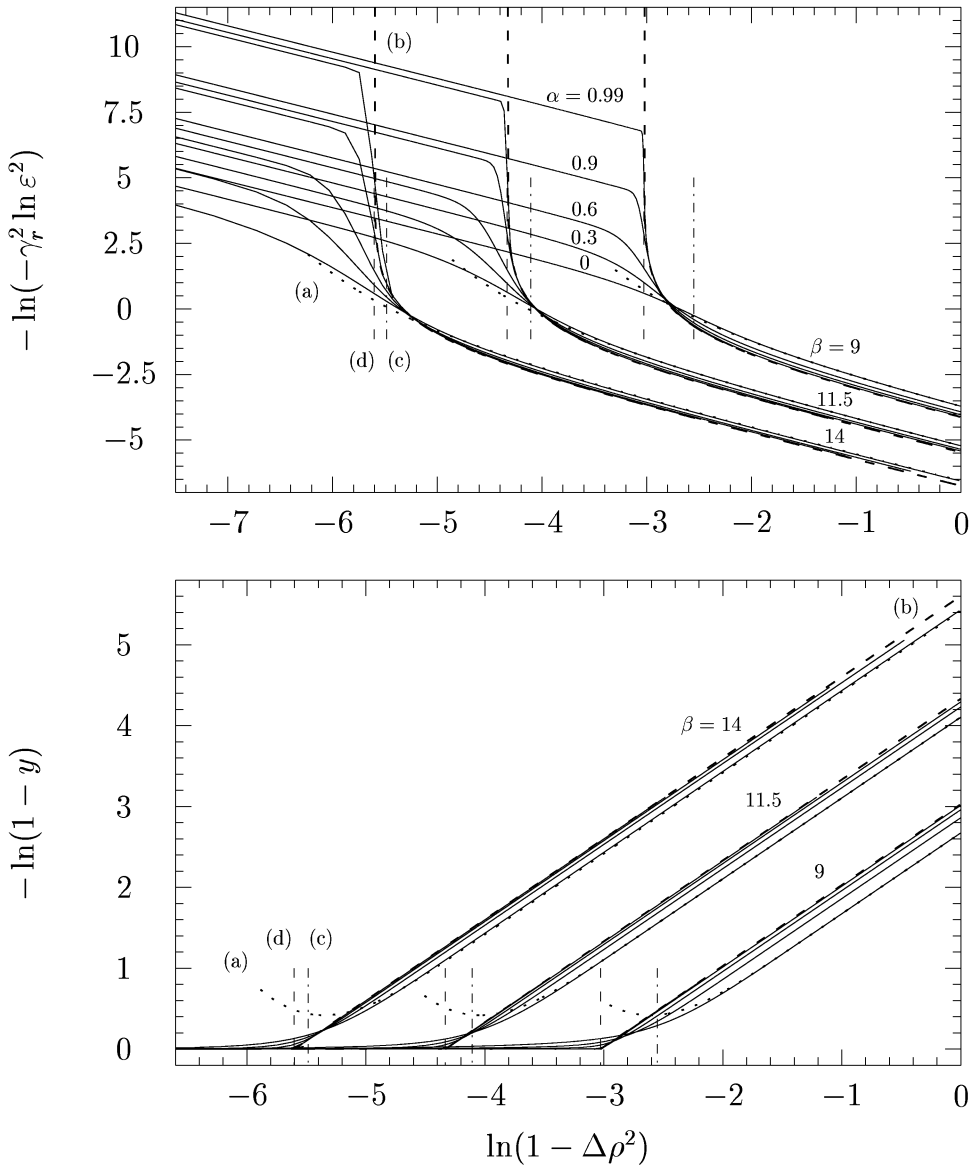

Figure 4.21: Isotherms showing $-\ln(-\gamma_r^2 \ln \varepsilon^2)$ and $-\ln(1-y)$ as functions of $\ln(1-\Delta\rho^2)$. At inverse temperatures $\beta = 9, 11.5$, and 14, the solutions for $\alpha = 0, 0.3, 0.6, 0.9$, and 0.99 have been plotted. Dotted curves (a) and dashed curves (b): Asymptotic behaviour at small densities $\Delta\rho$, for $\alpha = 0$ and $\alpha \to 1$, respectively. Vertical lines (c) and (d) mark the densities corresponding to exact phase coexistencies $\alpha = 0$ and 1, respectively.

internal energy y (lower plot) is described by the Gaussian approximation (4.93) (with $z = \frac{1}{4}\beta(1-\Delta\rho^2)$) outside the mean-field coexistence curve.

When $\gamma_r \to 0$ ($\alpha \gtrsim 0.99$) the SCOZA curves in Figs. 4.17 and 4.18 approach the mean field ones and at the same time the locations of the specific heat maxima approach the mean-field critical point; $\beta_c \to 4$, $\varepsilon_c \to 0$, and $y_c \to 0$. The ratio between the SCOZA critical temperature and the mean-field value $T_c^{MF} = 1/4$ is plotted in Fig. 4.22 as function of the inverse range of interaction squared (4.76). Results to compare with can be found in [16], in which Luijten *et al.* report a Monte Carlo simulation for an Ising model on the square lattice with variable interacting range. In their model each spin interacts equally strongly ($J_{ij} = J$) with its z neighbors lying within a radius R_m (in units of the lattice spacing). By Eq. (23) in [16] their effective range of interaction is

$$R^2 \equiv \frac{\sum_{j(\neq i)}(\boldsymbol{r_i}-\boldsymbol{r_j})^2 J_{ij}}{\sum_{j(\neq i)} J_{ij}} = \frac{1}{z}\sum_{j(\neq i)} |\boldsymbol{r_i}-\boldsymbol{r_j}|^2, \quad \text{with} \;\; r_{ij} \leq R_m.$$

Since R^2 gives the coefficient (4.15) in the Fourier series (4.14), and $R^2 = \gamma_r^{-2} = 1$ in case of nearest neighbor interactions ($z = 4, R_m = 1$), this definition matches (4.76), $R^2 \equiv \gamma_r^{-2}$. However, the shape of their potential is different from our. Tables I and II in [16] contain critical temperatures corresponding to values of R up to $\sqrt{7594/109} \approx 8.3$ (or $z = 436$). In Fig. 4.22 these results are marked by crosses. The curves for T_c/T_c^{MF} versus γ_r^2 approach unity with a finite slope when $\gamma_r \to 0$. But a slight curvature is seen all the way down to $\gamma_r = 0$. This was first noticed by Mon and Binder [33] who conjectured a logarithmic correction factor. However, the early MC-simulations of Mon and Binder covered only values up to $R \approx 3.7$. Indeed our results and the results of Luijten *et al.*, for much more long-ranged interactions, strongly suggest the presence of a logarithmic correction term. See the inset in Fig. 4.22 where the dotted straight lines indicate the asymptotic behavior

$$(1 - T_c/T_c^{MF})/\gamma_r^2 = a + b\ln\gamma_r^2, \tag{4.95}$$

when $\gamma_r \to 0$. The numerical constants are $a \approx 0.535$ and $b \approx -0.324$ for SCOZA, and $a \approx 0.288$ and $b \approx -0.301$ for the MC-data. Several perturbation schemes [34] in the region around the mean-field critical point support a shift of $\mathcal{O}(\gamma_r^2 \ln \gamma_r^2)$. Using renormalization theory Luijten *et al.* derive (4.95)

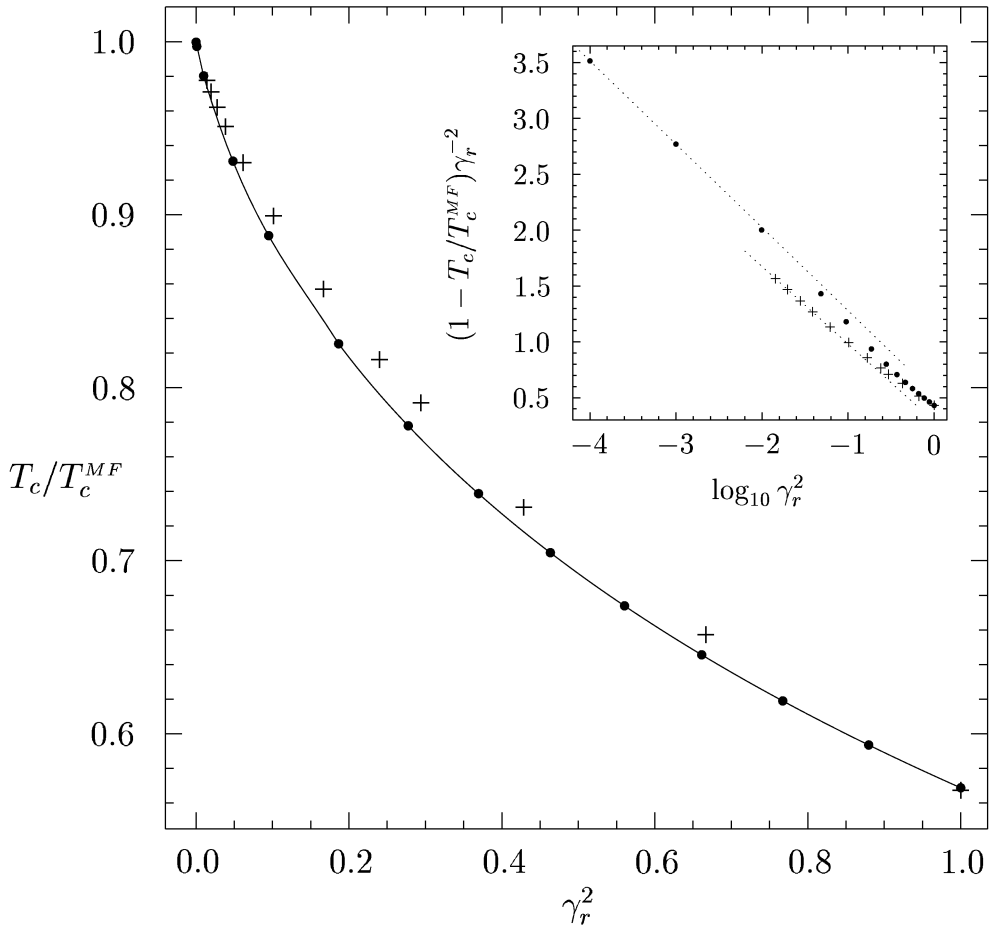

Figure 4.22: The ratio between the critical temperature T_c and the mean-field value T_c^{MF} shown as a function of the inverse range of interaction squared γ_r^2. Circles: SCOZA results. Crosses: MC-data after Luijten *et al.* [16]. For small γ_r^2 the dotted lines in the inset indicate a logarithmic correction to the shift $T_c^{MF} - T_c \sim \mathcal{O}(\gamma_r^2)$.

by studying leading corrections to scaling. For the corresponding shift in the critical internal energy we find the same asymptotic functional dependence upon γ_r. I. e., with $y^{MF} = 0$, the normalized critical internal energy y_c is given by

$$y_c/\gamma_r^2 = c + d \ln \gamma_r^2, \tag{4.96}$$

with $c \approx 1.91$ and $d \approx -0.319$. At the same time $\varepsilon_c^2/\gamma_r^2 \approx 2.39 \times 10^{-3}$ and $C_{Vc} \approx 2.26$ for small values of γ_r (Fig. 4.19). The values of c, d, and $\varepsilon_c^2/\gamma_r^2$ agree well with the asymptotic relation (4.94):

$$\varepsilon_c^2 = e^{-\pi y_c/\gamma_r^2} = e^{-\pi c}(\gamma_r^2)^{-\pi d} \tag{4.97}$$

By this the numerical value found for $\varepsilon_c^2/\gamma_r^2$ corresponds to $c \approx 1.92$ and $d = -1/\pi \approx -0.318$.

4.4.4 Effective critical behavior

Fig. 4.23 shows the magnetic susceptibility above T_c for various interaction ranges. In order to compare with the Monte Carlo results of Luijten and Blöte [35] we have plotted the scaled susceptibility

$$\bar{\chi} = \chi \gamma_r^2, \tag{4.98}$$

where

$$\chi = \frac{\partial M}{\partial H} = \frac{\beta}{\beta_c^{MF}} \varepsilon^{-2}, \tag{4.99}$$

as a function of the scaled temperature deviation

$$\bar{\tau} = \tau/\gamma_r^2, \tag{4.100}$$

where

$$\tau = (T - T_c)/T_c, \tag{4.101}$$

Eqs. (3.2) and (3.18). For large interaction ranges ($\alpha \gtrsim 0.99$) a data collapse is seen. At high temperatures $\tau \gg 1$ ($\bar{\tau} \gg 1/\gamma_r^2$), $\chi \simeq \beta/4 \simeq \beta_c/4\tau$ and the curves approach straight lines with slope -1; $\bar{\chi} = \beta_c/4\bar{\tau}$. As $\gamma_r \to 0$ these lines gradually coalesce with the classical critical asymptote $\bar{\chi} = 1/\bar{\tau}$ drawn as a dashed line in the plot. So far Fig. 4.23 looks almost identical to Fig. 4 in Ref. [35], in which interaction ranges $1.2 \leq R \leq 22$ ($0.7 \gtrsim \gamma_r^2 \gtrsim 0.002$) have been included. As SCOZA fails to give a critical point, $\bar{\chi}$ reaches a finite

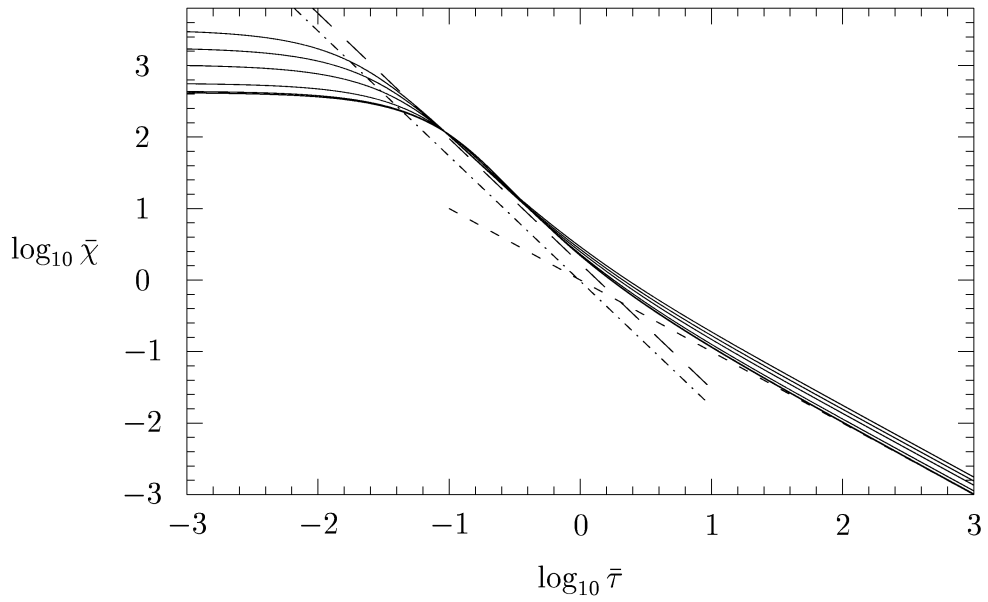

Figure 4.23: Scaled magnetic susceptibility $\bar{\chi}$ along the critical isochor plotted as function of the scaled temperature deviation $\bar{\tau}$ ($T > T_c$). The α values $0, 0.3, 0.6, 0.9, 0.99, 0.999, 0.9999$ and 0.99999 run from the top down and the curves for $\alpha \geq 0.99$ collapse. Short dashes: Mean-field critical asymptote. Dash-dotted curve: Critical asymptote for the nearest neighbour Ising model (slope $-7/4$). Long dashes: Ising-like critical asymptote obtained from MC-simulations [35].

value and the curves in Fig. 4.23 become horizontal when $\bar{\tau} \to 0$. But before this effect sets in, effective critical behavior resembling the exact critical one is observed. I. e., in a region around $\bar{\tau} \simeq 10^{-0.5}$, the effective critical exponent $\gamma = -\partial \log \chi / \partial \log \tau$ is not very different from the exact exponent 1.75. (See Fig. 4.24.) Furthermore we compare the magnitude of the susceptibility with critical Ising asymptotes $\bar{\chi} = \Gamma \bar{\tau}^{-7/4}$. From Fig. 4 in Ref. [35] we find $\Gamma \approx 1.7$ for the MC-data (all interaction ranges), whereas $\Gamma = 0.96258\ldots$ is known exactly for the nearest-neighbor Ising model [36, 35]. It is clear from Fig. 4.23 that around $\bar{\tau} \simeq 10^{-0.5}$ SCOZA gives a slightly higher susceptibility than the one given by the Monte Carlo simulations (dashed line). Fig. 4.24 shows the effective exponents γ calculated from the curves in Fig. 4.23. The dashed graph is an average of the six different curves (R values) in Fig. 5 of Ref.

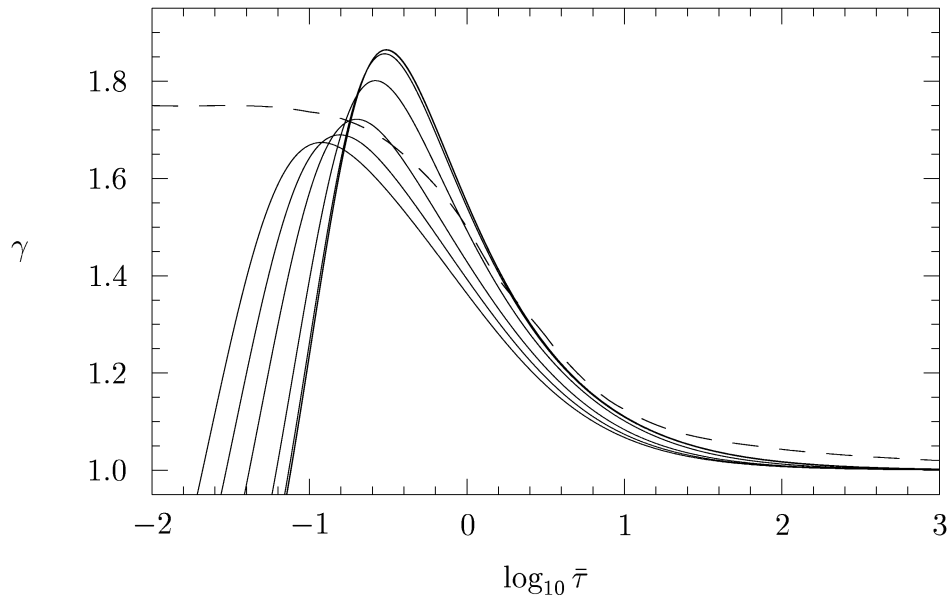

Figure 4.24: Effective critical exponent γ for the susceptibility curves in Fig. 4.23. The α values $0, \ldots, 0.99999$ run from left to right. The dashed curve shows the unique (γ_r independent) crossover curve obtained from MC-simulations [35].

[35], and shows the crossover from mean-field to Ising-like critical behavior obtained from the strictly collapsed MC suceptibility data. The uncertainty of this average graph easily amounts to as much as 0.1 units in the vertical direction. Thus the collapsed SCOZA curves ($\alpha \gtrsim 0.99$) are consistent with the universal MC-crossover for $\bar{\tau} \gtrsim 1$.

In analogy to Figs. 4.23 and 4.24, Fig. 4.25 shows the specific heat C_V and the associated effective critical exponent $\alpha = -\partial \log C_V / \partial \log \tau$. (The critical index α should not be confused with the interaction parameter α in (4.75).) At high temperatures, $\tau \gg 1$, $y \simeq \frac{1}{4} C\beta$ (from (4.87) with $z = \beta/4$) and $C_V \simeq \frac{1}{32} C\beta^2 \simeq \frac{1}{32} C\beta_c^2/\tau^2$. This behavior gives straight lines with slope -2 to the right in the upper plot of Fig. 4.25, and for large interaction ranges ($C \simeq \gamma_r^2/\pi$ and $\beta_c \simeq 4$) these lines are given by $C_V \simeq 1/(2\pi\gamma_r^2\bar{\tau}^2)$, $\bar{\tau} \gg 1/\gamma_r^2$. At the critical point C_V reaches a finite value whereas the exact C_V for the nearest neighbor Ising model diverges logarithmically. (See the dash-dotted lines in both figures for which τ measures the distance from the *exact* T_c.)

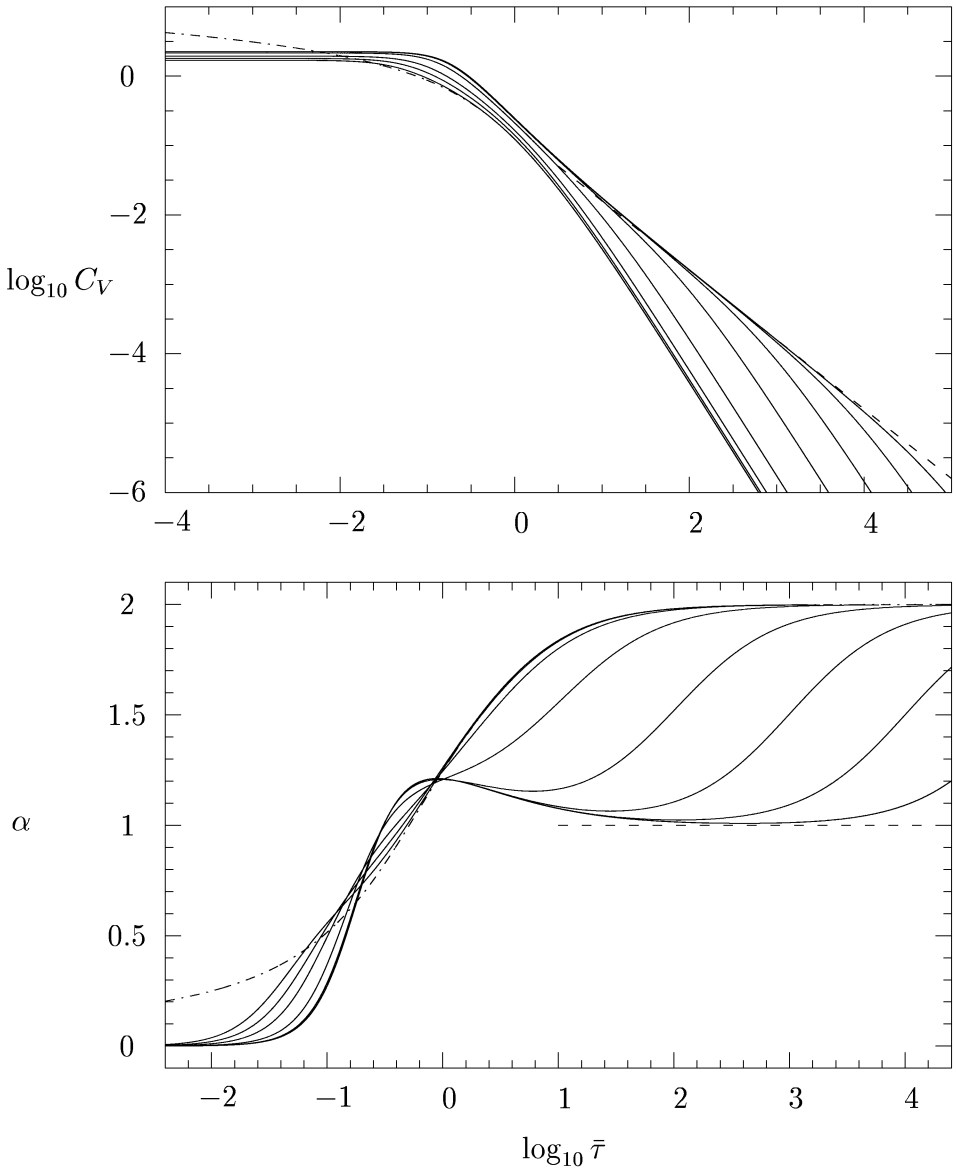

Figure 4.25: Specific heat C_V along the critical isochor and corresponding effective critical exponent α plotted as functions of the scaled temperature deviation $\bar{\tau}$ ($T > T_c$). The α values (interaction parameters) $0, 0.3, 0.6, 0.9, 0.99, 0.999, 0.9999$ and 0.99999 run from left to right. Dash-dotted curve: Exact solution for the nearest neighbour Ising model. Dashed line: Asymptotic behavior $\gamma_r \to 0$ for $\bar{\tau} \gg 1$.

SCOZA (with $\alpha = 0$) approximates the exact solution very well for $\tau \gtrsim 10^{-0.5} \approx 0.3$ (compare Fig. (4.19)) and the saturation of C_V does not become evident until $\tau \sim 10^{-2}$. As $\gamma_r \to 0$ the curves in Fig. 4.25 collapse except at the high-temperature asymptotes and an interval where $C_V \simeq 1/(2\pi\bar{\tau})$ and the effective exponent α takes the Gaussian value 1, Eq. (3.21), opens up outside the critical region. (See the dashed lines.) This result follows from (4.93) if one replaces $1 - z$ with τ. It is clear that this behavior is only seen for very large interaction ranges ($\gamma_r^2 \lesssim 10^{-5}$) for which the effective exponent $\alpha \approx 1$. Moreover the crossover from the Gaussian region to the critical one is nonmonotonic. I. e., the universal curve for the effective α varies smoothly from 1 to 0 but has a maximal value ≈ 1.2 at $\bar{\tau} \approx 1$. However this special behavior develops continuously for increasing interaction range and may be connected to the deviation between the exact nearest neighbor solution and the one for SCOZA (with $\alpha = 0$) close to the critical point. Since the internal energy satisfies the exact high and low temperature limits ($y = 0$ and 1), the specific heat integrates up to the exact value $\int_0^\infty C_V(\beta)\, d\beta$. Possibly, with $C_V \simeq 1/(2\pi\bar{\tau})$ for $\bar{\tau} \gg 1$ ($\gamma_r \to 0$), the effective exponent α exceeds 1, $\bar{\tau} \sim 1$, to compensate for the exact divergence, $\bar{\tau} \ll 1$. The effective critical behavior of the specific heat below T_c is shown in Fig. 4.26. At low temperatures $C_V \simeq \frac{1}{4}\beta^2 e^{-\frac{1}{2}\beta}$ vanishes due to saturation $\Delta\rho^2 \to 1$, Eqs. (4.85) and (4.86), for which the curves in Fig. 4.26 approach vertical asymptotes at $-\bar{\tau} = 1/\gamma_r^2$. As $\gamma_r^2 \to 0$, SCOZA is accurately described by the mean field outside the critical region. Hence a data collapse onto the maximal mean-field value $C_{Vc}^{MF} = 3/2$ (dashed asymptote (a) in Fig. 4.26.) is to be expected in the region $1 \ll -\bar{\tau} \ll 1/\gamma_r^2$. But due to numerical limitations at low temperatures, we were barely able to reach the maximum of C_V for $\alpha = 0.999$. However a clear tendency towards a unique asymptotic solution $\gamma_r \to 0$ is seen for our largest interaction ranges. Thus, for $\alpha \gtrsim 0.99$ and $-\bar{\tau} \lesssim 10^{-1}$, C_V approaches a maximal plateau. And outside the "critical" region mean-field theory seems to give a good description. (See the dashed curves calculated for $\alpha = 0.9$, 0.99, and 0.999.) In case of nearest neighbor interactions the SCOZA result follows the exact solution closely for $-\bar{\tau} \gtrsim 10^{-1.5}$.

4.4.5 The MSA solution

Also for the MSA one has $\varepsilon^2 \simeq 1 - z \sim \gamma_r^2$ at the critical point defined by the SCOZA solution. This follows from $x = zP(z) = \beta/4 = 1 + \mathcal{O}(\gamma_r^2 \ln \gamma_r^2)$, Eqs. (4.92) and (4.95). Via $x(1 - y) = 1 - \varepsilon^2$ and the asymptotic relation

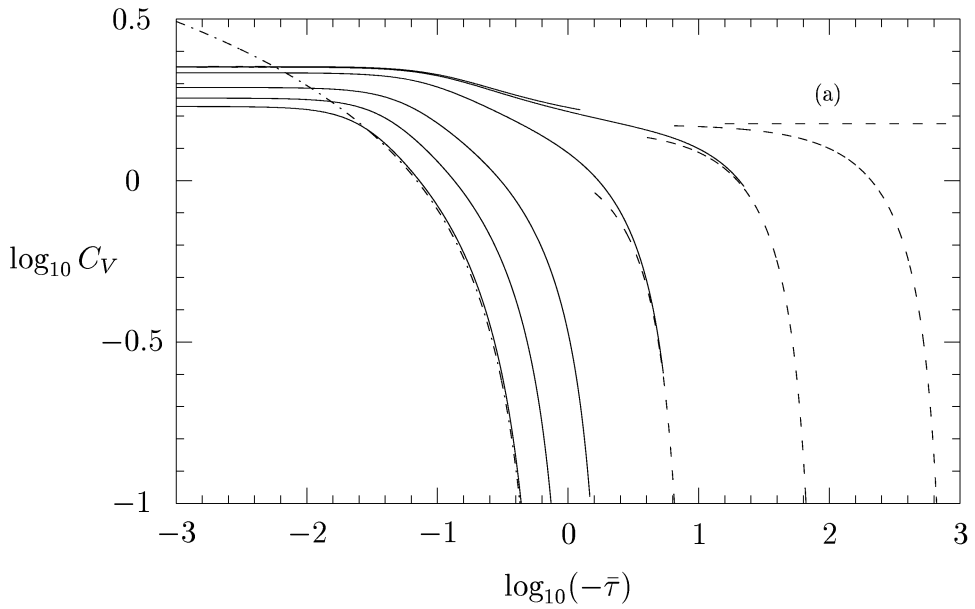

Figure 4.26: Specific heat C_V along the critical isochor plotted as function of the scaled temperature deviation $\bar{\tau}$ ($T < T_c$). The α values $0, 0.3, 0.6, 0.9, 0.99$ and 0.999 run from left to right. Dash-dotted curve: Exact solution for the nearest neighbour Ising model. Dashed curves: Mean-field solution for $\alpha = 0.9, 0.99$, and 0.999. Dashed line (a): Classical critical asymptote $\gamma_r \to 0$.

(4.94) we therefore use

$$x(1 + \frac{1}{\pi}\gamma_r^2 \ln \varepsilon^2) = 1 - \varepsilon^2 \tag{4.102}$$

to find the MSA solution $\varepsilon(x)$ in the limit $\gamma_r \to 0$. In order to have an asymptotic (i. e. γ_r-independent) solution we introduce

$$\bar{\varepsilon}^2 = \varepsilon^2/\gamma_r^2, \tag{4.103}$$

and one immediately realizes that

$$\bar{\Delta x} = \bar{\varepsilon}^2 + \frac{1}{\pi} \ln \bar{\varepsilon}^2, \tag{4.104}$$

where

$$\Delta x = \gamma_r^2 \bar{\Delta x} = 1 - \frac{1}{\pi}\gamma_r^2 \ln \gamma_r^2 - x. \tag{4.105}$$

Note that there is no natural choice of zero for $\bar{\Delta x}$ since a shift $\bar{\Delta x} \to \bar{\Delta x} - a$ does not bring us outside the critical region $x = 1 + \mathcal{O}(\gamma_r^2 \ln \gamma_r^2)$. By inverting (4.104) for large and small $\bar{\varepsilon}^2$ one gets

$$\bar{\varepsilon}^2 = \begin{cases} \bar{\Delta x}\left(1 - \frac{1}{\pi}\frac{\ln \bar{\Delta x}}{\bar{\Delta x}} + \cdots\right), & 1 \ll \bar{\Delta x} \ll 1/\gamma_r^2 \\ e^{\pi \bar{\Delta x}}\left(1 - \pi e^{\pi \bar{\Delta x}} + \cdots\right), & \ln \gamma_r^2 \ll \bar{\Delta x} \ll -1 \end{cases}, \tag{4.106}$$

respectively. These conditions follow from dropping higher order terms in (4.102). In particular $\bar{\Delta x} \gg \ln \gamma_r^2$ stems from demanding the smallest term kept to be dominant compared to the corrections of $\mathcal{O}(\gamma_r^2)$, Eq. (4.104). So by neglecting the term $\bar{\varepsilon}^2$ in (4.104), we obtain $\bar{\varepsilon}^2 \simeq e^{\pi \bar{\Delta x}}$ at "subcritical" values $-1/\gamma_r^2 \ll \bar{\Delta x} \ll -1$, in agreement with the asymptotic behavior $z \to 1$ and $\gamma_r \to 0$ (Eqs. (4.81), (4.84) and (4.105)). For large $\bar{\Delta x} > 0$ (4.106) reproduces the classical critical asymptote $\bar{\varepsilon}^2 = \bar{\Delta x}$ in accordance with the Ginzburg criterion (3.18). Provided that $\bar{\Delta x} = 0$ yields the dominant contribution to the shift (4.95) for SCOZA (i. e. $(1-1/x)\gamma_r^{-2} = -(1/\pi)\ln \gamma_r^2$ corresponding to $b = -1/\pi$), (4.106) shows that MSA is capable of renormalizing the first-order γ-expansion (diverging at $x = 1$) although $\bar{\Delta x} = 0$ does not correspond to a critical point. With $W(f)$ defined as the inverse function of $f(W) = We^W$ (Lamberts W function [37]) and W_0 being the only (real) branch for $f \geq 0$, the general solution of (4.104) is

$$\bar{\varepsilon}^2 = \frac{1}{\pi} W_0\left(\pi e^{\pi \bar{\Delta x}}\right). \tag{4.107}$$

Correspondingly

$$C_V = \frac{1}{2}\frac{1}{1 + W_0(\pi e^{\pi \bar{t}})} = \frac{1}{2\pi}\frac{1}{\bar{t}} + \frac{1}{2\pi^2}\frac{\ln \bar{t} - 1}{\bar{t}^2} + \cdots, \quad \bar{t} \gg 1, \tag{4.108}$$

for the specific heat along the critical isochor.

Beyond the classical result $\bar{\varepsilon}^2 = \bar{\Delta x}$, (4.106) gives the leading deviation outside the critical region. Assuming $b = -1/\pi$ and measuring $\bar{\Delta x}$ relative to SCOZA's critical point, $\bar{\Delta x} \to \bar{\Delta x} - a$,

$$\bar{\varepsilon}^2 - \bar{\Delta x} \simeq -\frac{1}{\pi}\ln \bar{\Delta x} - a, \qquad 1 \ll \bar{\Delta x} \ll 1/\gamma_r^2. \tag{4.109}$$

In Fig. 4.27 we have shown the deviation (4.109) for SCOZA along the critical isochor ($\Delta x = t$) and critical isotherm ($\Delta x = \Delta\rho^2$). As the MSA gives the

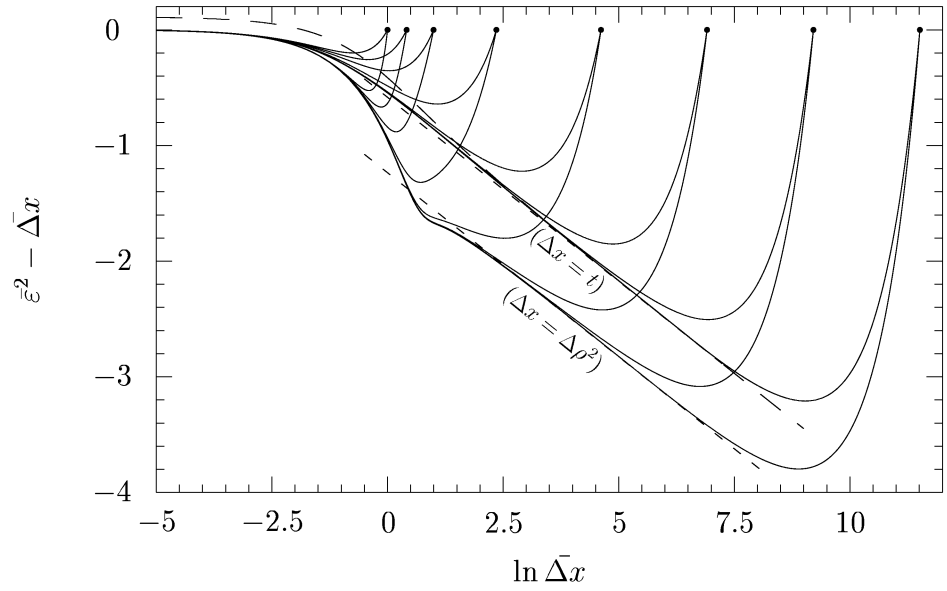

Figure 4.27: Deviation from the classical critical asymptote $\bar{\varepsilon}^2 = \bar{\Delta}x$ along the critical isochor ($\Delta x = t > 0$) and critical isotherm ($\Delta x = \Delta\rho^2$). Δx is measured from the critical point for SCOZA. Solid lines: SCOZA with the same values α as used in Fig. 4.23. Endpoints at $\beta = 0$ and $\Delta\rho^2 = 1$ (circles) run from left to right for increasing α. Short dashes: The asymptotic behaviour (4.109). Long dashes: The asymptotic MSA solution (4.107).

same solution along either direction, the constant a in (4.109) effectively increases for SCOZA along the critical isotherm. See Fig. 4.27 where the two straight lines, representing the asymptotic behavior (4.109), have been drawn with $a = 0.583$ ($\Delta x = t$) and $a = 1.23$ ($\Delta x = \Delta\rho^2$). The exact value of the constants b and d defined by (4.95) and (4.96) is in fact $-1/\pi$ for any long-range potential $\gamma_r \to 0$ on the square lattice. This follows from the MSA "critical" point $1 - z = \text{const}\,\gamma_r^2 \to 0$, and from (4.92), which gives the exact result $P(z) = 1 - (1/\pi)\gamma_r^2 \ln \gamma_r^2 + \mathcal{O}(\gamma_r^2)$. See the proof in Appendix A. With respect to the linear fitting performed on the SCOZA results one should note that $d \approx -0.319$ is quite accurate while $b \approx -0.324$ (in combination with $a \approx 0.535$) is less precise. On the other hand the straight line (4.95) with $a = 0.583$ and $b = -1/\pi = -0.318$ intersects our leftmost (smallest γ_r) point in the inset of Fig. 4.22, and this indicates that γ_r^2 typically has to be

less than 10^{-4} for the asymptotic result (4.95) to be valid. Presumably this explains the somewhat inaccurate Monte Carlo value $b \approx -0.301$ (my own fit) as $\gamma_r^2 \gtrsim 10^{-2}$ for those data.

With the successful renormalization (4.105) and the energy-compressibility relation (4.94) the energy route (4.48) leads to

$$\overline{\beta\Delta\mu} = 2\bar{\Delta\rho}\left(\bar{t} + \frac{1}{3}\bar{\Delta\rho}^2 - \frac{1}{\pi}\ln\bar{\varepsilon}^2\right), \tag{4.110}$$

for the scaled chemical potential $\overline{\beta\Delta\mu} = \beta\Delta\mu/\gamma_r^3$ to zeroth order in γ_r^2. In this way the mean-field phase coexistence is recovered outside the critical region $-t \gg \gamma_r^2$, or, more precisely, $\bar{\Delta x} \simeq -2\bar{t} \gg 1$. Furthermore an irregular thermodynamic behavior similar to the one found for the three-dimensional MSA solution (Sec. 4.3.2) is obtained close to the critical point $|t| \lesssim \gamma_r^2$. With $\bar{\Delta x} = \bar{t} + \bar{\Delta\rho}^2$, Eqs. (4.107) and (4.110) yield

$$-2\bar{t} = \frac{2}{3}\bar{\Delta\rho}^2 - \frac{2}{\pi}\ln\left(\frac{2}{3}\bar{\Delta\rho}^2\right), \tag{4.111}$$

for the coexistence curve $\overline{\beta\Delta\mu} = 0$. (Outlined in Appndix B.) $\bar{\Delta\rho}$ as a function of $\bar{t}$ has a branch-point at $\bar{t} = [\ln(2/\pi) - 1]/\pi \approx -0.46$, $\bar{\Delta\rho}^2 = 3/\pi$, analogous to the point $\bar{t} = 1/2$, $\bar{\Delta\rho}^2 = 3/2$ in $d = 3$, Eq. (4.51). To recover the mean-field result one must choose the outer branch W_{-1} of the Lambert function,

$$\frac{2}{3}\bar{\Delta\rho}^2 = -\frac{2}{\pi}W_{-1}[-(\pi/2)e^{\pi\bar{t}}] \tag{4.112}$$

Correspondingly it follows from (4.104) and (4.111) that

$$\bar{\varepsilon}^2 = \frac{2}{3}\bar{\Delta\rho}^2 = -2\bar{t} + \frac{2}{\pi}\ln(-2\bar{t}) + \cdots. \tag{4.113}$$

To zeroth order in γ_r^2 the mean-field configurational energy gives a contribution $C_{V0} = -\frac{1}{2}d(\bar{\Delta\rho}^2)/d\bar{t} \simeq 3/2 + (3/\pi)(-2\bar{t})^{-1}$ to the specific heat. Similarly $C_{V1} = \frac{1}{2\pi}d\ln\bar{\varepsilon}^2/d\bar{t} \simeq -(1/\pi)(-2\bar{t})^{-1}$ comes from the excess part of configurational energy along the coexistence curve. As found in $d = 3$, Eq. (4.53), the Gaussian correction (3.21) to the simple mean-field term 3/2 in the specific heat is positive. I.e.,

$$C_V = \frac{1}{2}\,\frac{1 + 3\,W_{-1}[-(\pi/2)e^{\pi\bar{t}}]}{1 + W_{-1}[-(\pi/2)e^{\pi\bar{t}}]} = \frac{3}{2} + \frac{2}{\pi}\frac{1}{(-2\bar{t})} + \cdots, \quad -\bar{t} \gg 1. \tag{4.114}$$

At the top of the coexistence curve (4.111) $C_V(> 0)$ diverges. In fact the leading behavior close to the branch-point is qualitatively equal to that described by Eqs. (4.51)–(4.53) in $d = 3$.

It is evident from the SCOZA results shown in Fig. 4.27 that the logarithmic correction term follows selfconsistently from the MSA also along the critical isotherm (MSA is fully thermodynamic selfconsistent along the critical isochor). More specifically the energy route yields

$$\bar{\varepsilon}^2 = \frac{1}{2}\left(\frac{\partial\overline{\beta\Delta\mu}}{\partial\bar{\Delta}\rho}\right)_{\bar{t}=0} = \bar{\Delta}\rho^2 - \frac{1}{\pi}\ln\bar{\Delta}\rho^2 - \frac{2}{\pi} + \cdots. \tag{4.115}$$

Eq. (4.106) cannot account for the constant $2/\pi \approx 0.637$. As this term in fact almost equals the height $1.23 - 0.583 = 0.647$ between both sets of SCOZA curves $\Delta x = \Delta\rho^2$ and $\Delta x = t$ in Fig. 4.27, (4.115) demonstrates how close the SCOZA is to yield a MSA-like phase coexistence (energy-route) just by lowering the critical point $\bar{t} \to \bar{t} - a$. With regard to selfconsistency the situation along the coexistence curve $\overline{\beta\Delta\mu} = 0$ is exactly the same, and the logarithmic term in the compressibility result (4.113) is reproduced by $\bar{\varepsilon}^2 = \frac{1}{2}\partial\overline{\beta\Delta\mu}/\partial\bar{\Delta}\rho$.

Unfortunately the numerical integration of the basic PDE (4.13) breaks down before reaching the asymptotic regime[8] $\bar{t} \ll -1$. However, as outlined in the previous paragraph we know that SCOZA will only have perturbative effects upon the MSA solution in this region. To compare with the subcritical results obtained from the Monte Carlo simulations of Luijten *et al.* [35] we therefore concentrate on the MSA solution. A special feature obtained by these simulations is the *nonmonotonic* variation of the effective critical exponent γ'. I. e., γ' drops below the interval set by the mean-field and Ising limits 1 and 1.75, respectively. (See Fig. 4.28.) This effect is well described by the MSA solution. By lowering the critical point $\bar{t} \to \bar{t} - a$, and taking the logarithmic derivative of (4.113), we obtain

$$\gamma' = 1 - \frac{2}{\pi}\frac{\ln(-2\bar{t}) + \pi a - 1}{(-2\bar{t})} + \cdots, \quad -\bar{t} \gg 1. \tag{4.116}$$

Whereas the correction term in (4.116) is dominated by the denominator both for large and small values of $-\bar{t}$, its sign is essentially governed by the logarithm. At $\ln(-2\bar{t}) = 2 - \pi a$, corresponding to $-\log_{10}(-\bar{t}) \approx -0.17$ for

[8] due to extremely small numbers which the computer cannot handle.

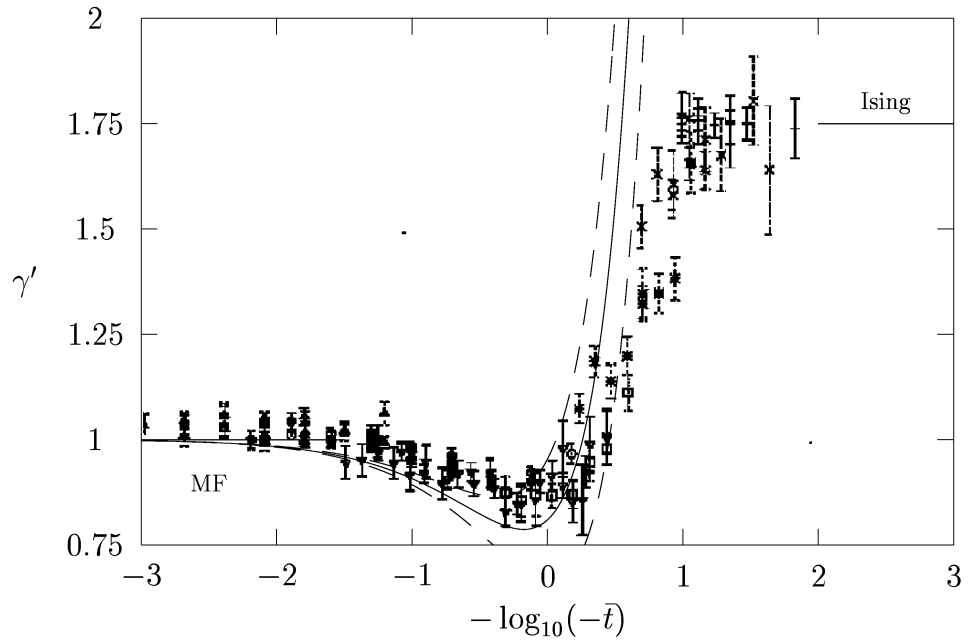

Figure 4.28: Effective subcritical exponent γ' for the compressibility, shown as function of reduced temperature $\bar{t}$. Points with error bars: Monte-Carlo results after Luijten *et al.* [35]. Curves: MSA solution (4.116) for $a/a_{MC} = 0.5, 1, 1.5$ with γ' decreasing with increasing a. Here $a_{MC} = 0.288$ is taken from Fig. (4.22). γ' varies nonmonotonically between the mean-field value 1 and the Ising value 1.75 for the MC-data.

the MC value $a_{MC} \approx 0.288$, γ' takes the minimum value $1 - 2e^{\pi a - 2}/\pi \approx 0.79$. From the MC-data shown in Fig. 4.28 it is clear that this is not a bad estimate although higher order terms in (4.116) dominate for $-\bar{t} \ll 1$. (See the solid line drawn with $a = a_{MC}$.) We have also plotted (4.116) with the values $a/a_{MC} = 0.5$ and 1.5. Judging from the curvature seen for the MC-data in the inset of Fig. 4.22, one should suspect the numerical value a_{MC} to be somewhat high. With slope $b = -1/\pi$ the straight line with $a = 0.215$ intersects the leftmost MC-point in Fig. 4.22. If so, a slightly better agreement between the MSA solution and the MC points is obtained for $-\bar{t} \gtrsim 1$. But inside the critical region, $-\bar{t} \lesssim 1$, where the MSA anyway becomes inconsistent, a worse coincidence is obtained.

Also for the other effective critical exponents following from the MSA

energy route, there will be deviations from the asymptotic mean-field value. But only the exponents α, γ', and ν' are pushed outside the "classical/Ising" interval and hence show a nonmonotonic variation. For ν' this is obviously so since $\gamma' \simeq 2\nu'$ in the critical region ($\xi^{-2} \sim \varepsilon^2 \sim 1 - z \sim \gamma_r^2$, Eq. (4.16)). Furthermore

$$\alpha = 1 + \frac{1}{\pi}\frac{\ln \bar{t} + \pi a - 2}{\bar{t}} + \cdots, \quad \bar{t} \gg 1, \tag{4.117}$$

follows from (4.108) and the shift $\bar{t} \to \bar{t} - a$. With $a = 0.583$ the truncated series (4.117) gives an excellent fit to the tail of the collapsed SCOZA solution $\gamma_r \to 0$ shown in Fig. (4.25). Its maximum point $\ln \bar{t} = 3 - \pi a$ ($\log_{10} \bar{t} = 0.51$), $\alpha = 1 - e^{\pi a - 3}/\pi = 1.10$ does not reach the top of the SCOZA solution though.

As we have seen the size of the leading MSA deviations from the mean-field behavior depend upon a. But their sign (direction) does not. The shift a of the critical point depends upon details of the interaction as demonstrated in Fig. 4.22. Therefore the MSA solution indicates that while the nonmonotonic variation of α, γ', ν', and the monotonic variations of the other effective exponents, represent universal behavior, the shift of the critical point does not. With one exception[9] exactly the same indications can be seen from the three-dimensional MSA solution in Sec. 4.3.2. However, with a "nonmonotonic" minimum value $\gamma' \approx 0.996$ obtained from our SCOZA results[10] ($\gamma_r^3 = 10^{-3}$ and 10^{-4}) it is clear that the influence of the MSA is very different in $d = 3$. In renormalization-group theory effective critical exponents are viewed as smooth crossover functions linking the classical and the Ising critical regime. Above the critical point several attempts have been made to calculate crossover functions [38]. They all suggest that the crossover behavior is universal. In discussing experiments on micellar solutions (Ising universality class), corresponding to $T > T_c$ in our case, Fisher [39] claims that nonmonotonic variations of effective critical exponents can be incorporated in standard scaling.

[9] Only for $a > 1/4$ the effective exponent α exceeds the Gaussian value $1/2$ in $d = 3$.

[10] This effect is barely visible in Fig. 5 in I. Here the classical critical asymptote, represented by the lower solid curve, is intersected by the curve with $\gamma_r^3 = 10^{-3}$.

4.5 Calculations for the one-dimensional case

4.5.1 Asymptotic relations

Also in the one-dimensional case we use the construction (4.75) to build up long-range interactions. Thus, with $I_\alpha = 1/\sqrt{1-\alpha^2}$ (Eq. (28) in Sec. IV of II), the range of interaction, γ_r^{-1}, is given by (4.76). But instead of measuring in units of the effective nearest neighbor range we here multiply the right-hand side of (4.76) by a factor 2 to keep the asymptotic form (30) in Sec. IV of II. So with B defined by (4.78), we define

$$\gamma_r^2 \equiv 2\frac{1-\alpha}{\alpha}B. \tag{4.118}$$

As $z \to 1$, $P(z)$ diverges as

$$P(z) = \frac{1}{2}\gamma_r \frac{1}{\sqrt{1-z}} + B + \mathcal{O}\left(\sqrt{1-z}\right). \tag{4.119}$$

Repeating the manipulations performed in Sec. 4.4.2 here leads to

$$1 - z = \frac{1}{4}\gamma_r^2(1-y)^2\left[1 + 2(B + \tfrac{1}{4}\gamma_r^2)(1-y) + \cdots\right], \tag{4.120}$$

and

$$\varepsilon^2 = \frac{1}{4}\gamma_r^2(1-y)\left[1 + 2(B + \tfrac{1}{8}\gamma_r^2)(1-y) + \cdots\right]. \tag{4.121}$$

Therefore, unless $\gamma_r = 0$, there will be finite corrections to $x = (1-\varepsilon^2)/(1-y) \simeq 1/(1-y)$ to all orders in $1-y$, Eq. (4.83). The other way around one gets

$$1 - y = \frac{1}{x}\left\{1 - \frac{1}{4}\gamma_r^2\frac{1}{x}\left[1 + 2B\frac{1}{x} + \mathcal{O}(\frac{1}{x^2})\right]\right\}. \tag{4.122}$$

As shown in the appendix in II SCOZA gives the exact solution for nearest neighbor interactions ($\gamma_r^2 = 2$ and $B = 0$). From Eq. (A7) in II[11],

$$1 - y \simeq 2\frac{e^{-\beta/4}}{\sqrt{1-\Delta\rho^2}} - 2\frac{e^{-\beta/2}}{1-\Delta\rho^2} \tag{4.123}$$

[11] where β must be replaced with $\beta/4$ in the present units.

at low temperatures near the critical isochor $\Delta\rho = 0$. Due to the non-singular relation (4.121) the PDE (4.13) can be linearized near $y = 1$ to yield

$$\frac{\partial\phi}{\partial\beta} = \frac{2}{\gamma_r^2}[\rho(1-\rho)]^2\frac{\partial^2\phi}{\partial\rho^2}, \tag{4.124}$$

in terms of the unknown function

$$\phi = \rho(1-\rho)(1-y). \tag{4.125}$$

For the constant C, defined by (4.87) and used to calculate the second virial coefficient (4.91), we have

$$C = \frac{1}{2}\sqrt{\frac{1-\alpha}{1+\alpha}} \overset{\alpha\to 1}{\simeq} \frac{1}{4}\gamma_r. \tag{4.126}$$

Generally

$$P(z) = 1 + \frac{1}{2}\left(\frac{1}{\sqrt{1-z}} - 1\right) z\ \gamma_r + \mathcal{O}(\gamma_r^2) \tag{4.127}$$

for small γ_r. As long as $1 - z \sim \gamma_r^p$, with $0 < p < 2$, (4.127) leads to the mean-field equation of state (compare the two-dimensional analogue in Sec. 4.4.2) and

$$y = \frac{1}{2}\left(\frac{1}{\sqrt{1-z}} - 1\right)\gamma_r + \mathcal{O}(\gamma_r^2), \tag{4.128}$$

for the internal energy (4.79). Hence the asymptotic relation between the compressibility $\varepsilon^2 \simeq 1 - z$ and $y \sim \gamma_r^{1-p/2} \ll 1$ turns out as

$$\varepsilon^2 \simeq \frac{1}{4}\gamma_r^2\frac{1}{y^2}. \tag{4.129}$$

Furthermore this relation matches the bracket (times the prefactor $\frac{1}{4}\gamma_r^2$) in (4.121) to first order in $1-y$ and lowest order in γ_r (since $B = 1 - \frac{1}{2}\gamma_r + \cdots$). I. e., with $1 - z \geq c\,\gamma_r^2$ and $c \ll 1$ ($p = 2$), y is no longer small and

$$\varepsilon^2 \simeq \frac{1}{4}\gamma_r^2\frac{1-y}{y^2} \tag{4.130}$$

generalizes (4.129) by including the low-temperature behavior (4.121) at least to order $(1-y)^2$. By some joinery

$$\varepsilon^2 \simeq \left(\frac{\frac{1}{2}\gamma_r}{\frac{1}{2}\gamma_r + y}\right)^2 (1-y) \tag{4.131}$$

also picks up the high-temperature relation (4.90) without violating (4.130).

4.5.2 Numerical results

We start the numerical investigations in one dimension by studying the configurational energy along the "critical" isochor $\rho = 1/2$. In Fig. 4.29 we have drawn both the internal energy function (4.79) and the specific heat per volume as functions of inverse temperature. The curves are calculated for $\alpha = 0, 0.3, 0.6, 0.9, 0.99, \ldots, 0.9999999$, and the crosses mark the specific heat maxima (same notation as in Sec. 4.4). With a finite interaction range the main qualitative difference compared with the two-dimensional situation (compare Figs. 4.18 (upper plot) and 4.19) merely reflects the absence of a critical point in one dimension. For SCOZA this means that the specific heat varies very smoothly as function of temperature instead of displaying a relatively sharp maximum. Moreover the low-temperature behavior shows a continuous variation between the nearest-neighbor and the mean-field results, Eqs. (4.123) and (4.85) (to leading order), respectively. This is shown more precisely in the upper plot of Fig. 4.30 where the negative logarithm of the small saturation difference $1 - y$ is plotted versus β. The lower plot in Fig. 4.30 focuses upon high temperatures. As $\alpha \to 1$ SCOZA approaches the Gaussian approximation, Eq. (4.128) with $z = \beta/4$, above the mean-field critical point ($\beta < 4$). (See the curve drawn with short dashes.) The essential features for the inverse compressibility along $\rho = 1/2$ are exhibited in Fig. 4.31. Here we have plotted $\ln(\varepsilon^2/\gamma_r^2)$ versus β to capture the asymptotic behavior $\gamma_r \to 0$ and the exponential decay at low temperatures implied by (4.121). Below the mean-field critical point and in the limit $\alpha \to 1$, the SCOZA result approaches the dashed curve calculated numerically from the mean-field phase equilibrium $y = \Delta\rho_0(\beta)^2$ and (4.130). To zeroth order in γ_r, $\varepsilon^2 \simeq 1 - \beta/4$ above the mean-field critical point, giving rise to the characteristic curves in the upper left corner of the figure.

The upper plot in Fig. 4.32 shows isotherms for both the inverse compressibility ε^2 and the internal energy y at inverse temperature $\beta = 10$. With α values 0, 0.3, 0.6, 0.9, 0.99, and 0.999, ε^2 and y are plotted versus $1 - \Delta\rho^2$ close to the boundary $|\Delta\rho| = 1$. The figure illustrates the continuous change of the mean-field equation of state as $\alpha \to 1$. (See the dashed lines.) I. e., $\varepsilon^2 = 1 - (1 - \Delta\rho^2)\beta/4$ and $y = 0$ outside the intersections with the mean-field coexistence curve $\Delta\rho_0(\beta)$. More precisely, y is given by the Gaussian approximation (4.128) with $z = \frac{1}{4}(1-\Delta\rho^2)\beta$. (See the inset in the lower plot, Fig. 4.32.) Inside $\Delta\rho_0$, $\varepsilon^2 = 0$ and $y = 1 - (1 - \Delta\rho_0^2)/(1 - \Delta\rho^2)$, Eq. (4.83). In contrast to the low-temperature situation in two dimensions, β_e for finite

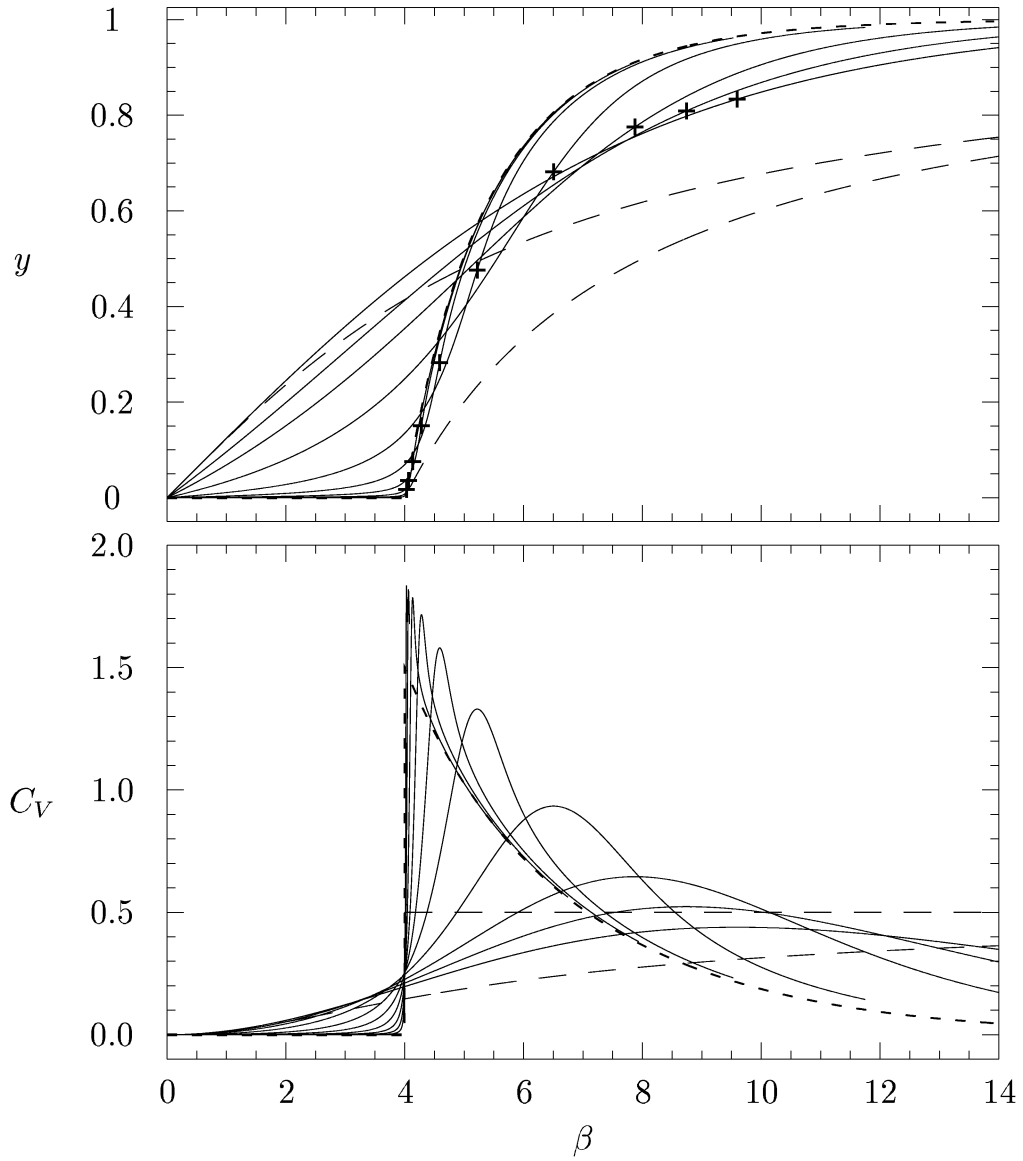

Figure 4.29: Internal energy y (upper plot) and specific heat per volume C_V (lower plot), along the critical isochor, shown as functions of inverse temperature β. Solid curves: SCOZA corresponding to α values $0, 0.3, 0.6$, and $1-10^{-n}$, with $n = 1, 2, \ldots, 7$. Short dashes: Asymptotic solution $\alpha \to 1$. Crosses correspond to the maximum for the specific heat, running from right to left for increasing α. Long dashes: MSA with $\alpha = 0$ and $\alpha \to 1$.

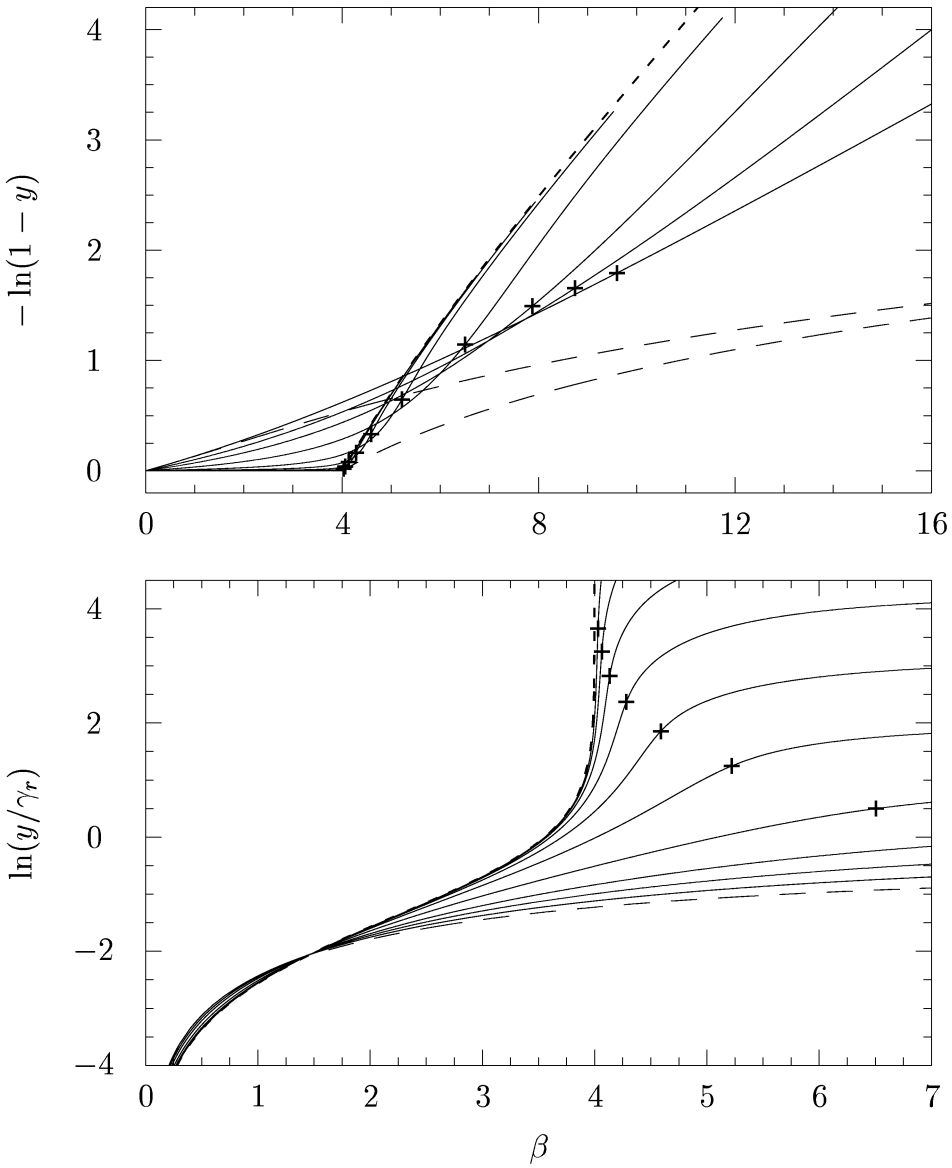

Figure 4.30: Internal energy y along the critical isochor, as function of inverse temperature β. Notation as in Fig. 4.29.

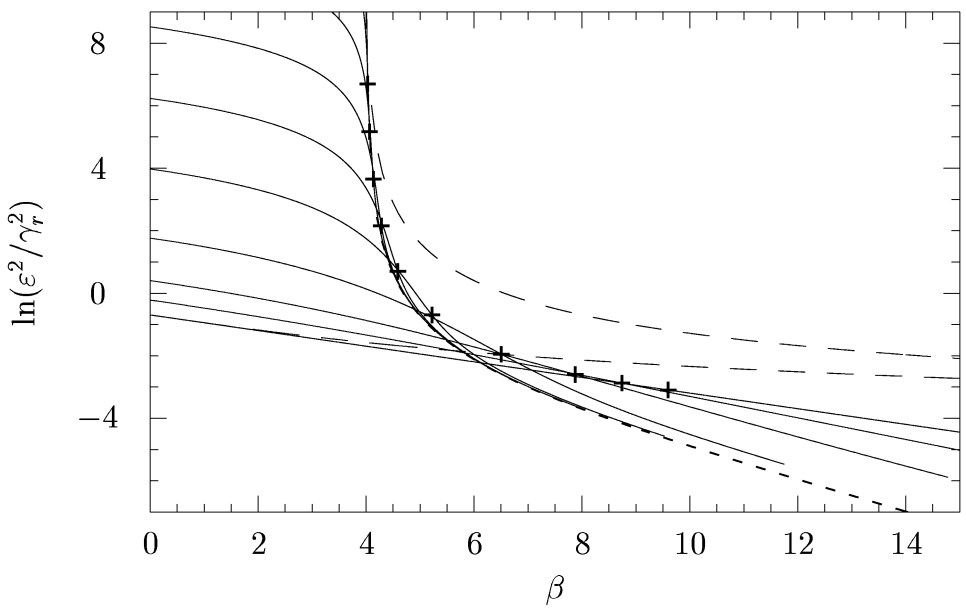

Figure 4.31: The inverse compressibility function ε^2 along the critical isochor, as function of inverse temperature β. Notation as in Fig. 4.29.

interaction ranges depends strongly upon density near the critical isochor $\Delta\rho = 0$. In Fig. 4.32 this is seen as deviations from the dashed straight line with slope 1 in the lower plot, representing the mean-field asymptote $-\ln(1-y) = \ln(\beta_e/4) + \ln(1-\Delta\rho^2)$, with $\beta_e = 4/(1-\Delta\rho_0^2)$. In particular, we have $\beta_e \simeq 2e^{\beta/4}/\sqrt{1-\Delta\rho^2}$ for nearest neighbor interactions. Although $\beta = 10$ is not a really low temperature for short interaction ranges (in the lower plot the curve for $\alpha = 0$ has slope ≈ 0.46 at $\Delta\rho = 0$), the numerical results suggest that $\beta_e \sim (1-\Delta\rho^2)^{-\upsilon}$ with υ varying continously between 1/2 and 0 as α takes values between 0 and 1. I. e., with K small (decaying exponentially as function of β), put $1/x \simeq K(1-\Delta\rho^2)^{\upsilon-1}$ (Eq. (4.83)) into (4.122). For finite interaction range and density deviation $\Delta\rho$, the expression between braces in (4.122) gives corrections to $-\ln(1-y) = -\ln K + (1-\upsilon)\ln(1-\Delta\rho^2)$, corresponding to a straight line in the lower plot in Fig. 4.32.

Indeed there exists a scaling solution

$$1 - y \simeq s^{\omega}, \tag{4.132}$$

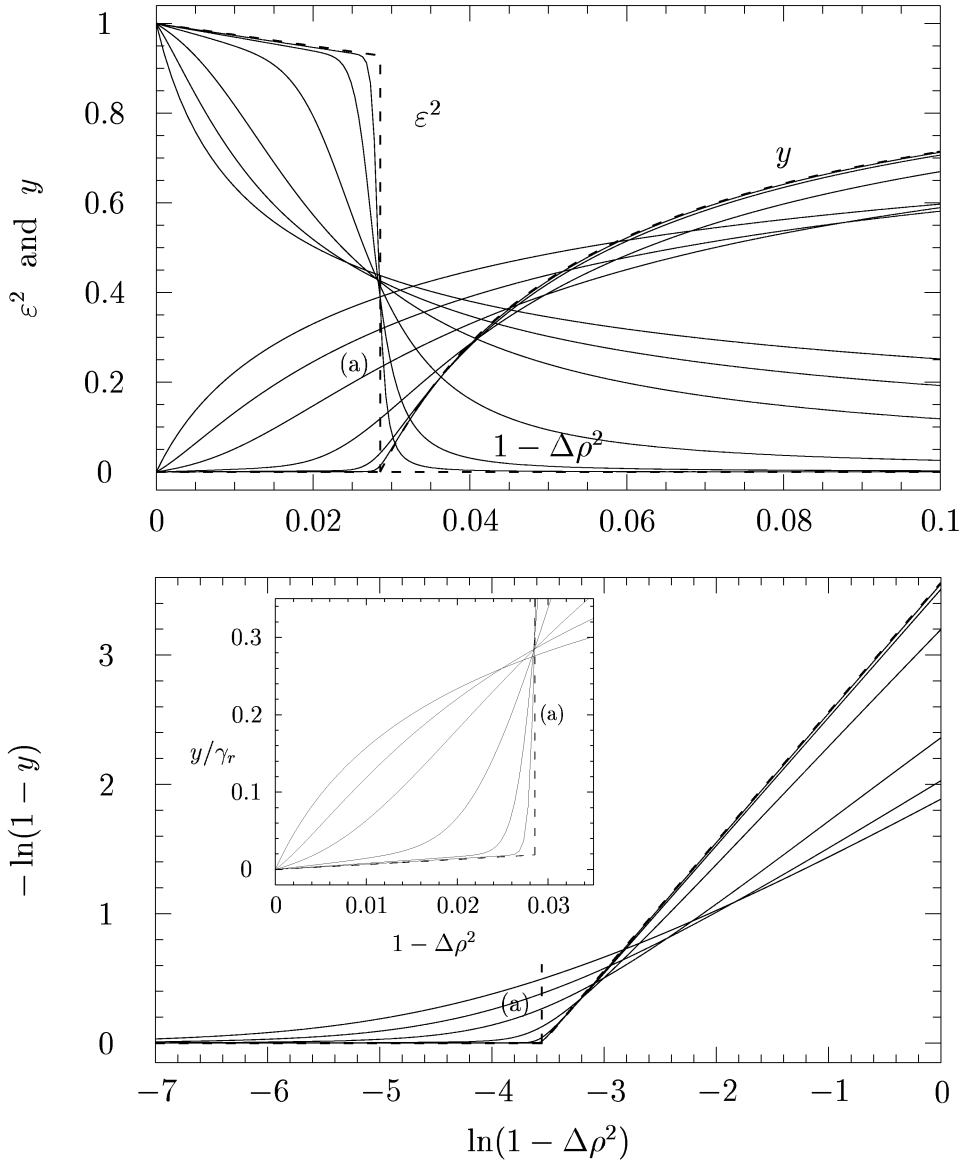

Figure 4.32: The inverse compressibility ε^2 and the internal energy y at inverse temperature $\beta = 10$ plotted as functions of $1-\Delta\rho^2$. For both quantities isotherms corresponding to α values 0, 0.3, 0.6, 0.9, 0.99, and 0.999 have been drawn. Dashed lines: Mean-field equation of state obtained in the limit $\alpha \to 1$. Vertical line (a): Intersection with the mean-field coexistence curve.

with

$$s = \frac{2e^{-\beta/4}}{\sqrt{1-\Delta\rho^2}} = 2e^{-\beta/4}(1 + \frac{1}{2}\Delta\rho^2 + \cdots), \tag{4.133}$$

for the asymptotic SCOZA equation, Eqs. (4.124) and (4.125). Solving (4.124) to zeroth order in $\Delta\rho^2$ one obtains for the index ω a γ_r-dependent equation whose solution is

$$\omega = \frac{2}{1 + \frac{1}{2}\gamma_r^2}. \tag{4.134}$$

Since putting $1 - y \sim s^2$ directly into (4.124) (via (4.125)) makes the right-hand side disappear ($\phi \sim e^{-\beta/2}[1 + \mathcal{O}(\Delta\rho^4)]$), (4.132)–(4.134) demonstrates how SCOZA produces the low-temperature behavior (4.85) in the limit $\gamma_r \to 0$. Moreover $\omega = 1$ corresponds exclusively to $\gamma_r^2 = 2$ (nearest-neighbor interaction). With an arbitrary value γ_r this means that there is no possibility of having a cross-over situation $1 - y \simeq c_1 s + c_2 s^2$, from mean-field to nearest-neighbor behavior, as $T \to 0$. As mentioned above the curves in Fig. 4.32 have slopes (at $\Delta\rho = 0$) somewhat below those given by (4.132). The deviations are typically 10%, 1%, and less than 0.1% when α is less than, equal to, and greater than 0.9, respectively. Needless to say the thermodynamically inconsistent MSA deviates severely at low temperatures as (4.132) corresponds to $\beta_e \simeq e^{\beta\omega/4}[\rho(1-\rho)]^{\frac{1}{2}\omega-1}$.

4.5.3 The MSA solution

In Sec. IV of II our treatment of the one-dimensional lattice gas with long-range interactions reduces to calculating the pair correlation function at the mean-field critical point. Starting with the MSA we now examine the equation of state outside the critical region.

From Eqs. (34) and (41) in II it follows that $\varepsilon^2 \simeq 1 - z \simeq 2^{-2/3}\gamma_r^{2/3}$ for the MSA at the mean-field critical point. Using the asymptotic relation (4.129) one therefore has

$$x(1 - \frac{\gamma_r}{2\varepsilon}) = 1 - \varepsilon^2, \tag{4.135}$$

analogous to the two-dimensional version (4.102). In terms of scaled quantities $\bar{\varepsilon}^2$ and $\bar{\Delta}x$ defined by

$$\bar{\varepsilon}^2 = \varepsilon^2/\gamma_r^{2/3} \quad \text{and} \quad \Delta x = \gamma_r^{2/3}\bar{\Delta}x = 1 - x, \tag{4.136}$$

the asymptotic equation for now reads

$$\bar{\Delta x} = \bar{\varepsilon}^2 - \frac{1}{2\bar{\varepsilon}}. \tag{4.137}$$

For large and small $\bar{\varepsilon}^2$ this gives

$$\bar{\varepsilon}^2 = \begin{cases} \bar{\Delta x}\left[1 + \frac{1}{2}\bar{\Delta x}^{-3/2} + \mathcal{O}(\bar{\Delta x}^{-3})\right], & 1 \ll \bar{\Delta x} \ll 1/\gamma_r^{2/3} \\ \dfrac{1}{4\bar{\Delta x}^2}\left[1 + \frac{1}{2}\bar{\Delta x}^{-3} + \mathcal{O}(\bar{\Delta x}^{-6})\right], & -1/\gamma_r^{1/6} \ll \bar{\Delta x} \ll -1 \end{cases}, \tag{4.138}$$

respectively. At supercritical temperatures, $1 \ll \bar{t} \ll 1/\gamma_r^{2/3}$, (4.138) is identical to the exact result along the critical isochor $\Delta x = t = 1 - \beta/4$, Eq. (22) in [40]. But along the critical isotherm $\Delta x = \Delta\rho^2$, $1 \ll \bar{\Delta\rho}^2 \ll 1/\gamma_r^{2/3}$, the leading correction beyond the mean-field asymptote $\bar{\varepsilon}^2 = \bar{\Delta x}$ vanishes in the exact solution. This can be shown from the first-order result (23) in Ref. [40] for the equation of state in the one-phase region. Unfortunately one has to go to $\mathcal{O}(\gamma_r^2)$ in the one-phase region (not reported) if higher order corrections are to be found. Note that a systematic derivation of $\bar{\varepsilon}(\bar{\Delta x})$ beyond the asymptotic relation (4.129) used in (4.135) gives a γ_r-dependent term which dominates the contribution of $\mathcal{O}(\bar{\Delta x}^{-3})$ when $\bar{\Delta x} \gg 1/\gamma_r^{1/6}$. I. e., including the two leading γ_r-dependent terms, we have

$$\begin{aligned} \bar{\varepsilon}^2 \;=\; & \bar{\Delta x}\left[1 + \frac{1}{2}\bar{\Delta x}^{-3/2} - \frac{1}{2}\gamma_r^{1/3}\bar{\Delta x}^{-1} - \frac{1}{8}\bar{\Delta x}^{-3} + \right. \\ & \left. \frac{1}{8}\gamma_r^{1/3}\bar{\Delta x}^{-5/2} + \mathcal{O}(\bar{\Delta x}^{-9/2}, \gamma_r^{1/3}\bar{\Delta x}^{-4})\right]. \end{aligned} \tag{4.139}$$

At the boundaries $\bar{\Delta x} = \bar{\varepsilon}^2 = 1/\gamma_r^{2/3}$ ($\beta = 0$, $|\Delta\rho| = 1$) the γ_r-dependent terms provide the pairwise cancellation needed.

As a final exercise we study the two-phase region implied by the energy route. From Eqs. (4.48), (4.129) and (4.136) the chemical potential $\overline{\beta\Delta\mu} = \beta\Delta\mu/\gamma_r$ becomes

$$\overline{\beta\Delta\mu} = 2\bar{\Delta\rho}\left(\bar{t} + \frac{1}{3}\bar{\Delta\rho}^2 + \frac{1}{2\bar{\varepsilon}}\right) \tag{4.140}$$

to zeroth order in $\gamma_r^{2/3}$. Via the solution $\bar{\varepsilon}(\bar{\Delta x})$ of the cubic equation (4.137) it can be shown that

$$-2\bar{t} = \frac{2}{3}\bar{\Delta\rho}^2 + \left(\frac{2}{3}\bar{\Delta\rho}^2\right)^{-1/2} \tag{4.141}$$

is the locus of $\overline{\beta\Delta\mu} = 0$. With a branch-point at $-\bar{t} = \bar{\Delta\rho}^2 = 3/2^{5/3} \approx 0.94$ the outer branch

$$\bar{\Delta\rho} = \sqrt{-3\bar{t}} - \frac{1}{2}\sqrt{\frac{3}{2}}\frac{1}{(-2\bar{t})} + \mathcal{O}(-2\bar{t})^{-5/2} \tag{4.142}$$

matches the mean-field solution outside the critical region $-\bar{t} \gg 1$. Again (compare Secs. 4.3.2 and 4.4.5) the asymptotic relation between the compressibility and the MSA variable $\bar{\Delta x} = \bar{t} + \bar{\Delta\rho}^2$, in combination with the locus for $\overline{\beta\Delta\mu} = 0$ (Eqs. (4.137) and (4.141)), implies the generalized mean-field result $\bar{\varepsilon}^2 = \frac{2}{3}\bar{\Delta\rho}^2$. Hence

$$\bar{\varepsilon}^2 = -2\bar{t} - \frac{1}{\sqrt{-2\bar{t}}} + \mathcal{O}(-2\bar{t})^{-2}. \tag{4.143}$$

By analogy with the two- and three-dimensional treatments we find $C_{V0} = -\frac{1}{2}d(\bar{\Delta\rho}^2)/d\bar{t} \simeq 3/2 + (3/4)(-2\bar{t})^{-3/2}$ and $C_{V1} = -\frac{1}{4}d(\bar{\varepsilon}^{-1})/d\bar{t} \simeq -(1/4) \times(-2\bar{t})^{-3/2}$ along $\overline{\beta\Delta\mu} = 0$. Altogether

$$C_V = \frac{3}{2} + \frac{1}{2}\frac{1}{(-2\bar{t})^{3/2}} + \mathcal{O}(-2\bar{t})^{-3}, \quad -\bar{t} \gg 1. \tag{4.144}$$

Correspondingly we obtain

$$C_V = \frac{1}{8}\frac{1}{\bar{t}^{3/2}} + \mathcal{O}(\bar{t})^{-3}, \quad \bar{t} \gg 1, \tag{4.145}$$

which agrees both with the exact result[12] [40] and the numerical solution obtained for SCOZA. However, for $-\bar{t} \gg 1$, the exact result becomes

$$C_V = \frac{3}{2} - \frac{1}{4}\frac{1}{(-2\bar{t})^{3/2}} + \cdots. \tag{4.146}$$

This result follows from the MSA if one drops the contribution due to the deformation of the mean-field coexistence curve (the second term in C_{V0}), or, equivalently, if one only uses the simple mean-field result $\bar{\Delta\rho}^2 = -3\bar{t}$ to calculate both contributions C_{V0} and C_{V1}. With some knowledge of the solution

[12] In Ref. [40] Δc_v is given per particle and the specific volume at the critical point $l_c = 3$ in our units. To compare with our C_V one must divide Δc_v by $3k_B$. Furthermore ν_1 and l_1^2 correspond to our $-\bar{t}$ and $\frac{4}{3}\bar{\Delta\rho}^2$ (since mean-field coexistence curve is $4\nu_1 = l_1^2$ in the continuum case).

of the Kac integral equation in the critical region this result should not be unreasonable. I. e., in zeroth approximation the van der Waals equation plus the Maxwell rule appears exactly without any "deformations". But higher order perturbations are extremely weak for $-\bar{t} \gg 1$, although sufficient to remove the zeroth order phase transition. (See Sec. III in [40].) For instance the specific heat becomes extremely flat inside the mean-field coexistence. I. e., for fixed $\bar{t} \ll -1$, $C_V = C_V(\bar{\Delta}\rho = 0) - \frac{3}{2\pi}\sqrt{-2\bar{t}}\exp[-(-2\bar{t})^{3/2}]\bar{\Delta}\rho^2 + \cdots$. This means that the MSA cannot handle the corrections to the mean field quantitatively correct and the price to pay is that even the sign is wrong. In one dimension there is no critical point and (4.146) smoothes out the discontinuity which follows from the mean-field equation of state (the step from 0 to 3/2 at T_c) whereas the MSA (4.144) sharpens it. To see the thermodynamic inconsistency connected to this inaccuracy compare (4.143) with the energy route result

$$\bar{\varepsilon}^2 = \frac{1}{2}\left(\frac{\partial\overline{\beta\Delta\mu}}{\partial\bar{\Delta}\rho}\right)_{\overline{\beta\Delta\mu}=0} = -2\bar{t} + \frac{5}{4}\frac{1}{\sqrt{-2\bar{t}}} + \mathcal{O}(-2\bar{t})^{-2}. \tag{4.147}$$

One should also note that along the critical isochor $\bar{\varepsilon}^2 = \frac{1}{2}\partial\overline{\beta\Delta\mu}/\partial\bar{\Delta}\rho = \bar{t} + 1/(2\bar{\varepsilon})$, which is identical to the compressibility equation (4.137). But close to the critical point $\bar{t} = 0$ things get inconsistent outside $\bar{\Delta}\rho = 0$ and the MSA becomes inaccurate.

4.5.4 Effective critical behavior

In Fig. 4.33 we have plotted the relative deviation from the classical critical asymptote $\bar{\varepsilon}^2 = \bar{\Delta}x$ along the critical isochor ($\Delta x = t$) and critical isotherm ($\Delta x = \Delta\rho^2$). Δx measures the distance from the mean-field critical point. As it turns out numerically SCOZA gives the same leading γ_r-dependent term as the MSA (4.139), $\frac{1}{2}\gamma_r^{1/3}$ has been added to $\bar{\varepsilon}^2$ in the ordinate. Thus we avoid using $\bar{\varepsilon}^2/\bar{\Delta}x - 1$ which becomes negative along the critical isotherm for $\bar{\Delta}\rho^2 \gtrsim 1/(\sqrt{2}\,\gamma_r^{1/6})$. I. e., for the asymptotic ($\gamma_r \to 0$) solutions $(\bar{\varepsilon}^2 + \frac{1}{2}\gamma_r^{1/3})/\bar{\Delta}x - 1$ we find $\simeq \frac{1}{2}\bar{t}^{-3/2}$ and $\approx \frac{1}{4}(\bar{\Delta}\rho^2)^{-3}$ along the two directions. (See the dashed lines in the figure.) This means that $\bar{\varepsilon}^2 \simeq \bar{\Delta}\rho^2 + \frac{1}{4}\bar{\Delta}\rho^{-4}$ along the critical isotherm when $1 \ll \bar{\Delta}\rho^2 \ll 1/\gamma_r^{1/6}$. Hence SCOZA agrees with the exact results mentioned in the previous subsection. The other advantage of using the ordinate in Fig. 4.33 is that the endpoints (circles) at $\beta = 0$ and $|\Delta\rho| = 1$ lie on the asymptote ($\Delta x = t$) for the critical isotherm. To be specific

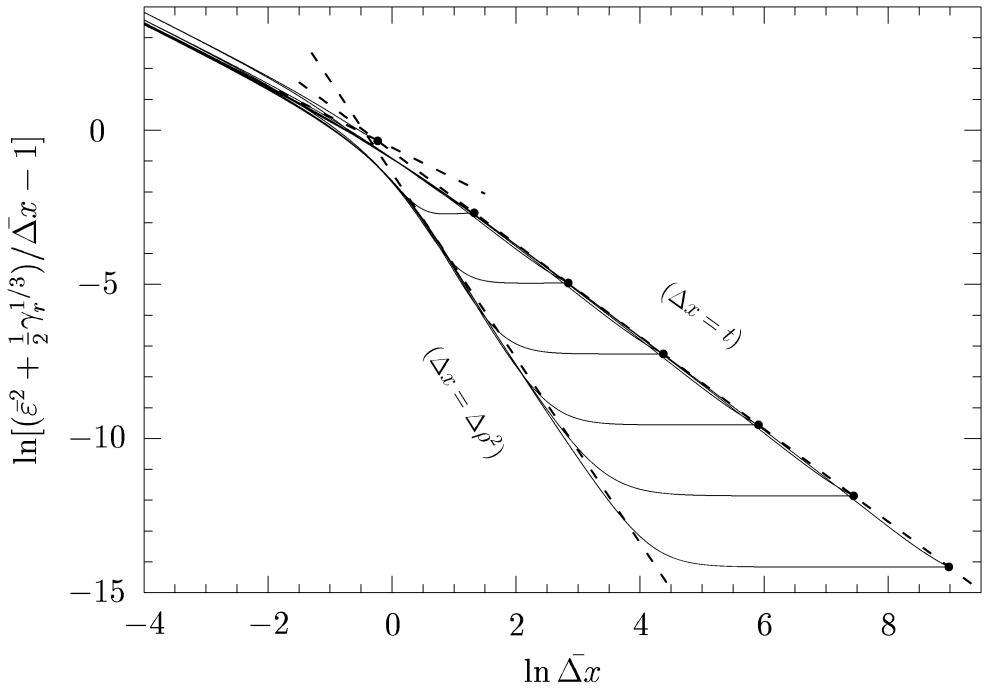

Figure 4.33: Relative deviation from the classical critical asymptote $\bar{\varepsilon}^2 = \bar{\Delta x}$ (see the text) along the critical isochor ($\Delta x = t$) and along the critical isotherm ($\Delta x = \Delta\rho^2$). The curves are calculated with $\alpha = 1 - 10^{-n}$ where $n = 0, 2, 4, \ldots, 12$. Circles: Endpoints at $\beta = 0$ and $|\Delta\rho| = 1$, running from left to right for increasing n. Dashed lines: Asymptotic behaviour in the limit $\alpha \to 1$ ($\gamma_r \to 0$).

$(\bar{\varepsilon}^2 + \frac{1}{2}\gamma_r^{1/3})/\bar{\Delta x} - 1 = \frac{1}{2}\bar{\Delta x}^{-3/2} = \frac{1}{2}\gamma_r$ for $\bar{\varepsilon}^2 = \bar{\Delta x} = 1/\gamma_r^{2/3}$. To fulfill the boundary conditions the critical isotherms are almost horizontal close to the endpoints. So $\bar{\varepsilon}^2 \simeq (1 + \frac{1}{2}\gamma_r)\bar{\Delta\rho}^2 - \frac{1}{2}\gamma_r^{1/3}$ for $\bar{\Delta\rho}^2 \gg 1/\gamma_r^{1/3}$. At the critical point $\bar{\varepsilon}^2 \to a^2$, $\gamma_r \to 0$, with $a \approx 0.756$ (Eq. (42) in II). This correponds to the dashed line $2\ln a - \ln \bar{\Delta x}$ in the upper left corner of Fig. 4.33.

With respect to thermodynamic selfconsistency the leading correction term along the critical isotherm follows from the MSA solution. It is readily seen that each order in $\bar{\Delta x}^{-3/2} = \bar{\Delta\rho}^{-3}$ beyond the leading mean-field term in the compressibility (4.138) corresponds to a term of order one higher via

the energy route. E. g., by dropping the γ_r-dependency in (4.139),

$$\bar{\varepsilon}^2 = \bar{\Delta x}\left(1 + \frac{1}{2}\bar{\Delta x}^{-3/2} - \frac{1}{8}\bar{\Delta x}^{-3} + \cdots\right) \tag{4.148}$$

corresponds to the superior energy route result

$$\bar{\varepsilon}^2 = \frac{1}{2}\left(\frac{\partial\overline{\beta\Delta\mu}}{\partial\bar{\Delta\rho}}\right)_{\bar{t}=0} = \bar{\Delta x}\left(1 + \frac{3}{8}\bar{\Delta x}^{-3} - \frac{15}{32}\bar{\Delta x}^{-9/2} + \cdots\right). \tag{4.149}$$

Chapter 5

Summary

We have applied the thermodynamically self-consistent Ornstein-Zernike approximation (SCOZA) to lattice gases with attractive pair interactions of arbitrary interaction range.

In the case of nearest neighbor interaction in three dimensions the SCOZA yields remarkably accurate predictions for the overall thermodynamics, the critical point, and the phase coexistence. Its critical properties are such that the equation of state does not scale in the standard way. Above the critical temperature the critical exponents are those of the mean spherical approximation $\alpha = 0$, $\gamma = 2$, and $\delta = 5$ while below they are $\alpha' = -1/10$, $\beta = 7/20$, and $\gamma' = 7/5$. Away from the critical point one obtains effective critical exponents consistent with experimental ones. Likewise the deviation from scaling also seems to be a feature of real systems. This is demonstrated by comparison with experimental data for CO_2 where by closer inspection one finds that different isotherms lie on different curves in a scaling plot. In two dimensions SCOZA does not give a critical point. But the deviation from the Onsager solution is only appreciable close to the exact critical point. However, the sharp maximum of the specific heat along the critical isochor may be identified with the location of the critical point. Compared with the Onsager solution this maximum is less than 0.3% away from the exact critical temperature. Also the extrapolated index γ is near the exact value 7/4. For nearest neighbor interaction in one dimension the SCOZA is exact.

As a function of inverse range of interaction γ the critical region has an extension that agrees with the Ginzburg criterion. In the limit $\gamma \to 0$ the SCOZA solution describes a unique crossover from mean-field to SCOZA-like critical behavior. However, for larger γ there is not a full crossover to mean-

field exponents, consistent with more recent analysis. Similar results, also in agreement with MC simulations, are found in 2 dimensions, and likewise in 1 dimension, comparing with exact results in the latter case. To leading order in γ the shift of the critical temperature compared to the mean-field limit, agrees with previous estimates. Far away from the critical point the mean spherical approximation gives the leading deviations from the simple mean-field behavior. In two dimensions this leads to a nonmonotonic variation of the effective critical exponent γ' for the susceptibility below the critical temperature. This effect agrees well with the one originally observed in MC simulations.

The SCOZA yields an accurate equation of state over the whole temperature-density plane, and is not restricted as to dimensionality or any specific type of interaction.

Appendix A

Exact result in two dimensions

In this appendix we show that for any long-range potential ($\gamma_r \to 0$)

$$\tilde{\varphi}(\boldsymbol{k}) = 1 - \frac{1}{4}\left(\frac{k}{\gamma_r}\right)^2 + \cdots \tag{A.1}$$

on the square lattice, the leading correction to the mean-field result $P(z) = 1$ (integral (4.7)) is given by

$$P(z) = 1 - \frac{1}{\pi}\gamma_r^2 \ln \gamma_r^2 + \text{const}\, \gamma_r^2 + \mathcal{O}(\gamma_r^4), \tag{A.2}$$

when

$$1 - z = \mathcal{O}(\gamma_r^2). \tag{A.3}$$

γ_r^{-1} is the range of interaction in units of the effective range for the nearest neighbor interaction (Eqs. (4.75) and (4.76) with $\tilde{\psi}''(0) = 1/2$).

Following the same line of reason as in Sec. 4.2.2 for the integral $I(\xi)$ we then have

$$P(z) - 1 \simeq \frac{z}{1-z}\frac{1}{(2\pi)^2}\int\limits_{k<k_0} \frac{d\,\boldsymbol{k}}{1 + \epsilon^2 k^2} \tag{A.4}$$

with

$$\epsilon^{-2} = 4(1-z)\gamma_r^2. \tag{A.5}$$

For (A.4) to be a good approximation we must have

$$k_0^2 \gg (1-z)\gamma_r^2. \tag{A.6}$$

Without specifying the cut-off k_0, we have

$$P(z) - 1 = \frac{1}{\pi} z \gamma_r^2 \ln \left[\frac{k_0^2/4}{\gamma_r^2 (1-z)} \right] + \mathcal{O}\left(\gamma_r^4 (1-z)/k_0^2 \right). \tag{A.7}$$

This result is essentially (4.77) for the limit $z \to 1$, and higher order terms like (4.82) are needed for (4.77) to be consistent with the γ_r-expansion (4.92). Such corrections are beyond the scope of this simple calculation. To extract merely the leading contribution (A.2) one must shrink the cut-off k_0 without violating (A.6). For small values of γ_r^2 this is carried out by choosing

$$k_0^2 = \text{const}\,(1-z). \tag{A.8}$$

Appendix B

The MSA phase equilibrium in two dimensions

In this appendix we show that

$$-2\bar{t} = \frac{2}{3}\bar{\Delta\rho}^2 - \frac{2}{\pi}\ln\left(\frac{2}{3}\bar{\Delta\rho}^2\right) \tag{B.1}$$

is the locus of the phase equilibrium

$$\bar{t} + \frac{1}{3}\bar{\Delta\rho}^2 = \frac{1}{\pi}\ln\bar{\varepsilon}^2 \tag{B.2}$$

for the two-dimensional MSA (4.110).

Taking the logarithm of π times (B.2) and inserting for the solution (4.107) we have

$$Y = W_0(X), \tag{B.3}$$

where

$$X = \pi\exp\left[\pi e^{\pi(\bar{t}+\bar{\Delta\rho}^2)}\right] \quad \text{and} \quad Y = \pi\exp\left[\pi e^{\pi(\bar{t}+\frac{1}{3}\bar{\Delta\rho}^2)}\right]. \tag{B.4}$$

From the definition of Lamberts W function

$$X = Ye^Y \tag{B.5}$$

or

$$\ln X = \ln Y + Y. \tag{B.6}$$

Inserting for X and Y and deleting the common factor π,

$$\frac{2}{3}\bar{\Delta\rho}^2 = \exp\left[\pi\left(\bar{t} + \frac{1}{3}\bar{\Delta\rho}^2\right)\right], \tag{B.7}$$

from which (B.1) follows.

Bibliography

[1] C. A. Croxton, *Liquid State Physics : A Statistical Mechanical Introduction* (Cambridge University Press, London, 1974).

[2] H. E. Stanley, *Introduction to Phase Transitions and Critical Phenomena* (Oxford Univ. Press, New York, 1987).

[3] E. H. Hauge, *Phase Transitions and Critical Phenomena*, lecture notes, NTH, Trondheim (1991).

[4] J. P. Hansen and I. R. McDonald, *Theory of Simple Liquids* (Academic Press, London, 1986).

[5] L. S. Ornstein and F. Zernike, Proc. Acad. Sci. (Amsterdam) **17**, 793 (1914). F. Zernike, Proc. Acad. Sci. (Amsterdam) **18**, 1520 (1916).

[6] M. Kac, G. E. Uhlenbeck, and P. C. Hemmer, J. Math. Phys. **4**, 216 (1963).

[7] P. C. Hemmer, J. Math. Phys. **5**, 75 (1964). J. L. Lebowitz, G. Stell, and S. Baer, J. Math. Phys. **6**, 1282 (1965).

[8] J. S. Høye, in *New Approaches to Problems in Liquid State Theory*, edited by C. Caccamo *at al.* (Kluwer Academic Publishers, The Netherlands, 1999).

[9] J. S. Høye, thesis NTH, Trondheim (1973).

[10] J. L. Lebowitz and J. K. Percus, Phys. Rev. **144**, 251 (1966).

[11] T. H. Berlin and M. Kac, Phys. Rev. **86**, 821 (1952). H. W. Lewis and G. H. Wannier, Phys. Rev. **88**, 682 (1952); **90**, 1131 (1953).

[12] J. K. Percus and G. J. Yevick, Phys. Rev. **110**, 1 (1958).

[13] C. F. Baillie *et al.*, Phys. Rev. B **45**, 10 438 (1992).

[14] M. E. Fisher, in *Proceedings of the Summer School on Critical Phenomena, Stellenbosch, South Africa, 1982*, edited by F. J. W. Hahne (Springer, Berlin, 1983).

[15] V. L. Ginzburg, Fiz. Tverd. Tela **2**, 2031 (1960) [Sov. Phys. Solid State **2**, 1824 (1960)].

[16] E. Luijten, H. W. J. Blöte and K. Binder, Phys. Rev. E **54**, 4626 (1996).

[17] B. Widom, J. Chem. Phys. **43**, 3898 (1965); **43**, 3898 (1965).

[18] M. S. Green *et al.*, Phys. Rev. Lett. **18**, 1113 (1967).

[19] J. S. Kouvel and J. B. Comly, Phys. Rev. Lett. **20**, 1237 (1968).

[20] J. S. Høye and G. Stell, Mol. Phys. **52**, 1071 (1984).

[21] J. S. Høye and G. Stell, Int. J. Thermophys. **6**, 561 (1985).

[22] R. Dickman and G. Stell, Phys. Rev. Lett. **77**, 996 (1996).

[23] G. S. Joyce, J. Phys. A **5**, L65 (1972).

[24] D. Pini, G. Stell, and R. Dickman, Phys. Rev. E, **57**, 2862 (1998).

[25] W. F. Ames, *Numerical Methods for Partial Differential Equations* (Academic Press, New York, 1977).

[26] A. V. Voronel, in *Phase Transitions and Critical Phenomena Vol. 5b* (Academic Press, London, 1976), p. 348.

[27] A. M. Ferrenberg and D. P. Landau, Phys. Rev. B **44**, 5081 (1991). A. J. Liu and M. E. Fisher, Physica A **156**, 35 (1989).

[28] A. Michels *et al.*, Proc. Roy. Soc. (London) **A153**, 201, 214 (1935); **A160**, 358 (1937).

[29] M. Vicentini-Missoni, J. M. H. Levelt Sengers, and M. S. Green, Phys. Rev. Lett. **22**, 389 (1969).

[30] A. Aharony and P. C. Hohenberg, Phys. Rev. B **13**, 3081 (1976).

[31] J. S. Høye and G. Stell, J. Stat. Phys. **89**, 177 (1997).

[32] K. Huang, *Statistical Mechanics* (Wiley, New York, 1987), Chap. 15.

[33] K. K. Mon and K. Binder, Phys. Rev. E **48**, 2498 (1993).

[34] P. C. Hemmer and J. L. Lebowitz, in *Phase Transitions and Critical Phenomena Vol. 5b* (Academic Press, London, 1976), p. 187.

[35] E. Luijten and H. W. J. Blöte, Phys. Rev. Lett. **79**, 561 (1997).

[36] E. Barouch, B. M. McCoy, and T. T. Wu, Phys. Rev. Lett. **31**, 1409 (1973).

[37] R. M. Corless *et al.*, Advances in Computational Mathematics **5**, 329 (1996).

[38] J. F. Nicoll and J. K Bhattacharjee, Phys. Rev. B **23**, 389 (1981). C. Bagnuls and C. Bervillier, Phys. Rev. B **32**, 7209 (1985). M. Y. Belyakov and S. B. Kiselev, Physica A **190**, 75 (1992).

[39] M. E. Fisher, Phys. Rev. Lett. **57**, 1911 (1986).

[40] P. C. Hemmer, M. Kac, and G. E. Uhlenbeck, J. Math. Phys. **5**, 60 (1964).

Paper 1

Critical properties of the self-consistent Ornstein–Zernike approximation for three-dimensional lattice gases with varying range of interaction

A. Borge and J. S. Høye
Institutt for fysikk, NTNU, N-7034 Trondheim, Norway

(Received 9 July 1997; accepted 9 December 1997)

The self-consistent Ornstein–Zernike approach (SCOZA) is solved numerically, and its properties in the critical region are investigated for the lattice gas or Ising model in three dimensions. We especially investigate how critical properties depend upon the inverse range of interaction. We find effective critical indices that depend upon this range. However, the SCOZA does not fulfill scaling. Nevertheless, comparing with experimental results for fluids and magnets we find good agreement. Away from the critical point we find that SCOZA yields deviations from scaling that seem similar to experiments. © *1998 American Institute of Physics.* [S0021-9606(98)50211-5]

I. INTRODUCTION

Recently Dickman and Stell succeeded in numerically solving the self-consistent Ornstein–Zernike approach (SCOZA) partial differential equation such that a well-defined solution was also obtained below the critical temperature T_c where one has phase coexistence.[1] They considered the Ising model or the equivalent lattice gas in three dimensions with nearest-neighbor interactions. A striking feature of their results was the accuracy with which the best estimates for Ising model thermodynamics were approximated for the three possible types of cubic lattices. This accuracy is present both in the values of T_c, which were within 0.2% of such estimates, as well as the general behavior in the critical region with effective critical exponents close to the best analytic estimates.

The critical region has been an especially complicated region to treat more accurately by statistical mechanics. Usually theories have been restricted to various types of mean-field or Van der Waals-like theories. In this way density fluctuations that are important and crucial in the critical region have been neglected. Thus mean-field theories are most inaccurate in this region, and they are in no way able to capture the singular behavior experienced by thermodynamic quantities as the critical point is approached. This singular behavior is again connected to the correlation length that grows to infinity.

New insight and major progress towards understanding the mechanism of critical behavior was obtained by Widom[2] and Kadanoff[3] by introduction of homogeneity from which the well-known scaling relations followed. Further on, renormalization group methods were introduced by Wilson,[4] after which Wilson and Fisher[5] showed how quantitative predictions of critical exponents could be obtained as expansions in $4-d$ where d is dimension.

However, globally more accurate treatments of systems at thermal equilibrium have been less developed. But some work has been performed as was done by one of the authors in his thesis.[6] This work was based on the γ ordering for long-range forces that was used by Hemmer[7] and by Lebowitz *et al.*[8] to obtain corrections to the well-known Van der Waals equation of state for fluids. From this study it became clear that corrections to mean-field theory (or here a three-dimensional version of Van der Waals equation) beyond the usual high-temperature contribution were relatively small except in a region around the critical point where corrections due to the finite range of interaction would be crucial. A noteable problem with the critical point is its singular nature such that corrections to mean field tend to diverge. To some extent this was rectified by a resummation or renormalization of the leading contribution beyond mean field. In this way results that quantitatively compared well with experimental results for Ar were obtained using the Lennard–Jones potential. However, close to the critical point remaining thermodynamic inconsistencies were crucial in the sense that isotherms became ''irregular'' by which, for instance, the gas–liquid phase equilibrium no longer remained well defined. But nevertheless, extrapolation of results towards the critical point indicated a critical index $\beta \approx 1/3$ for the phase equilibrium while the one for the critical isotherm was $\delta \approx 5$.

For the lattice gas it later became clear[6] that the resummed γ ordering above was essentially the MSA (mean spherical approximation). Thus the critical properties were those of the MSA. However, the MSA result is less satisfactory in the latter case with nearest-neighbor interaction. In the view of the above analysis this can be understood from the correction to mean field. For the Lennard–Jones fluid the lowering of T_c was less than 10% compared to the T_c from the high-temperature result while the lattice gas case yields a lowering of 34% for the simple cubic lattice. That is corrections and thus inconsistencies will be considerably larger in the latter case.

The MSA for fluids and modified versions of it were studied extensively by Chandler *et al.*,[9–12] and accurate results were obtained outside the critical region. However, critical properties remained mean-field-like. This is the case with MSA for continuum fluids which is thermodynamicly inconsistent in such a way that the divergence of the correlation function will take place inside the two-phase region from the energy route and not at the critical point itself. Further various integral equations methods have been devel-

oped and refined to describe fluids.[13] Høye and Stell then proposed to apply thermodynamic self-consistency in connection with the MSA solution for fluids.[14] Further they fully developed equations necessary for solving the self-consistency problem. Preliminary numerical results suggested that the SCOZA approach might yield rather accurate thermodynamic results,[15] which recently was verified.[1] The high accuracy actually found may be surprising. But as argued by Høye and Stell[16] there is reason to believe that this accuracy partly can be connected to the fact that in three dimensions the critical index η for the correlation function is close to zero. Thus the spatial dependence of the assumed MSA form of the correlation function is close to the exact correlation function too. So the main defect of the MSA itself is apparently its thermodynamic inconsistency which is remedied by the SCOZA.

Recently another theory of global accuracy has also appeared. This is the hierarchical reference theory (HRT) of Parola and Reatto.[17,18] This theory is based on renormalization group ideas that build in scaling, but is not self-consistent in our sense. However, it results in a similar numerical problem of solving a nonlinear partial differential equation of diffusion type.

In view of the accuracy of the results obtained[1] we found reason to believe that SCOZA will yield accurate information about properties in the critical region too as there is not much room for corrections due to higher-order perturbing terms. As is already clear, the SCOZA will not yield exact critical indices very close to the critical point. However, away from this very small region there seems to be an effective critical behavior near the exact one as reported.[1] One purpose of this work is to investigate this more closely by performing more accurate and detailed evaluations especially in the critical region. Another purpose is to investigate the effect upon critical properties when varying the range of interaction. According to γ ordering, results should be more accurate and reliable the smaller the inverse range of interaction is.

In view of standard scaling theory we understand that critical properties are expected to be independent of the range of interaction, i.e., they are universal. However, the preliminary SCOZA results indicated that effective critical exponents were sensitive to interaction range. For example, by comparing the results of Refs. 1 and 15 one got an indication that the effective supercritical index γ for the inverse susceptibility had such a behavior as results obtained differed. Also some previous unpublished numerical work by one of the authors in connection with a student project indicated the same.[19] In this latter case the continuum fluid with Yukawa interaction whose range could be varied was considered. By the more precise and accurate evaluations performed here we actually find such a dependence upon the range of interaction. This sensitivity to interaction range for effective exponents may be related to the expected crossover behavior as one approaches the critical point, with the crossover occurring at a ''Ginzburg temperature'' that depends upon the sixth power of the inverse potential range γ_r.[20–22] That is, inside this crossover temperature which turns out to be very small, our results indicate universal behavior while outside effective critical exponents vary.

In Ref. 15 the presence of scaling solutions of the SCOZA were shown. However, the results of Ref. 1 were not in accordance with these as the index γ approached the MSA value 2 and not the scaling value 1 close to T_c. Thus the boundary conditions of the SCOZA are in conflict with the family of possible scaling solutions. Later analytic work by Høye *et al.*[33] shows the presence of a solution with index $\gamma = 2$ where scaling is not present. What seems to happen is that the true solution approaches the trivial scaling solution that does not contain temperature and is thus nothing but the critical isotherm near the critical density.

In Sec. II we sketch the SCOZA theory, and in Sec. III we discuss the numerical method. In Sec. IV we discuss numerical results for critical indices while in Sec. V results for the equation of state and its deviations from scaling are discussed. We have evaluated the various critical indices for thermodynamic quantities and our results are presented in the figures. The indices, defined as slopes of curves in log-log plots, are evaluated for various ranges of interaction. Also the equation of state with scaled variables is evaluated and then compared with experimental results for fluids and magnets. Although SCOZA does not scale it turns out to be close to scaling in the part of the critical region usually covered by experimental results. This is also the region best described by effective exponents. In fact a closer examination of the experimental results indicate a similar deviation from scaling. That is the nonscaling properties of SCOZA seem to describe the exact behavior in a way that goes beyond previous descriptions. However, deviations from and corrections to scaling are nothing new as considerable effort has been devoted to this to describe properties close to the critical point.[23,24] Furthermore, crossover has been studied by Fisher[25] and by Bagnuls and Bervillier[26] using renormalization group methods while Anisimov *et al.*[27] have used a phenomenological approach, Mon and Binder[28] have performed Monte Carlo simulations, and Parola and Reatto[17] have used a liquid-state theory.

II. THEORY

As mentioned in the Introduction SCOZA builds upon the MSA by combining it with thermodynamic self-consistency where one can utilize the thermodynamic relation

$$\frac{\partial(\beta\chi^{-1})}{\partial\beta} = \frac{\partial^2(\rho u)}{\partial\rho^2}, \tag{1}$$

where $\rho\chi^{-1}$ is the inverse compressibility $\partial p/\partial\rho$. Here $\beta = 1/k_B T$, p is the pressure, ρ is the density, and u is the average energy per particle which has a contribution of mean-field form $u_0 = -(q/2)\rho$ and a contribution from correlations u_1.

$$u = u_0 + u_1. \tag{2}$$

Here we incorporate the coordination number q as used in Ref. 1. For the Ising model ρ, χ^{-1}, ρu, and ρu_0 are replaced by $\frac{1}{2}(1+m)$, $\partial H/\partial m$, U, and $U_0=-(1/2)m^2$ as done in Ref. 15.

For an interaction $-\psi(\mathbf{r})$ the SCOZA pair correlation function $h(\mathbf{r})$ has Fourier transform

$$1+\rho\tilde{h}(\mathbf{k})=\frac{1}{1-\rho\tilde{c}(\mathbf{k})}, \tag{3}$$

where the direct correlation function $\tilde{c}(\mathbf{k})$ is assumed to be of MSA form

$$\tilde{c}(\mathbf{k})=c_0+c_1\tilde{\psi}(\mathbf{k}). \tag{4}$$

Equation (3) is nothing but the Fourier transform of the usual Ornstein–Zernike equation. Approximation (4) for $c(\mathbf{r})$ or its Fourier transform $\tilde{c}(\mathbf{k})$ is of Ornstein–Zernike form assuming $c(\mathbf{r})$ to be of a range corresponding to the range of the potential. (This relation to Ornstein–Zernike[29] theory explains the name SCOZA of our approach.) At the same time we utilize the MSA form to define $\tilde{c}(\mathbf{k})$ explicitly except for c_1 which is determined by thermodynamic self-consistency via Eq. (1) that yields Eq. (12) below. As in Ref. 1 we normalize $\psi(\mathbf{r})$ such that $\tilde{\psi}(0)=q$. The core condition $h(0)=-1$ then implies

$$1-\rho=\frac{1}{(2\pi)^3}\int(1+\rho\tilde{h}(\mathbf{k}))d\mathbf{k}=\frac{1}{1-\rho c_0}P(z), \tag{5}$$

where

$$P(z)=\frac{1}{(2\pi)^3}\int\frac{d\mathbf{k}}{1-z\tilde{\psi}(\mathbf{k})/q} \tag{6}$$

with

$$z=\frac{\rho c_1 q}{1-\rho c_0}=\frac{q\rho(1-\rho)c_1}{P(z)}. \tag{7}$$

From the pair correlation function one can now obtain the equation of state in two different ways. First the internal energy due to correlations becomes

$$\rho u_1=-\frac{1}{2}\frac{1}{(2\pi)^3}\int(\rho+\rho^2\tilde{h}(\mathbf{k}))\tilde{\psi}(\mathbf{k})d\mathbf{k}$$
$$=-q\rho(1-\rho)F(z), \tag{8}$$

where by use of Eqs. (5) and (7)

$$F(z)=\frac{P(z)-1}{2zP(z)}. \tag{9}$$

Second, from the compressibility relation we further get

$$\beta\chi^{-1}=\frac{1}{\rho}(1-\rho\tilde{c}(0))=\frac{\epsilon^2}{\rho(1-\rho)}, \tag{10}$$

where with (5) and (7) $[\tilde{c}(0)=c_0+qc_1]$

$$\epsilon^2=(1-z)P(z). \tag{11}$$

The SCOZA partial differential equation now follows by inserting (8), (2), and (10) into (1) to obtain

$$\frac{\partial\epsilon^2}{\partial\beta}=-q\rho(1-\rho)\left\{1+\frac{\partial^2}{\partial\rho^2}[\rho(1-\rho)F(z)]\right\}. \tag{12}$$

The solution of this equation along with relations (6), (9), and (11) will determine the parameter c_1 in Eq. (4) and all other quantities of interest in Eqs. (2)–(11) above. This also includes the pair correlation function $h(\mathbf{r})$ [or $\tilde{h}(\mathbf{k})$] in Eq. (3). Note that the whole influence of the pair interaction, besides the mean-field piece u_0, goes via the function $P(z)$ as given by Eq. (6) which is not restricted to dimensionality three as studied here.

III. NUMERICAL SOLUTION

The preliminary SCOZA results reported by Høye and Stell in Ref. 15 were limited to supercritical temperatures as the problem of going below the critical temperature T_c turned out to be nontrivial. The SCOZA equation is mathematically equivalent to a highly nonlinear diffusion process which becomes seriously instable by numerical solution when one tries to go below T_c. The reason is that the ϵ in Eqs. (10) and (12) goes towards zero at the critical point and continues to stay at this value along the on beforehand unknown spinodal curve below T_c. Close to $\epsilon=0$ the $F(z)$ is linear in ϵ (not ϵ^2) due to the singular nature of integral (6) when $z\to1$. From Eq. (12) this means that one will have a diffusion constant $D\sim1/\epsilon\to\infty$ which creates numerical problems along an unknown curve, inside which the equation will be invalid.

Originally we started our numerical work by using the form of the SCOZA equation established in Ref. 15. There a quantity S, that is essentially Helmholtz free energy, was used as the quantity to solve for. In terms of S the ϵ^2 used here is essentially its second derivative $\partial^2S/\partial\rho^2$. By numerical differentiation errors in S amplify seriously when one also takes the square root to obtain ϵ near the spinodal $\epsilon=0$. Although we otherwise developed a stable numerical procedure the determination of the spinodal did not stabilize as far as we went. In the meantime the numerical results of Ref. 1 were obtained. The crucial step taken in this work was to use Eq. (1) as basis for the SCOZA equation instead of relating u and χ via Helmholtz free energy and its derivatives. In this way the ϵ comes out directly from solution, not via a second derivative, and the determination of the spinodal $\epsilon=0$ becomes a stable procedure, although care has to be shown.

The numerical procedure used in Ref. 1 was not stable unless very small steps in β direction were used. To rectify this Pini developed an unconditionally stable, accurate, and efficient numerical procedure based on previous experience in related work using a predictor-corrector method.[18,30] Our continued work is thus based directly upon programs developed by Pini. Then we solved Eq. (12) with respect to ρu_1 as given by (8) expressing other quantities in Sec. II including the derivatives of Eq. (12) in terms of it by numerical tabulation in the general case. [However, ρu_1 and ϵ are essentially the same and no separate tabulation is required when using expression (13) below.] To obtain accurate results close to the critical point we had to show special care in order to keep accuracy high.

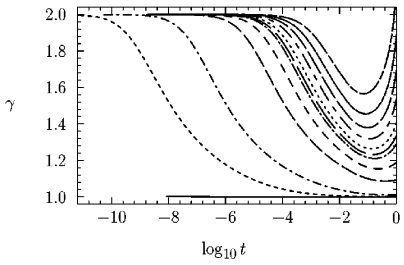

FIG. 1. Effective critical index γ for the susceptibility along the critical isochor versus $\log_{10} t$ where $t=1-T_c/T$. The different curves correspond to γ_r^3 values 10^{-3}, 10^{-2}, 0.1, 0.2, 0.3, 0.34, 0.4, 0.5, 0.6, 0.7, and 0.8, respectively, starting with the lower dashed curve for 10^{-3}. The solid line $\gamma=1$ is the mean-field result $\gamma_r\to 0$ (i.e., we used $\gamma_r^3=10^{-6}$ to run the program). In Figs. 2–6 below the same set of γ_r^3 values (including $\gamma_r\to 0$) and corresponding dashed curves are used. (The γ_r is the inverse range parameter.)

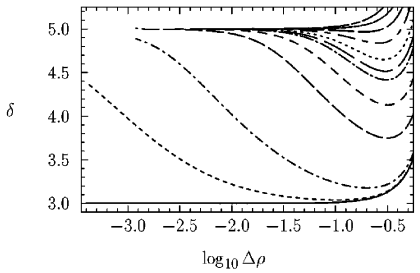

FIG. 2. Effective critical index δ for the critical isotherm versus $\log_{10}\Delta\rho$, where $\Delta\rho=|(\rho-\rho_c)/\rho_c|(\rho_c=1/2)$ (notation as in Fig. 1).

The properties of the function $F(z)$ follow from the interaction and depend crucially on its range and dimensionality. With inverse range γ_r the latter can be written as $\psi(r)=\gamma_r^3 f(\gamma_r r)$. Its Fourier transform is $\tilde{\psi}(k)=\tilde{f}(k/\gamma_r)=a-b(k/\gamma_r)^2+\cdots$ in the continuum case. In the lattice case this will be modified slightly as integration is replaced by summation. Inserted in (6) this $\tilde{\psi}(k)$ ($\tilde{\psi}(0)/q=1$) by integration yields $F(z)\sim P(z)-1=\gamma_r^3(A-B\epsilon+\cdots)$ for small $\epsilon\to 0$ or $z\to 1$ in three dimensions. (The quantities a, b, A, and B are constants.) Thus to simplify during the greater part of our work we approximated the internal energy function (8) by

$$F(z)=\tfrac{1}{2}\gamma_r^3(1-\epsilon). \tag{13}$$

Here and below we write γ_r for the inverse range of interaction to distinguish it from the critical index γ. Via (9) this function approximates integral (6) for $P(z)$ and yields the proper form of its singularity near the critical point at $\epsilon=0$. In addition it immediately incorporates the inverse range of interaction γ_r, the effect of which upon critical properties we want to study. It can be noted that γ_r is the same as the range parameter γ introduced by Uhlenbeck *et al.*[31] in their works on one-dimensional systems using the Kac potential $\gamma e^{-\gamma|x|}$ to obtain a model that is exactly solvable in the form of an integral equation that was analyzed obtaining Van der Waals equation in the limit $\gamma\to 0$. This parameter γ was then also introduced in the more general situation considered in Refs. 6–8.

One might think that the precise form of $F(z)$ would be important. But from previous analysis of γ ordering[6] and preliminary numerical work by Pini[30] we had reason to believe that this was not the case. However, in the present work we also performed detailed SCOZA computations to evaluate effective critical indices using the correct $P(z)$ for nearest-neighbor interaction on the SC lattice as done in Ref. 1. And in accordance with the above assumption the results were near those with $\gamma_r^3=0.34$. By near we mean that with the choice $\gamma_r^3=0.3405...$, which gives the SC value $P(1)=1.516...$, the critical temperature was nearly the same (0.7% deviation) and corresponding curves for the various critical indices were essentially the same. (For example, in Fig. 1 the curve for γ in the SC case was shifted about a distance 0.2 to the right of the $\gamma_r^3=0.34$ curve for $t\lesssim 0.1$ and the minimum value for γ was lowered about 0.03. On the other hand it nearly coincided the $\gamma_r^3=0.4$ curve in the same region.) Doing the same for the BCC and FCC lattices gave essentially the same results for the indices although a somewhat smaller γ_r^3 would be more appropriate to yield the correct T_c. That is, details of the pair interaction have minor influence compared with its range, and with respect to critical properties there will be no influence in the qualitative sense. Thus to investigate how effective critical indices depend upon γ_r^3 we kept form (13). Clearly it is possible to γ_r parametrize the correct nearest-neighbor function too.[32] But we did not do so here as this will not change our conclusions as just argued.

IV. NUMERICAL RESULTS

Above T_c evaluations were relatively straightforward to perform with high accuracy. For the critical indices γ and δ for the susceptibility at critical density and the critical isotherm, respectively, the asymptotic values 2 and 5 were easily verified.[1,33] However, away from the critical point one finds effective values and these vary with the γ_r^3 parameter, as can be clearly seen from Figs. 1 and 2. Here and below effective critical indices are defined by the logarithmic derivative of the quantity in question. That is, $\alpha=\partial(\log C_v)/\partial(\log t)$, $\delta=\partial(\log(p_2-p_1))/\partial(\log\Delta\rho)$, etc. where C_v is the configurational specific heat, and p_2 and p_1 are the pressures on the critical isotherm at densities $\rho_2=\rho_c(1+\Delta\rho)$ and $\rho_1=\rho_c(1-\Delta\rho)$, respectively. For example, the curves for γ typically each have a minimum that defines an effective exponent that dominates the critical region except very close to T_c, i.e., the effective exponent dominates when $t\gtrsim 10^{-2}$ for $\gamma_r^3=0.34$ that is near to the Ising model with nearest-neighbor interaction. Here $t=1-T_c/T$ for $T>T_c$ while for $T<T_c$ we use $t=1-T/T_c$. As in Ref. 1 we find γ near 1.25 in good agreement with best estimates. Here we find it interesting to note that the best estimate $\gamma\approx 1.25$ coincides well with the dominant effective SCOZA γ for nearest-neighbor interaction (or $\gamma_r^3\approx 0.34$). However, when γ_r^3 is changed the effective γ changes too. Thus we find reason to ask ourselves whether this latter nonuniversal behavior is accidental or will estimates for more long-ranged

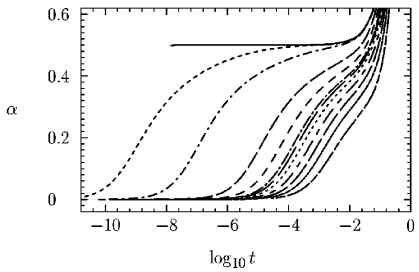

FIG. 3. Effective critical index α for the specific heat along the critical isochor versus $\log_{10} t$ where $t=1-T_c/T$ (notation as in Fig. 1). (Note $\alpha=1/2$ in the mean-field limit as long as γ_r^3 is kept finite by which configurational internal energy $\sim\gamma_r^3$ is finite.)

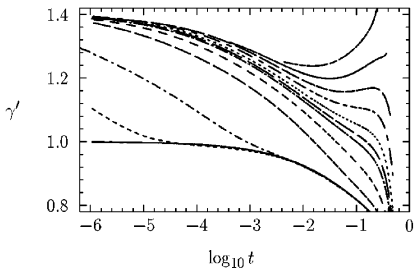

FIG. 5. Effective subcritical index γ' for the susceptibility along the coexistence curve versus $\log_{10} t$ where $t=1-T/T_c$ (notation as in Fig. 1).

interactions also follow effective SCOZA values. As far as we can understand this feature has not been investigated, although the universality hypothesis will say that the true γ is fixed. The situation is similar with the exponent δ as seen in Fig. 2.

In view of the accuracy of SCOZA as shown in Ref. 1 we find reason to expect that this nonuniversal behavior away from the critical point is part of the exact behavior as discussed in Sec. V. But as we do not know about independent investigations in this respect we cannot check to which extent the SCOZA results are correct. Although this behavior is a type of correction to scaling we do not find it directly comparable to previous work.[23,24]

In the way Fig. 1 (and other figures) are presented one may ask why a value of γ close to the minimum of the curve can define a dominant effective exponent. The reason is that it represents a stationary point of the slope of the susceptibility versus t on a log-log plot. And restricting the latter to the region $10^{-4.4}\leqslant t\leqslant 1$ as done in Ref. 1 one sees almost a straight line that curves somewhat on the end. (That is, $\gamma\approx 1.25$ is restricted to $10^{-2}<t<1$.) Our computations have been made accurate much closer to the critical point, however, to capture crossover phenomena for varying γ_r^3 and to obtain the SCOZA limiting values that we find independent of γ_r^3. Due to this the tiny region more or less unattainable by experiments covers a dominating part of our figures when using logarithmic variables while the easily attainable region where effective exponents vary with γ_r^3, is less dominating.

Note that as one might expect, the effective exponents change smoothly into the mean-field behavior as $\gamma_r\to 0$. How this ''crossover'' to mean-field behavior takes place more precisely can be seen from the figures. However, for small γ_r^3 one generally has MSA behavior for $t\gtrsim c(\gamma_r^3)^2$ where c is a constant $(T>T_c)$. Typically the effective MSA exponents change with t and they become the mean-field ones as t increases. For $t>c(\gamma_r^3)^2$ we expect this MSA behavior to be close to the exact result. But for $t\lesssim c(\gamma_r^3)^2$ the MSA will be too inconsistent, and modifications from SCOZA become important. These latter, however, are not exact either, but we expect them to represent the exact behavior well as was demonstrated with nearest-neighbor forces.[1] The condition $t\lesssim c(\gamma_r^3)^2$ is also in accordance with the Ginzburg criterion that tells that crossover from mean-field behavior takes place when entering this region.[20–22] Crossover from mean-field behavior to limiting SCOZA behavior in accordance with this criterion can be clearly seen in Figs. 1–6 for small γ_r^3. For larger γ_r^3 there is no clear mean-field region that separates out.

The MSA solution

$$\epsilon=-\gamma_r^3 x+\sqrt{(\gamma_r^3 x)^2-2(1-\gamma_r^3)x+1} \tag{14}$$

with $x=\frac{1}{2}q\rho(1-\rho)\beta$ follows from Eqs. (7), (9), (11), and (13) with $c_1=\beta$ inserted. From (14) follows the MSA critical temperature $(\epsilon=0)\,T_c^M=(q/4)(1-\gamma_r^3)$. For the SCOZA critical temperature T_c^{SC} we numerically found the shift $T_c^{SC}/T_c^M\approx 1+0.9(\gamma_r^3)^2$ for $\gamma_r^3\lesssim 0.5$. Also it should be noted from Fig. 1 that in the SCOZA the critical exponent γ approaches its asymptotic value 2 much more slowly than in the MSA where it follows from (14). For values of $\gamma\gtrsim 1.5$ the ratio between corresponding values of t is about a factor

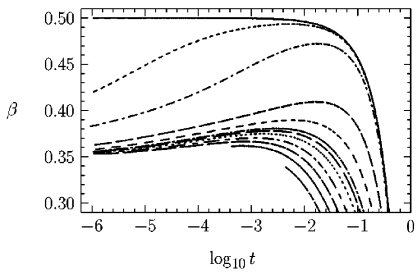

FIG. 4. Effective critical index β for the coexistence curve versus $\log_{10} t$ where $t=1-T/T_c$ (notation as in Fig. 1).

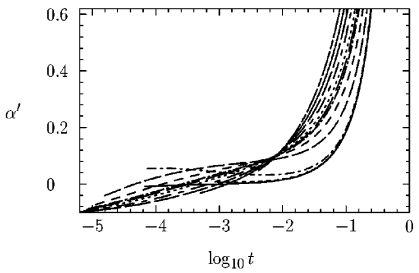

FIG. 6. Effective subcritical index α' for the specific heat along the coexistence curve versus $\log_{10} t$ where $t=1-T/T_c$ (notation as in Fig. 1).

100. That is in SCOZA $\gamma=2$ is located in a much smaller region by which this asymptotic value of γ will have a small influence upon the general accuracy.

Concerning the critical index α for the specific heat it is clear from Fig. 3 and Ref. 1 that it does not follow best estimates so well as the other indices ($\gamma_r^3=0.34$). This accuracy of α is connected to the way SCOZA in its present form closely ties α to γ since for susceptibility we here have $\epsilon^2\sim t^\gamma$ and for change in internal energy $\epsilon\sim t^{1-\alpha}$ as $t\to 0$. Thus $\alpha=1-\frac{1}{2}\gamma$ by which it varies along with γ in a way not dictated by scaling. So this is a clear defect of the SCOZA.

For subcritical temperatures the numerical evaluations are more challenging with respect to accuracy to determine the phase transition once one has a numerically stable procedure. Due to symmetry around $\rho=1/2$ it is sufficient to use either equal pressures or chemical potentials for this purpose. We used the former as in Ref. 1 obtaining the pressure p by integration of the susceptibility from both $\rho=0$ and $\rho=1$. (Alternatively one could go via Helmholtz free energy by integration of the internal energy.) To determine the constant of integration one notes that the mean-field result is exact for $\rho=0$ and $\rho=1$. (Due to division by zero one must start integration at neighboring values of $\rho=0$ and $\rho=1$ where analytic exact expansions are also used to maintain desired accuracy.) However, due to numerical inaccuracy (using the Simpson rule) the p values will differ slightly at $\rho=1/2$ for $T>T_c$ when integrating from both sides. To eliminate this error to which determination of phase equilibrium is very sensitive close to T_c we corrected for the difference obtained at T_c and kept this correction as an added constant below T_c. The justification for this is that the error of integration will stay essentially constant as the integrand is almost the same by small changes in temperature near T_c where this is important.

Near T_c the determination of phase equilibrium turned out very sensitive to numerical accuracy. Thus some of our preliminary values for the critical exponent β for the curve of coexistence was misleading. That is, for $t\to 0$, $\beta\to 1/5$ when $\gamma_r^3>0.5$. This we later found wrong by performing a sensitive check of consistency using the thermodynamic relation for magnetic systems

$$C_H-C_M=T\left(\frac{\partial M}{\partial T}\right)_H^2\left(\frac{\partial H}{\partial M}\right)_T, \tag{15}$$

where the derivatives are taken along the curve of coexistence. With this relation fulfilled the results became acceptable. Close to T_c this relation would easily fail especially for larger values of γ_r^3. Increasing the number of grid points improved upon this situation. Thus we typically used 10^3 (and in a few cases up to 10^4) grid points for the density in the region from zero density to ρ_c.

For the effective critical exponents β, γ', and α' one from Figs. 4–6 sees that they also vary with γ_r^3. Down to $\gamma_r^3\approx 0.1$ the variation is relatively slow, but from there on the change to mean-field effective exponents is more rapid. As far as the accuracy of our computations went using standard double precision, it seems clear that each of these exponents has a common asymptotic or universal value as $t\to 0$ independent of γ_r^3 as long as it is finite. Figs. 4–6 show that these asymptotic values are something like $\beta\approx 0.35$, $\gamma'\approx 1.40$, and $\alpha'\approx -0.10$. [These values are related via the usual scaling relation $\alpha'+2\beta+\gamma'=2$ that follows from Eq. (15) whenever C_H is dominant compared to C_M.] We find these values interesting especially the one for β which is close to best estimates of its exact value. Somehow, for some reason SCOZA tries to aim for something near the exact β.

Concerning the asymptotic value $\alpha'\approx -0.10$ one must expect this to be a defect of SCOZA as a negative α' does not seem reasonable as an exact value. Thus the value $\gamma'\approx 1.40$, which is connected to α' via the scaling relation above, is somewhat large too. However, away from T_c the γ' lowers its value such that more reasonable values for the effective γ' are then obtained. (Corresponding values obtained by the HRT theory of Ref. 18 are $\beta\approx 0.345$ and $\gamma'\approx 1.378$.)

The asymptotic exponents can be given some additional comments. For example, the limiting value $\gamma=2$ itself is no improvement over the MSA value. However, instead the improvement is the major increase in general accuracy such that the asymptotic region with $\gamma=2$ has moved about two decades closer to the critical point as discussed below Eq. (14).

However, for the exponent β (and to some extent γ') the situation is more spectacular as the asymptotic value $\beta\approx 0.35$ is in fact close to best estimates that can vary somewhat depending on approach.[23,24] Thus the β is clearly no longer tied to mean-field and spherical model value $\beta=0.5$. (As indicated in the Introduction the MSA defines no β, as meaningful phase coexistence is destroyed near T_c.)

The specific heat exponent $\alpha\to 0.5$ in the mean-field limit $\gamma_r^3\to 0$ needs a special comment (Fig. 3). The reason for this Gaussian model value is that kinetic energy is not included, and the mean-field configurational energy does not contribute to the specific heat above T_c. Thus only the correction to it contributes, and from Eqs. (8), (9), and (14) one has $u_1\sim\gamma_r^3\sqrt{t}\,(\gamma_r\to 0)$ or $C_v\sim\gamma_r^3/\sqrt{t}$. So $\alpha=0.5$, but on the other hand C_v itself vanishes anyway along with γ_r.

From the viewpoint of scaling it is clearly unsatisfactory that $\gamma\neq\gamma'$ and $\alpha\neq\alpha'$. However, again this is of most concern in the small asymptotic region close to the critical point where it is clear that SCOZA fails anyway.

The nonuniversal behavior of effective exponents depending upon γ_r^3 may look strange and be unexpected in view of scaling. As discussed in Sec. V this may be part of the exact behavior too such that true scaling will be present only very close to the critical point, i.e., for something like $t\lesssim 10^{-3}$ for real systems.

V. NONSCALING AND SCALED EQUATION OF STATE

As mentioned in the Introduction the SCOZA does not yield a scaled equation of state in the critical region due to its boundary conditions. Despite this SCOZA seems to yield very accurate results as verified by the results obtained for the three-dimensional Ising model in Ref. 1. Thus we were lead to speculate that somehow the SCOZA would yield something close to a scaling solution in a relatively large region that may fit into experimental results. To do this com-

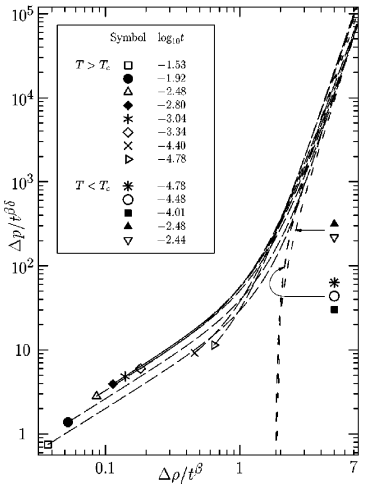

FIG. 7. Equation of state for SCOZA with $\gamma_r^3=0.34$ using scaled variables. Symbols designating the various supercritical isotherms are plotted on the various curves. For $T<T_c$ the symbols on the curves have been omitted since the curves are so close together.

parison we chose the $\gamma_r^3=0.34$ case that gave results close to the ones for the Ising model with nearest-neighbor interaction on the SC lattice. To plot SCOZA results we then introduced scaled variables in Figs. 7 and 8. (These variables were not used in the SCOZA equation itself as it does not scale.) They are

$$x=\Delta\rho/t^{\beta},$$
$$y=\Delta p/t^{\delta\beta}, \tag{16}$$

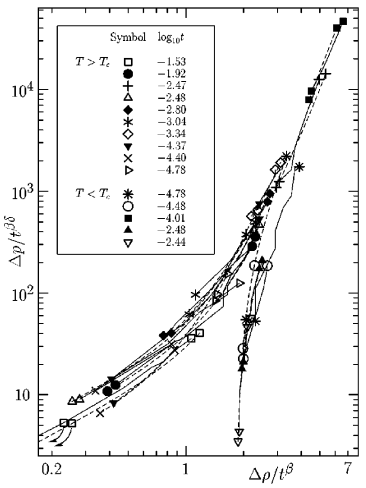

FIG. 8. Scaled equation of state for SCOZA with $\gamma_r^3=0.34$ (dashed curves) compared to experimental results for CO_2 (solid curves) taken from Ref. 34. Start and end points of both sets of curves are indicated with symbols corresponding to the actual temperatures (see inset). (The solid curves are somewhat wiggly as they connect various experimental points.)

with

$$\Delta\rho=\left|\frac{\rho_c-\rho}{\rho_c}\right|,$$
$$\Delta p=\frac{p_2-p_1}{2p_c}, \tag{17}$$

where ρ_1 and ρ_2 are the coexisting densities and p_1 and p_2 are the corresponding pressures. (Alternatively we could have used the corresponding chemical potential, or in spin system language the magnetic field, which is fully symmetric around ρ_c.)

We found experimental results with which to compare in the work by Green *et al.*[34] where the equation of state for various fluids were plotted using the scaled variables above. With some spreading these points fall along scaling curves, and they represent various isotherms with given deviations from their critical temperatures. Thus the range of t values and $\Delta\rho$ values covered is easily estimated, and the corresponding region (extended somewhat) using the SCOZA results was plotted. From Fig. 7 one sees that isotherms with small separations are obtained, and these lines fall within the experimental points as shown in Fig. 8. The only change from the experimental results in this log-log plot is a minor translation in position which we have performed. Such a shift in position should not be unexpected since we are in fact comparing experimental data for continuum fluids with SCOZA results for lattice gases. Also for the lattice gas considered here we obtained the critical ratio $\beta_c p_c/\rho_c=0.227...$ which is somewhat lower than usually found experimentally for fluids. The SCOZA results we have drawn with indices $\delta=5$ and $\beta=0.38$ gave the best fit while Ref. 34 used $\beta=0.35$. When the results in Fig. 7 are extended beyond the temperature region considered there, they start to spread markedly on the lower left side. Thus for the region plotted SCOZA yields an equation of state that is close to a scaled equation which would yield two single lines on such a plot.

We have also compared our SCOZA results with experimental results for the magnetic system Ni that has a FCC structure.[35] (Thus the extreme anisotropy in the z direction of the Ising model interactions is clearly not present.) In Ref. 35 scaled magnetization $m=M/|t|^{\beta}$ and scaled magnetic field $h=H/|t|^{\beta\delta}$ is used. In Figs. 2(a) and 2(b) of Ref. 35 subcritical and supercritical results, respectively, are plotted on log-log plots. In the subcritical case $m^2-m_0^2$ is plotted as a function of h/m while in the supercritical case m^2 is plotted as a function of $h/m-h_0/m_0$. The m_0 and h_0/m_0 are limiting $t\to 0$ values of m and h/m in the two cases, and are determined by Fig. 1 of Ref. 35. By suitable choice of parameters we find that the SCOZA results coincide fully with the experimental ones except for a small shift in position. Due to this coincidence we have not drawn here these figures that can be found in Ref. 35. There is quite a bit of flexibility with respect to choice of such parameters as within certain limits a choice of γ_r^3 can be compensated by a choice of effective β and γ. For example, we found full agreement with these experimental results with the two sets of choices

$$\gamma_r^3=0.34 \quad \beta=0.371 \quad \gamma=1.33,$$
$$\gamma_r^3=0.25 \quad \beta=0.382 \quad \gamma=1.28, \tag{18}$$

for $T>T_c$, while for $T<T_c$ a small deviation beyond experimental uncertainty can be seen. On the other hand the experimental results for Ni for $T>T_c$ shown in Fig. 3(b) in Ref. 36, slightly different from those in Ref. 35, agrees fully with the choice of parameters $\gamma_r^3=0.2$, $\beta=0.388$, and $\gamma=1.26$. Unlike the results for CO_2 presented in Fig. 8 we do not see significant nonscaling in the result for Ni and similarly the corresponding SCOZA curves are very close together along a single line in the relatively narrow region of temperature and density covered in this case. (Outside this region the SCOZA curves start to diverge somewhat with respect to density.) However, a choice of parameters different from (18) will easily yield curves that spread quite a bit. Also it should be mentioned that the determination of the SCOZA values for m_0 and h_0 defined above yield values somewhat different from the dimensionless ones reported in Table I of Ref. 35. For the SCOZA ($\gamma_r^3=0.34$) we find $m_0\approx1.76$ and $h_0\approx2.38$ while from Ref. 35 $m_0=1.487$ and $h_0=1.524$ for the Ising model, and $m_0=1.422$ and $h_0=1.037$ for Ni. Why especially the value for h_0 disagrees significantly is unclear (as we recover the mean-field values $m_0=h_0=\sqrt{3}$ when $\gamma_r^3\to0$).

One can ask why SCOZA despite its nonscaling properties nevertheless almost scales in a region with available experimental values. If one follows the shift in isotherms by changing t one notes that first the isotherms are shifted in one direction and then the shift is returned as can be seen from Fig. 7 where the end points of the curves are marked for $T>T_c$. Thus this shift goes through a stationary point (like passing through an extremum). Accordingly a whole range of isotherms locate themselves close to a single line. The range of these values for some reason coincides rather well with the one covered by the experimental data used. (For $T<T_c$ the situation is similar but cannot be directly seen in Fig. 7 since the curves are already so close together.)

In view of the accuracy demonstrated by SCOZA[1] we found reason from the above to speculate whether the type of corrections to scaling present in SCOZA might be present in real fluids too. The plotting made in Ref. 34 assumed full scaling in the region considered such that all deviations from a single line could be regarded as experimental uncertainties. On the basis of our SCOZA results we found it possible that part of these deviations might be related to the nonscaling properties found in SCOZA. Thus we made a closer examination of the experimental data where several isotherms for CO_2 were plotted using different symbols. These were not easy to identify in the figure in Ref. 34. However, by scrutinizing it we were able to identify points belonging to the same isotherm. Then for changing t one, in Fig. 8 actually sees (by looking carefully), a clear tendency of the same systematic shift of lines as found above from SCOZA. (That is in Fig. 8 one sees that the various symbols for end points of curves mostly occur pairwise.) Thus it seems that this nonscaling behavior of the SCOZA represents properties of real fluids too away from the critical point. As mentioned in the Introduction corrections to scaling is nothing new and close to the critical point such corrections have been worked out and used to compare with experimental data and to make estimates of critical exponents.[23,24] However, the specific features exhibited by the SCOZA solution do not seem to have been noticed before.

VI. CONCLUSION

As demonstrated in Ref. 1 the SCOZA yields accurate results. Its critical properties are such that the equation of state does not scale. Except very close to the critical point this does not seem to be a defect or inaccuracy of the SCOZA but instead seems to represent properties that would be present by an exact treatment too as demonstrated in Figs. 7 and 8. Furthermore, except very close to the critical point this leads to nonuniversal behavior and thus effective critical exponents that vary with the inverse range of interaction as demonstrated by Figs. 1–6. However, very close to the critical point the SCOZA will fail somewhat as the expected full scaling cannot be obtained. But, nevertheless, the SCOZA critical exponents $\delta=5$ and $\beta\approx0.35$ (as $t\to0$) are near estimated exact values.

ACKNOWLEDGMENTS

We are very grateful to Davide Pini for sending us his program for the SCOZA in the lattice gas case and to George Stell for helpful comments.

[1] R. Dickman and G. Stell, Phys. Rev. Lett. **77**, 996 (1996).
[2] B. Widom, J. Chem. Phys. **43**, 3898 (1965).
[3] L. Kadanoff, Physics (Long Island City, NY) **2**, 263 (1966).
[4] K. G. Wilson, Phys. Rev. B **4**, 3174 (1971); K. G. Wilson and J. B. Kogut, Phys. Rev. C **12**, 2 (1974).
[5] K. G. Wilson and M. E. Fisher, Phys. Rev. Lett. **28**, 240 (1972).
[6] J. S. Høye, thesis NTH, 1973.
[7] P. C. Hemmer, J. Math. Phys. **5**, 75 (1964).
[8] J. L. Lebowitz, G. Stell, and S. Baer, J. Math. Phys. **6**, 1282 (1965).
[9] H. C. Andersen and D. Chandler, J. Chem. Phys. **57**, 1918 (1972).
[10] H. C. Andersen, D. Chandler, and J. D. Weeks, J. Chem. Phys. **57**, 2626 (1972).
[11] H. C. Andersen, D. Chandler, and J. D. Weeks, J. Chem. Phys. **56**, 3812 (1972).
[12] D. Chandler and J. D. Weeks, Phys. Rev. Lett. **25**, 149 (1970).
[13] C. Caccamo, Phys. Rep. **274**, 1 (1996).
[14] J. S. Høye and G. Stell, Mol. Phys. **52**, 1071 (1984). See also Sec. IV of J. S. Høye and G. Stell, J. Chem. Phys. **67**, 439 (1977).
[15] J. S. Høye and G. Stell, Int. J. Thermophys. **6**, 561 (1985).
[16] J. S. Høye and G. Stell, Physica A **244**, 176 (1997).
[17] A. Parola and L. Reatto, Phys. Rev. Lett. **53**, 2417 (1984); Phys. Rev. A **31**, 3309 (1985); A. Parola, A. Meroni, and L. Reatto, Phys. Rev. Lett. **62**, 2981 (1989); A. Parola and L. Reatto, Phys. Rev. A **44**, 6600 (1991).
[18] D. Pini, A. Parola, and L. Reatto, J. Stat. Phys. **72**, 1179 (1993).
[19] C. B. Jensen, F. Rinnan, and J. S. Høye (unpublished).
[20] M. E. Fisher, Phys. Rev. Lett. **71**, 3826 (1993).
[21] R. F. J. Leote de Carvalho and R. Evans, J. Phys.: Condens. Matter **7**, L575 (1995).
[22] V. L. Ginzburg, Sov. Phys. Solid State **2**, 1824 (1960).
[23] D. S. Gaunt and C. Domb, J. Phys. C **3**, 1442 (1970).
[24] J. V. Sengers and J. M. H. Sengers, Annu. Rev. Phys. Chem. **37**, 189 (1986).
[25] M. E. Fisher, Phys. Rev. Lett. **57**, 1911 (1986).
[26] C. Bagnuls and C. Bervillier, Phys. Rev. Lett. **76**, 4094 (1996).
[27] M. A. Anisimov, S. B. Kiselev, J. V. Sengers, and S. Tang, Physica A **188**, 487 (1992).

[28] K. K. Mon and K. Binder, Phys. Rev. E **48**, 2498 (1993).
[29] L. S. Ornstein and F. Zernike, Proc. R. Acad. Sci. Amsterdam **7**, 793 (1914).
[30] D. Pini (unpublished); see also W. F. Ames, Numerical Methods for Partial Differential Equations (Academic, New York, 1977) pp. 82–86.
[31] M. Kac, G. E. Uhlenbeck, and P. C. Hemmer, J. Math. Phys. **4**, 216 (1963); G. E. Uhlenbeck, P. C. Hemmer, and M. Kac, *ibid.* **4**, 229 (1963); P. C. Hemmer, M. Kac, and G. E. Uhlenbeck, *ibid.* **5**, 60 (1964).
[32] J. S. Høye and G. Stell, J. Stat. Phys. **89**, 177 (1997).
[33] J. S. Høye, G. Stell, and G. Tarjus (unpublished).
[34] M. S. Green, M. Vicentini-Missoni, and J. M. H. Levelt Sengers, Phys. Rev. Lett. **18**, 1113 (1967).
[35] J. S. Kouvel and J. B. Comly, Phys. Rev. Lett. **20**, 1237 (1968).
[36] J. S. Kouvel and D. S. Rodbell, Phys. Rev. Lett. **18**, 215 (1967).

Paper 2

Self consistent Ornstein–Zernike approximation compared with exact results for lattice gases in one and two dimensions

J. S. Høye and A. Borge
Institut for Fysikk, Norwegian University for Science and Technology (NTNU), N-7034 Trondheim, Norway

(Received 19 December 1997; accepted 27 February 1998)

We evaluate numerically results for the self consistent Ornstein–Zernike approximation (SCOZA) for the Ising model or the lattice gas in one and two dimensions where exact results are known. The cases we consider thus include the Ising model with nearest-neighbor interaction in two dimensions, and in one dimension the cases with a Kac interaction or exponential potential in the infinite range limit and the one with nearest- and next-nearest neighbor interactions. As earlier found for the three-dimensional Ising model, results with high general accuracy are found, although the phase transition of the two-dimensional Ising model is smeared out a bit, as SCOZA at least in its present form, does not yield a phase transition in two dimensions. In the two-dimensional case more long-range interactions are also considered to see to what extent SCOZA approximates the expected universal critical behavior. By extrapolation we find our numerical results quite consistent with a value near the exact one $\gamma=1.75$ for the supercritical exponent of isothermal susceptibility. In the case with the nearest- and next-nearest neighbor interactions a situation that clearly favors ferromagnetic configurations is needed. Otherwise the present version of SCOZA will fail, i.e., the solution becomes less accurate and finally ceases to exist. © *1998 American Institute of Physics.* [S0021-9606(98)01921-7]

I. INTRODUCTION

Earlier the SCOZA was solved for the three-dimensional case, and results with high accuracy compared with best estimates have been generally obtained so far. The first results in this respect were those of Dickman and Stell that were able to solve the SCOZA partial differential equation also below the critical temperature T_c (Ref. 1). They considered the three-dimensional Ising model with nearest-neighbor interaction on the various cubic lattices, and the values of T_c obtained were within 0.2% of best estimates. Recently a more detailed investigation of the critical region of three-dimensional systems was performed by the authors, and again results close to expected exact behavior were obtained.[2] (Also the influence of the range of interaction was then investigated, and away from the critical point, effective critical indices that varied with this range were found.) Further SCOZA evaluations for the three-dimensional Ising model with nearest-neighbor interaction have also been performed by Pini, Stell, and Dickman, and again new results with good accuracy were obtained.[3]

As the SCOZA is not restricted to lattice systems it can be extended to continuum systems too. In this respect the situation with interaction of Yukawa type besides hard spheres has been considered by Pini, Stell, and Høye, and numerical results again seem close to real fluid behavior (including the critical region) and previous estimates.[4]

The SCOZA has also been generalized to D-dimensional spins and continuous spins.[5] However, so far numerical results have not been published for the latter.

A strength of the SCOZA is that it is not tied to a specific interaction or dimension. It is closely related to the MSA (mean spherical approximation) upon which it builds. One then imposes thermodynamic self-consistency that gives rise to an effective temperature that depends upon temperature and density. As SCOZA will be applicable in quite general situations for fluids and lattice gases, it is of interest to test its general accuracy more precisely in various situations. In this respect comparisons with known exact results are useful, and the purpose of the present work is to do so for lattice gases, in which we must restrict ourselves to one and two dimensions where three different situations are considered. Thus in Sec. III we consider the two-dimensional Ising model with n. n. (nearest-neighbor) interaction where the exact solution is known in zero magnetic field.[6,7] In Sec. IV the situation with Kac (exponential) interaction in one dimension is considered and compared with the known exact result (beyond mean field) in the infinite long-range limit. In Sec. V we compare with exact results for the one-dimensional Ising model with nearest- and next-nearest neighbor interactions. In Sec. II we reestablish briefly the SCOZA equation and relations connected to it.

II. THE SCOZA EQUATION

In lattice gas language the SCOZA self-consistency is based upon the thermodynamic relation,[1,2]

$$\frac{\partial(\beta\chi^{-1})}{\partial\beta}=\frac{\partial^2(\rho u)}{\partial\rho^2}, \tag{1}$$

where $\rho\chi^{-1}$ is inverse compressibility, $\beta=1/k_BT$, ρ is density, and u is average energy per particle. The latter can be written

$$u=u_0+u_1, \tag{2}$$

which has a mean-field contribution $u_0=-(1/2)q\rho$ and a contribution from correlations u_1 where the coordination number q as used in Refs. 1 and 2 is incorporated. In Ising model language the ρ, χ^{-1}, ρu, and ρu_0 are replaced by $(1/2)(1+m)$, $\partial H/\partial m$, U, and $U_0=-(1/2)m^2$.

For an interaction $-\psi(\boldsymbol{r})$ the SCOZA pair correlation function $h(\boldsymbol{r})$ has a Fourier transform

$$1+\rho\tilde{h}(\boldsymbol{k})=\frac{1}{1-\rho\tilde{c}(\boldsymbol{k})}, \tag{3}$$

where the direct correlation function $\tilde{c}(\boldsymbol{k})$ is assumed to be of MSA form,

$$\tilde{c}(\boldsymbol{k})=c_0+c_1\tilde{\psi}(\boldsymbol{k}). \tag{4}$$

As done in Refs. 1 and 2, we normalize $\psi(\boldsymbol{r})$ such that $\tilde{\psi}(0)=q$. The core condition $h(0)=-1$ implies (d is dimensionality),

$$1-\rho=\frac{1}{(2\pi)^d}\int(1+\rho\tilde{h}(\boldsymbol{k}))\,d\boldsymbol{k}=\frac{1}{1-\rho c_0}P(z), \tag{5}$$

where

$$P(z)=\frac{1}{(2\pi)^d}\int\frac{d\boldsymbol{k}}{1-z\tilde{\psi}(\boldsymbol{k})/q}, \tag{6}$$

with

$$z=\frac{\rho c_1 q}{1-\rho c_0}=\frac{q\rho(1-\rho)c_1}{P(z)}. \tag{7}$$

The internal energy due to correlations is then

$$\rho u_1=-\tfrac{1}{2}\frac{1}{(2\pi)^d}\int(\rho+\rho^2\tilde{h}(\boldsymbol{k}))\tilde{\psi}(\boldsymbol{k})\,d\boldsymbol{k}$$

$$=-q\rho(1-\rho)F(z), \tag{8}$$

where by use of Eqs. (5) and (7),

$$F(z)=\frac{P(z)-1}{2zP(z)}. \tag{9}$$

From the compressibility relation we have

$$\beta\chi^{-1}=\frac{1}{\rho}(1-\rho\tilde{c}(0))=\frac{\varepsilon^2}{\rho(1-\rho)}, \tag{10}$$

where with (5) and (7),

$$\varepsilon^2=(1-z)P(z). \tag{11}$$

Inserting (8), (2), and (10) into (1), the SCOZA partial differential equation is obtained,

$$\frac{\partial\varepsilon^2}{\partial\beta}=-q\rho(1-\rho)\left\{1+\frac{\partial^2}{\partial\rho^2}[\rho(1-\rho)F(z)]\right\}. \tag{12}$$

The SCOZA equation can now be solved, for instance, with respect to the parameter ε in terms of which $F(z)$ can be expressed via the relations above. However, as before, our present work is based upon programs developed by D. Pini, who worked out an unconditionally stable, accurate, and efficient numerical procedure based upon previous experience.[8,9] Thus we followed the latter and used $F(z)$ as a quantity for which to solve, expressing other quantities in terms of it using numerical tabulation.

III. THE TWO-DIMENSIONAL ISING MODEL

For the two-dimensional case with nearest-neighbor interaction on the square lattice $(q=4)$, the interaction Fourier transformed is

$$\tilde{\psi}(\boldsymbol{k})=\tfrac{1}{2}q(\cos(k_x)+\cos(k_y))=q\,\cos(u)\cos(v), \tag{13}$$

where the Fourier variables k_x and k_y are replaced by

$$u=\tfrac{1}{2}(k_x+k_y),\quad v=\tfrac{1}{2}(k_x-k_y),$$

such that $du\,dv=(1/2)dk_x\,dk_y$. To obtain $P(z)$, the k_x and k_y are integrated over a full period $(-\pi,\pi)$. In terms of u and v only half of the same two-dimensional region will be covered. Extending both the u and v to a full period each will double the integral, and one finds

$$P(z)=\frac{1}{(2\pi)^2}\int\frac{du\,dv}{1-z\,\cos u\,\cos v}$$

$$=\frac{2}{\pi}\int_0^{\pi/2}\frac{du}{\sqrt{1-z^2\,\sin^2 u}}=\frac{2}{\pi}K(z), \tag{14}$$

where $K(z)$ is the complete elliptic integral of first kind which is tabulated or can be obtained numerically. As $z\to1$ the $P(z)$ diverges logarithmically and one has

$$P(z)=\frac{1}{\pi}\ln\left(\frac{8}{1-z}\right)+\mathcal{O}(1-z), \tag{15}$$

which we used in this limit to obtain satisfactory accuracy.

As $P(z)$ diverges, although slowly when $z\to1$, it became clear that a sharp phase transition could not be obtained, which is the case with the MSA too. From this viewpoint the situation looked worse for the SCOZA in two dimensions compared with three, where the phase transition and critical properties are described with good accuracy.[1,2] Therefore, the present case is also a test on how SCOZA acts under conditions where it clearly will give a wrong prediction. A crucial question in this connection is to what extent this wrong qualitative feature will affect the general accuracy and, for instance, to what extent the corresponding MSA solution will be improved.

The MSA follows by putting $c_1=\beta$ in Eq. (4), and by combining Eqs. (7)–(9), this yields

$$U_{\mathrm{MSA}}=\rho u_1=-\frac{1}{2}\frac{P(z)-1}{\beta}, \tag{16}$$

with

$$q\rho(1-\rho)\beta=zP(z).$$

In zero magnetic field $\rho=(1/2)(1+m)=1/2$ such that $(q=4)$,

$$\beta=zP(z), \tag{17}$$

and U_{MSA} is then also the full energy, as the mean field piece $U_0=-(1/2)qm^2$ mentioned below Eq. (2) is zero. With

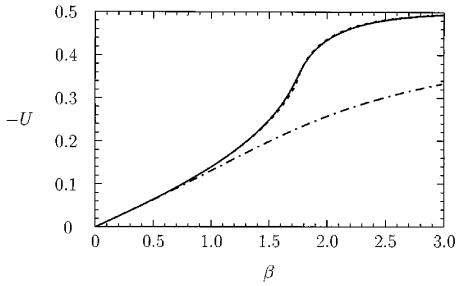

FIG. 1. Internal energy per spin U in zero magnetic field vs β for the two-dimensional Ising model on the square lattice. The solid curve is the SCOZA result, while the dashed curve is the exact result. The dashed-dotted curve is the MSA result.

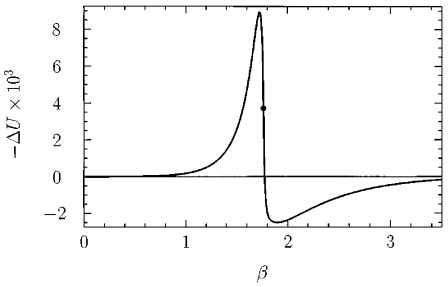

FIG. 2. Deviation between the SCOZA and the exact internal energy per spin ΔU vs β for the two-dimensional Ising model. The circle is the value of ΔU at the critical point of the exact solution.

$P(z)=(2/\pi)K(z)$ from Eq. (14), both U_{MSA} and β are easily evaluated as functions of z by which the MSA result $U_{\mathrm{MSA}}(\beta)$ can be plotted.

The exact result for the internal energy U_{ex} as first obtained by Onsager[6] is given by,[7]

$$U_{\mathrm{ex}}=-\frac{1}{4}\coth(\beta/2)\left[1+\frac{2}{\pi}\kappa' K(\kappa)\right], \tag{18}$$

with

$$\kappa=\frac{2\sinh(\beta/2)}{\cosh^2(\beta/2)}$$

and

$$\kappa'=2\tanh^2(\beta/2)-1.$$

In Fig. 1 we have plotted the internal energy in zero magnetic field comparing the MSA and SCOZA results with the exact result. From this figure it is clear that the SCOZA result follows the exact one very closely. Only near the critical point of the exact solution is there a visible deviation on the figure. Further, this deviation changes sign almost precisely at the critical point where the SCOZA solution is smoothed out a bit compared to the exact one. Compared with the MSA result the SCOZA is clearly a great improvement in accordance with the earlier results for three-dimensional systems.[1,2] Thus enforcing thermodynamic self-consistency along with the MSA or Ornstein–Zernike form of the direct correlation function seems crucial to obtain accurate results. And even near the critical point in two dimensions, remarkably accurate results are obtained, despite the fact that SCOZA does not yield a critical point, i.e., the corresponding singularity is smoothed out a little bit. (An obvious fault in the critical region is that SCOZA, as treated here, is missing a long-range piece in the direct correlation function. In two dimensions such a piece will be crucial to obtain a phase transition.) One can integrate the internal energy to obtain the free energy and then we find that the deviation from the exact solution integrates out to zero when $\beta\to\infty$. Thus the SCOZA free energy, as well as the internal energy, is exact in the low temperature limit. [This can be understood from the fact that as $T\to 0$ there will be a phase transition with coexistence of $m=1$ and $m=-1$ (or $\rho=0$ and $\rho=1$) that can be described by the mean field, which SCOZA faithfully preserves.]

In Fig. 2 the difference between the SCOZA and exact internal energies is shown more clearly. Although SCOZA does not yield a critical point one may use it to predict its location by prescribing it to be where the maximum of the specific heat $C_V=(\partial U/\partial T)_V$ is. By doing so we find $\beta_c=1.758\,28$ compared with the exact value $\beta_c=1.762\,75$ that follows from[7]

$$\sinh(\beta_c/2)=1. \tag{19}$$

In view of the accuracy obtained for u_1, it is also of interest to study the inverse susceptibility, comparing its exactly known critical behavior with critical index $\gamma=1.75$, i.e. in Fig. 3 $\chi^{1/\gamma}$ where χ is the inverse susceptibility is shown as a function of β. And with $\gamma=1.75$ we find an almost straight line that curves a bit near β_c, as SCOZA does not give a sharp phase transition. Further, for $\beta>\beta_c$ the χ approaches 0 rapidly in an exponential way (e.g., for $\beta=2.0$ the $\chi\approx 5.5\times 10^{-9}$). In this connection it also was of interest to investigate the properties of the SCOZA "critical" iso-

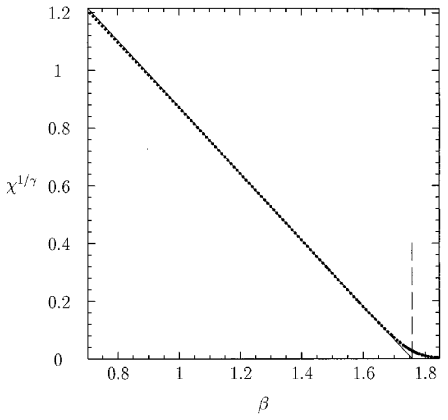

FIG. 3. Inverse susceptibility χ raised to the power $1/\gamma$ plotted vs β. For the critical index γ the exact value 1.75 is used for the two-dimensional Ising model. A straight line through the SCOZA results extrapolates into the critical point of the exact solution marked by the dashed line.

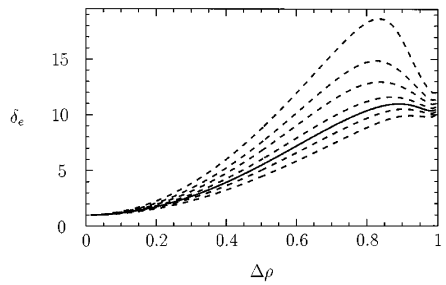

FIG. 4. Effective critical index δ_e defined below (19) vs $\Delta\rho$. The solid curve is for the "critical isotherm" $T=T_c$ or $t=0$. The dashed curves are neighboring isotherms with $\log_{10}t$ equal to -1.6 and -2.0 for $T>T_c$ and equal to -2.0, -1.6, -1.4, and -1.2 for $T<T_c$.

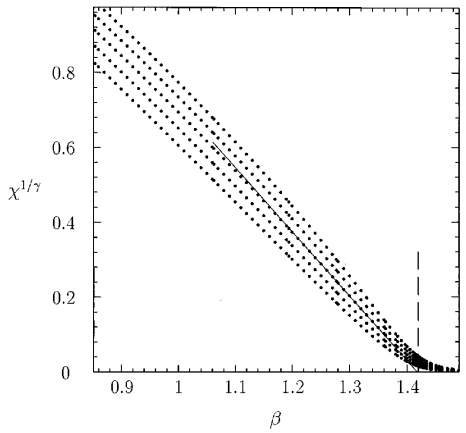

FIG. 5. Inverse susceptibility χ using interaction (20) with $\alpha=0.5$, raised to the power $1/\gamma$ and plotted vs β where the different curves correspond to γ-values 1.55, 1.65, 1.75, 1.85, and 1.95, respectively, from below. The straight line through the $\gamma=1.75$ curve goes through the "critical" point (vertical line) as defined by the maximum of the SCOZA specific heat.

therm at $\beta=\beta_c$. For small m the exact one behaves like $\chi \sim m^{\delta-1}$ where $\delta=15$. The SCOZA isotherm will have a finite slope for $m=0$ that can be subtracted. Then the logarithmic derivative is taken of the remainder $\Delta\chi$ to obtain an effective critical index $\delta_e-1=\partial(\ln m)/\partial \ln \Delta\chi$. In Fig. 4 it is shown how this index varies with m, and it shows that δ_e peaks at a value not so far below the exact value $\delta=15$. (To see how neighboring SCOZA isotherms behave close to $\beta=\beta_c$, some additional δ_e for isotherms are also drawn in Fig. 4.) Thus extrapolated SCOZA results indicate critical properties that resemble the exact ones.

Since critical properties are expected to be universal we found it of interest to investigate more long-range interactions in two dimensions too. Building upon the nearest-neighbor interaction this can be done by the prescription of Høye and Stell[10] such that the new integral $P(z)$ can be expressed in terms of the one for nearest neighbors that here we can call $P_0(z)$. The interaction is then

$$\tilde{\varphi}(k)=qA\left(\frac{1}{1-\alpha\tilde{\psi}(k)/q}-I_\alpha\right), \tag{20}$$

where in the present case $\tilde{\psi}(k)$ is as given by Eq. (13). Further,

$$A=\frac{1-\alpha}{1-(1-\alpha)I_\alpha}, \qquad I_\alpha=P_0(\alpha). \tag{21}$$

The constant I_α is used in (20) to make $\varphi(0)=\psi(0)=0$ as was assumed when deriving the relations for the SCOZA equation, and A is determined such that $\tilde{\varphi}(0)=q$. With this new interaction the integral of interest becomes

$$P(z)=\frac{1}{1+zAI_\alpha}\left[1+\frac{zA}{1-zA(1-I_\alpha)}P_0(W)\right], \tag{22}$$

where

$$W=\alpha\frac{1+zAI_\alpha}{1-zA(1-I_\alpha)}.$$

In two dimensions the inverse range of interaction is now $\gamma_r\sim(1-\alpha)^{1/2}$. With various values of α we then studied the inverse susceptibility χ in zero magnetic field as was done in Fig. 3 (i.e., for $\alpha=0$). If one considers all values of β below an estimated critical value β_c one finds an exponent γ that changes with γ_r and approaches its mean-field value $\gamma=1$ as $\gamma_r\to 0$. A somewhat similar situation was found in Ref. 2, where critical properties in three dimensions were studied. However, if one focuses upon the region close to β_c one sees a more universal behavior. The estimated value for β_c can be determined by the maximum of the specific heat, which as found above gave a value close to the exact one with nearest-neighbor interaction ($\alpha=0$). Then $\chi^{1/\gamma}$ can be plotted using various values of γ as done in Fig. 5 for the case $\alpha=0.5$. Studying the behavior in the critical region near β_c, one then sees that the curve with $\gamma\approx 1.75$ most accurately extrapolates with a straight line that crosses the $\chi=0$ axis at $\beta=\beta_c$. Thus in Fig. 6 the temperature dependent index γ defined as the logarithmic derivative

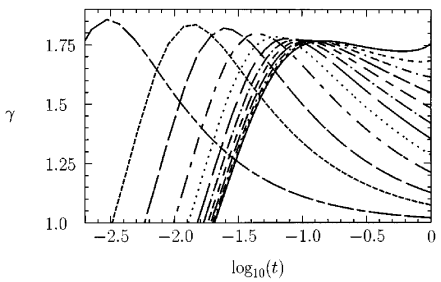

FIG. 6. Effective critical index γ for the susceptibility in zero field as defined by (23) vs $\log_{10}t$ ($t=1-T_c/T$) for varying range of interaction. The various curves correspond to α-values [see Eq. (20) and below] 0 (nearest-neighbor interaction), 0.1, 0.2, 0.2, 0.3, 0.4, 0.5, 0.6, 0.7, 0.8, 0.9, and 0.99, respectively, from above down along the right-hand side of the figure.

$$\gamma=\frac{\partial \ln \chi}{\partial \ln t} \tag{23}$$

with $t=1-\beta/\beta_c$ has been plotted for various α. For small β (i.e., large t) the γ has a nonuniversal behavior approaching the mean-field value $\gamma=1$ as $\alpha\to 1$. But for small $t\to 0$ the γ rises, reaching a maximum value around 1.80 before it drops. This yields a universal plateau for γ with an effective value of γ near its universal exact value 1.75. So somehow SCOZA for some unknown reason seems to aim for the exact behavior before it fails close to β_c.

Altogether our conclusion is that the Ornstein–Zernike or MSA form of $c(\boldsymbol{r})$ also describes two-dimensional systems well except close to β_c. As mentioned before, the latter is connected to the divergence of $P(z)$ $(z\to 1)$ by which a sharp phase transition is excluded. This contrasts somewhat the situation in three dimensions where a well defined phase transition with a critical point was obtained.[2] Furthermore, in the critical region, behavior close to the exact one was found although standard scaling was not obtained. But one striking result was the value $\beta=0.35$ for the critical index of the coexistence curve. So although the Ornstein–Zernike form used in SCOZA can not describe critical correlations or fluctuations correctly, the error, especially in three dimensions, must be small. However, in two dimensions $c(\boldsymbol{r})$ must develop a long-range tail to create a critical point. But clearly this tail can only give small corrections to thermodynamic quantities, although it will be crucial for determining the exact universal critical behavior for Ising systems or lattice gases in two dimensions.

IV. KAC INTERACTION IN ONE DIMENSION

The Kac interaction is the exponential

$$u(x)=-\gamma_r e^{-\gamma_r|x|}. \tag{24}$$

With this interaction in addition to hard cores, Kac, Uhlenbeck, and Hemmer showed that an exact solution could be obtained in terms of an integral equation in the continuum as well as the lattice case.[11] Explicit analytic solutions of this integral equation are not so easily obtained, but there is a nontrivial one upon which we will concentrate. This explicit result is the pair correlation function at the mean-field critical point in the limit $\gamma_r\to 0$ for the lattice case which is given by[12] $(r=|x|)$,

$$\begin{aligned} h(r)&=\gamma_r^{2/3}[0.656\exp(-0.754\gamma_r^{4/3}r)\\ &\quad+0.0019\exp(-2.91\gamma_r^{4/3}r)\\ &\quad+0.000\,06\exp(-5.6\gamma_r^{4/3}r)+\cdots]\\ &\approx\gamma_r^{2/3}(0.656+0.0019+0.000\,06+\cdots). \end{aligned} \tag{25}$$

In the limit $\gamma_r\to 0$ this immediately gives the internal energy correction to mean-field $(\rho=1/2)$,

$$\rho u_1=-\tfrac{1}{4}\gamma_r^{2/3}(0.656+0.0019+\cdots)=-0.1645\gamma_r^{2/3}. \tag{26}$$

The MSA and thus SCOZA give a simple exponential like the first term in (25) which is by far the dominating one. So the SCOZA can in no way give the exact result due to the correction terms in (25). So the question is to what extent SCOZA can approximate the leading term and the internal energy (26). Also, the MSA form enforces a certain relation between coefficients which, as will be seen, is not quite fulfilled by the leading term.

As in Sec. II the Kac interaction (24) can be expressed in terms of the nearest-neighbor interaction whose Fourier transform in one dimension is $(q=2)$,

$$\tilde{\psi}(k)=q\cos k \tag{27}$$

[when normalized as before such that $\tilde{\psi}(0)=q$]. Use of relations (20)–(22) then give the expressions needed for solution of the SCOZA equation (12). With expression (27) one finds for $P_0(W)$ [like the first integration in (14)]

$$P_0(W)=\frac{1}{2\pi}\int_{-\pi}^{\pi}\frac{dk}{1-W\cos k}=\frac{1}{\sqrt{1-W^2}}. \tag{28}$$

For small γ_r interaction, (24) is easily Fourier transformed, as one can integrate to obtain

$$\tilde{u}(k)=-\frac{2\gamma_r^2}{\gamma_r^2+k^2}. \tag{29}$$

Comparing this with Eq. (20) when Eq. (27) is inserted, one finds the identification $(\cos k=1-(1/2)k^2+\cdots)$

$$\gamma_r^2=2(1-\alpha)\quad(\gamma_r\to 0), \tag{30}$$

with $\tilde{\varphi}(k)=-(1/2)q\tilde{u}(k)$. Using Eqs. (3)–(7) replacing $\tilde{\psi}(k)$ with $\tilde{\varphi}(k)$, one now finds for the pair correlation function,

$$\rho+\rho^2\tilde{h}(k)=\frac{\rho(1-\rho)}{P(z)}\frac{1}{1-z\tilde{\varphi}(k)/q}. \tag{31}$$

At the mean-field critical point, which we want to investigate, we have $P(z)\to 1$ as $\gamma_r\to 0$. Thus by expanding (31) in k^2 with critical density $\rho=1/2$ inserted we find (i.e., formally regarding $k\ll\gamma_r$ and z close to 1),

$$\rho^2\tilde{h}(k)=\frac{1}{4}\frac{1}{1-z\dfrac{\gamma_r^2}{\gamma_r^2+k^2}}=\frac{1}{4}\frac{\gamma_r^2}{(1-z)\gamma_r^2+k^2}. \tag{32}$$

Inverting the transform by comparing Eqs. (24) and (29) one finds $(\gamma_r\to 0)$,

$$\rho^2 h(r)=\frac{1}{8a}\gamma_r^{2/3}\exp(-a\gamma_r^{4/3}r), \tag{33}$$

where

$$a=\sqrt{1-z}/\gamma_r^{1/3}. \tag{34}$$

By determination of the coefficient a this can be compared with the exact result (25). Here one notes that (33) can not coincide fully with the dominating term of the exact result as the two coefficients in the latter will correspond to two slightly different values of a that differ nearly 1%.

In this connection it is of interest to rederive the known MSA result.[13] Then $P(z)$, which is most easily obtained via

the internal energy, is needed. Integrating Eq. (8) in r-space (one dimension) one then has [$\rho=1/2$, the ρ-term does not contribute as $\int \tilde{\psi}(\boldsymbol{k})\, d\boldsymbol{k}=\psi(0)=0$],

$$\rho u_1=-\tfrac{1}{2}\int (\rho\delta(r)+\rho^2 h(r))\varphi(r)\, d\boldsymbol{r}=-\frac{q}{4}\frac{P(z)-1}{zP(z)}. \tag{35}$$

Now $h(r)$ as given by (33) (with a finite) is more long ranged than $\varphi(r)$ and can thus be regarded as a constant during integration ($\gamma_r\to 0$). Also with $z\to 1$ and $P(z)\to 1$, expression (33) inserted in (35) thus yields [$\tilde{\varphi}(0)=q$],

$$P(z)-1=-8\rho u_1/q=\frac{1}{2a}\gamma_r^{2/3}. \tag{36}$$

This latter result can be checked in an independent way via evaluation of W as given by (22). With (28) one then has $I_\alpha=1/\sqrt{1-\alpha^2}=1/\gamma_r$ and thus $A=(1/2)\gamma_r^2$. So expanding in $1-z$ one finds

$$W=1-\tfrac{1}{2}(1-z)\gamma_r^2, \tag{37}$$

which inserted in (28) and (22) then yields result (36) with a given by (34).

In MSA the coefficient $c_1=\beta$ such that Eq. (7) yields

$$P(z)z=q\rho(1-\rho)c_1=q\rho(1-\rho)\beta. \tag{38}$$

At the mean-field critical point ($\beta=\beta_c$, $\gamma_r=0$) $P(z)=1$ and $z=1$, i.e., $q\rho(1-\rho)\beta_c=1$. Thus with β_c unchanged for finite γ_r we still must have

$$P(z)z=1, \tag{39}$$

or

$$\begin{aligned} 1&=(1+(P(z)-1))(1-(1-z))\\ &=1+(P(z)-1)-(1-z)+\cdots,\\ 1-z&=P(z)-1. \end{aligned} \tag{40}$$

Inserting from Eqs. (34) and (36) we obtain

$$\begin{aligned} a^2\gamma_r^{2/3}&=\frac{1}{2a}\gamma_r^{2/3},\\ a&=1/2^{1/3}=0.7937, \end{aligned} \tag{41}$$

which is the known MSA result.

By doing SCOZA computations one (at critical density at least) generally finds an effective inverse temperature $\beta_e=c_1>\beta$. This will make $P(z)z>1$ by which the value of a becomes lower in direction of the exact result (25).

Numerically one can not put $\alpha=1$ or $\gamma_r=0$ directly, as deviation from a mean-field result is wanted. So α has to be chosen close to one, i.e., γ_r close to zero. The a turned out to vary quite a bit close to $\gamma_r=0$, and to obtain a reliable estimate we had to make $\gamma_r^2=2(1-\alpha)$ as small as possible. With standard double precision we found our results significant down to $1-\alpha=10^{-10}$. Thus in Fig. 7 we have plotted a as a function of $(1-\alpha)^{1/6}$ by which we find a straight line as $1-\alpha\to 0$. By extrapolation down to $1-\alpha=0$ we obtain the SCOZA value,

$$a=0.756\pm 0.001. \tag{42}$$

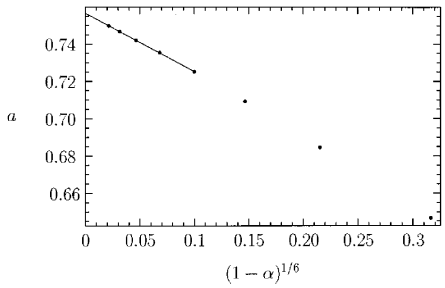

FIG. 7. The constant a defined by Eq. (34) for the SCOZA pair correlation function at the mean-field critical point for the one-dimensional model with exponential interaction plotted vs $(1-\alpha)^{1/6}$ [see Eq. (30)]. The points correspond to $(1-\alpha)$-values 10^{-3}, 10^{-4}, . . . ,10^{-10}. The straight line is extrapolation down to $1-\alpha=0$ which is the limit of infinitely long-ranged interaction.

The a can also be obtained via a similar plot using the internal energy (36). Extrapolation of the latter gave $a=0.756\pm 0.002$.

As a conclusion one sees that the SCOZA value (42) agrees closely with the exact result (25) when comparing exponents. For the coefficient in front of expression (26) the SCOZA via (36) yields (apart from sign)

$$\frac{1}{8a}=0.1654\pm 0.0004, \tag{43}$$

which again is near to the exact result. The same is the case when relating (25) to (33). In view of the comment below Eq. (26), it seems like the SCOZA result is a kind of best possible approximation to the exact result when using a single exponential term for $h(r)$.

V. NEAREST- AND NEXT-NEAREST NEIGHBOR INTERACTION IN ONE DIMENSION

With nearest- and next-nearest neighbor interaction the Fourier transform of it can be written

$$\tilde{\psi}(k)=\frac{q}{1+\alpha}(\cos k+\alpha\cos 2k), \tag{44}$$

where $q=2$ was used. To solve the SCOZA problem one again needs to evaluate integral (6) to obtain $P(z)$. As $\cos 2k=2\cos^2 k-1$ the resulting integrand can be split in two (partial fractions) that give integrals like (28). Altogether we find

$$P(z)=C\left(\frac{W_+}{\sqrt{1-W_+^2}}-\frac{W_-}{\sqrt{1-W_-^2}}\right), \tag{45}$$

where

$$\begin{aligned} C&=\frac{1+\alpha}{2\alpha z}\frac{W_+W_-}{W_--W_+},\\ 1/W_\pm&=-\frac{1}{4\alpha}\left[1\pm\sqrt{1+8\alpha^2+\frac{(1+\alpha)8\alpha}{z}}\right]. \end{aligned}$$

In the case with nearest-neighbor interaction only it is clear that SCOZA in fact yields the exact solution. This is con-

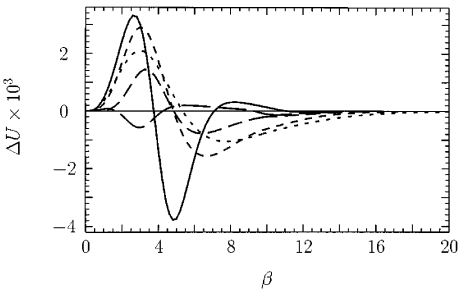

FIG. 8. Deviation between the SCOZA and the exact internal energy per spin ΔU vs β for the one-dimensional Ising model with nearest- and next-nearest neighbor interactions. The curves correspond to α-values [see Eq. (44)] 0.1, 0.5, 1.0, 2.0, and 10 drawn with increasing length of line segments for increasing α such that the fully drawn curve is for $\alpha=10$.

nected to the known property that the exact direct correlation function is restricted to nearest-neighbor sites which then is its SCOZA form too. In this case $\alpha=0$ such that $P(z)=1/\sqrt{1-z^2}$, and in the Appendix we verify that the exact solution is obtained. This was further used to test the accuracy of the numerical evaluation. When doing this for $m=0$ (or $\rho=1/2$) we found a deviation for the internal energy that had a maximum near $\beta\approx 13$. This deviation, which was negative, had the form of a ''bump'' of width $\Delta\beta\approx 10$, and its height went down such that it extrapolated to zero when increasing the number of grid points in the β- and/or ρ-directions. (In Fig. 8 using 1000 gridpoints for $0<\rho\leqslant 1/2$ this error will be barely visible as its height corresponds to 0.06 units and its area when integrated will be something like 0.5 units on the figure.)

The next-nearest neighbor interaction can now be added, solving the SCOZA problem with $P(z)$ given by (45), and comparing it with the exact solution. For $H=0$ or $m=0$ the exact result is[14]

$$\lambda=2e^{2\beta K}\cosh^2(\beta J)-2\sinh(2\beta K)+[e^{4\beta K}\sinh^2(2\beta J)+4\cosh^2(\beta J)]^{1/2}, \tag{46}$$

where $\lambda^{N/2}$ is the partition function for N spins. When related to interaction (44) we here have $4J=1/(1+\alpha)$ and $4K=\alpha/(1+\alpha)$. The internal energy per spin is thus $-(1/2)\partial(\ln\lambda)/\partial\beta$. (The exact solution could also be considered for $m\neq 0$, but then the exact λ is rather complex depending upon the solution of a quartic equation, and furthermore m should be substituted in favor of the magnetic field H. Due to this we have not tried such a comparison here.)

In Fig. 8 we have plotted the difference between the SCOZA internal energy and the exact one for $\alpha=0.1,0.5,1.0,2.0,10$ $(m=0)$. Quite similar to the two-dimensional case in Fig. 2 one sees that the deviation is largest somewhat above the mean-field critical point $\beta_c q=4$ i.e., $\beta_c=2$ (with $q=2$) where it typically also changes sign. The relative magnitude of the error $\Delta U/U$ is reaching a maximum of about 1%. [For $\alpha=0$ the exact internal energy is $-(1/2)\tanh(\beta/4)$.] Note that total area of the error when integrated with respect to β is zero (within numerical accuracy) when subtracting the $\alpha=0$ inaccuracy discussed above. This means that as in the two-dimensional case the SCOZA free energy as well as the internal one becomes exact when $\beta\to\infty$.

One can also evaluate the specific heat which is the derivative of the internal energy with respect to temperature. The error in this latter quantity that follows from the slope of the curves in Fig. 8 will of course have a relative magnitude that is greater than the one for the internal energy simply because derivation will always magnify ''bumpy'' behavior. The maximum of the latter is about 3%–7%.

Note that the exact solution again is recovered when $\alpha\to\infty$ as then there will be no nearest-neighbor interaction, and the next-nearest one alone on a sublattice is equivalent to the nearest one.

One can also make α negative, and one finds that SCOZA works for not too large $|\alpha|$. However, the error is getting larger and at $\alpha=-1/4$ the SCOZA starts to break down. This then also shows the limitation of SCOZA as defined here. Relation (4) for $\tilde{c}(\boldsymbol{k})$ is adapted to and thus works well when ferromagnetic arrangements are clearly favored. It is easily understood from integral (6) for $P(z)$ that SCOZA will start to fail seriously at $\alpha=-1/4$. The reason is that the maximum and thus the divergence of the integrand in (6) will no longer be at $k=0$ when $\alpha<-1/4$. (This for instance will prevent $z\to 1$ or $\varepsilon^2\to 0$.) Thus in the latter situation the simple assumption (4) is too much in conflict with the exact $c(r)$.

ACKNOWLEDGMENTS

We are very grateful to Davide Pini for sending us his program for the SCOZA in the lattice gas case and to George Stell for helpful suggestions and comments.

APPENDIX: EXACT SOLUTION WITH NEAREST-NEIGHBOR INTERACTION

We will show that with nearest-neighbor interaction in one dimension the SCOZA yields the known exact solution. Using the standard transfer matrix method one has the eigenvalues

$$\lambda_{\pm}=e^{\beta J}(\cosh(\beta H)\pm\sqrt{\sinh^2(\beta H)+e^{-4\beta J}}), \tag{A1}$$

where using Ising spin language H is the magnetic field, and J is the nearest-neighbor interaction. The λ_+^N is the partition function from which one can obtain the magnetization per spin $m=\partial(\ln\lambda_+)/\partial(\beta H)$. When rearranged this yields the relation

$$\sinh^2(\beta H)=\frac{m^2e^{-4\beta J}}{1-m^2}, \tag{A2}$$

which is used below to substitute βH by m to establish the SCOZA solution.

The exact spin correlation function and its Fourier transform is now

$$\Gamma(n)=(1-m^2)\sigma^{|n|},\qquad \tilde{\Gamma}(k)=(1-m^2)\frac{1-\sigma^2}{1+\sigma^2-2\sigma\cos k}, \tag{A3}$$

with

$$\sigma=\lambda_-/\lambda_+. \tag{A4}$$

In Ising spin language mentioned below Eq. (2), the SCOZA equation (12) reads [$\rho=(1/2)(1+m)$ putting $q=4$],

$$\frac{\partial\varepsilon^2}{\partial\beta}=-(1-m^2)\left(1+\frac{\partial^2}{\partial m^2}(1-m^2)F(z)\right), \tag{A5}$$

with other relations unchanged. As the solution of this equation is expected to be consistent with Eqs. (A1)–(A3) the value of the parameter z suggests itself comparing (6) and (A3) as

$$z=\frac{2\sigma}{1+\sigma^2}. \tag{A6}$$

With this z using (A1), (A2), and (A4), one then obtains the following explicit expressions,

$$P(z)=\frac{1}{\sqrt{1-z^2}}=\frac{1+\sigma^2}{1-\sigma^2},$$

$$\varepsilon^2=(1-z)P(z)=\frac{1-\sigma}{1+\sigma}=\frac{e^{-\beta}}{\sqrt{1-m^2(1-e^{-2\beta})}}, \tag{A7}$$

$$F(z)=\frac{P(z)-1}{2zP(z)}=\tfrac{1}{2}\sigma=\frac{(\sqrt{1-m^2(1-e^{-2\beta})}-e^{-\beta})^2}{2(1-m^2)(1-e^{-2\beta})},$$

where here the interaction has been normalized such that $2J=1$, which corresponds to $\tilde{\psi}(0)=q=4$. When inserted one finds that these expressions solve Eq. (12). They are also the exact ones, as their dependence upon σ is consistent with (A3) [$\tilde{\Gamma}(0)=(1-m^2)\varepsilon^{-2}$ and $\Gamma(1)=2(1-m^2)F(z)$]. [One can also differentiate (A1) to obtain ε^2 and $F(z)$ as given above from $\partial^2(\ln\lambda_+)/\partial(\beta H)^2=\tilde{\Gamma}(0)^{-1}$ and $\partial(\ln\lambda_+)/\partial\beta=-(1/2)m^2-\Gamma(1)$.]

[1] R. Dickman and G. Stell, Phys. Rev. Lett. **77**, 996 (1996).
[2] A. Borge and J. S. Høye, J. Chem. Phys. **108**, 4516 (1998).
[3] D. Pini, G. Stell, and R. Dickman, Phys. Rev. E **57**, 2862 (1998).
[4] D. Pini, G. Stell, and J. S. Høye, SUSB College of Eng. and Applied Sciences Report #738 (April 1997).
[5] J. S. Høye and G. Stell, Physica A **244**, 176 (1997); **247**, 497 (1997).
[6] L. Onsager, Phys. Rev. **65**, 117 (1944).
[7] K. Huang, *Statistical Mechanics* (Wiley, New York, 1987), p. 389.
[8] D. Pini, A. Parola, and L. Reatto, J. Stat. Phys. **72**, 1179 (1993).
[9] D. Pini, unpublished notes; see also W. F. Ames, *Numerical Methods for Partial Differential Equations* (Academic, New York, 1977), pp. 82–86.
[10] J. S. Høye and G. Stell, J. Stat. Phys. **89**, 177 (1997).
[11] M. Kac, G. E. Uhlenbeck, and P. C. Hemmer, J. Math. Phys. **4**, 216 (1963); G. E. Uhlenbeck, P. C. Hemmer, and M. Kac, *ibid.* **4**, 229 (1963); P. C. Hemmer, M. Kac, and G. E. Uhlenbeck, *ibid.* **5**, 60 (1964).
[12] M. Kac and E. Helfand, J. Math. Phys. **4**, 1078 (1963).
[13] G. Stell and W. K. Theumann, Phys. Rev. **186**, 581 (1969).
[14] W. K. Theumann and J. S. Høye, J. Chem. Phys. **55**, 4159 (1971).